Ph.D. Thesis

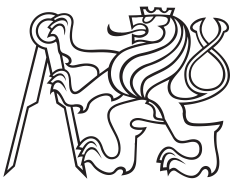

Czech Technical University in Prague

F3

Faculty of Electrical Engineering
Department of Physics

Numerical Studies of Plasma Instabilities

Ing. Miroslav Horký
Electrical Engineering and Information Technology, Plasma Physics

May 2015
Supervisor: prof. RNDr. Petr Kulhánek, CSc.
Consultee: prof. RNDr. Vladimír Karas, DrSc.

Acknowledgement / Declaration

This doctoral thesis is dedicated to my wife Barbara and son Miroslav for their fulltime support and patience during my doctoral studies.

I would like to acknowledge my supervisor prof. Petr Kulhánek and co-supervisor prof. Vladimír Karas for their guidance and willingness to help and answer any question throughout my entire studies. Many thanks belongs to Dr. Wojciech Jacek Miloch from the Unversity of Oslo for his patience and optimism even in times when research did not go so well.

Projects included in this thesis were supported from CTU internal grants Nos. SGS10/266/OHK3/3T/13, SGS12/181/OHK3/3T/13, SGS13/194/OHK-3/3T/13, GA CR grants GD205/09/H-033, 14-37086G, and Norway grant NF-CZ07-INS-3-002-2014.

I hereby declare that this thesis is the result of my own work and all the sources I used are in the list of references, in accordance with the Methodological Instructions on Ethical Principles in the Preparation of University Theses.

In Prague, 14. 5. 2015

.....

Abstrakt / Abstract

Plazmové nestability jsou v současnosti intenzivně zkoumány, protože představují procesy, které například stojí v pozadí pozorovaných astrofyzikálních dějů jako je ohřev sluneční chromosféry nebo geneze specifických elektromagnetických vln. Vzhledem k silně nelineárnímu chování plazmových nestabilit, jsou tyto dnes zkoumány hlavně za použití numerických metod. Numerické metody umožňují nalezení přibližného řešení i u takových dějů, které jsou popsány analyticky neřešitelnými rovnicemi. Při současném rozvoji výpočetní techniky se jedná o velmi efektivní nástroj, který má vedle experimentů a teoretických výpočtů své nezastupitelné místo.

Za pomoci numerických metod zkoumáme oba dva typy nestabilit: makro- a mikronestability. Práce poskytuje základní přehled o teorii plazmatu (pohyb částic, kinetická teroie, magnetohydrodynamika), jeho nestabilitách a numerických simulacích následovaný souborem publikovných prací ze dvou tématů. První dva články jsou zaměřené na analýzu numerického řešení zobecněné disperzní relace pro Bunemanovu nestabilitu, která je typickým příkladem makronestability. Zbylé tři články pokrývají výzkum na téma numerických simulací stability slabě srážkového plazmatu, kde v případě nestabilit jde o mikronestability vznikající z poruch v rychlostním rozdělení částic.

V prvním tématu byla nalezena a analyzována závislost koeficientu nárůstu nestability na všech parametrech disperzní relace. V druhém tématu byla nalezena závislost stability na typu iontově-neutrálních srážek.

Klíčová slova: plazmové nestability, PIC, numerické simulace, disperzní relace.

The subject of this Ph.D. thesis covers plasma instabilites that are nowadays intensively studied, because they represent processes which are for instance behind of observed astrophysical phenomena such as solar chromosphere heating or generation of particular electromagnetic waves. Due to the highly nonlinear behaviour of plasma instabilities the studies are carried out using numerical methods. Numerical methods allow to find an approximate solution even in cases of processes described by equations which are not analytically solvable. With actual growth of computational power they represent very useful tool and they have regular place between theory and experimental physics.

We numerically study both macro- and microinstabilities. This work describes the basic theoretical background of plasmas (particle motion, kinetic theory, and magnetohydrodynamics), their instabilities and numerical simulations. This part is followed by a collection of papers on the two topics. The first two papers deal with analysis of a numerical solution of the generalized dispersion relation for Buneman instability which is typical macroinstability. The remaining three papers focus on Particle-In-Cell simulations of the stability of weakly collisional plasma where instabilities are on microscopic scale originating from the distortions in velocity phase space.

The dependence of plasma instability growth rate on all plasma parameters in the relation is found and analysed in the first topic. The stability dependence on the type of ion-neutral collisions is found in the second part.

Keywords: plasma instabilities, PIC, numerical simulations, dispersion relation.

Contents / Figures

Chapter 1
Introduction

1.1 Aims and structure of this Ph.D. thesis

This Ph.D. thesis focuses on numerical studies of plasma instabilities. It deals with linear analysis of a plasma jet interaction with plasma background and Particle-In-Cell simulations of instabilities in weakly collisional plasmas. It is written in the format of collection of papers in accordance with the FEE CTU internal regulation of 1 November 2014 governing the dissertation defences ("Směrnice děkana pro obhajoby disertačních prací na FEL"). The main aim of the thesis is to gain a better understanding of studied phenomena, namely analyzing the dispersion relation for jet-background plasma interaction and finding stability properties of weakly collisional plasmas.

The structure of this thesis is as follows. The first part of the thesis is the introduction. The second part, Chapter 2, focuses on theoretical description of plasmas, especially three approaches of a general description and an introduction to instabilities. The basics of numerical simulations and particularly PIC simulations are covered in Chapter 3. Chapter 4 consists of a commented collection of scientific papers on two main subjects of my doctoral research and finally the conclusions constitute Chapter 5 of the dissertation. The lists of publications, grants, and used symbols complement the dissertation at the end in appendices.

1.2 What is plasma and where to find it.

Plasma, sometimes called the fourth state of matter, is a state of matter in which atoms are ionized thus it contains free charge carriers (ions and electrons) [1–2]. The origin of ionization can be different, i. e. heating, electromagnetic radiation. The term *plasma* was firstly used by Irwing Langmuir (1881-1957) who also made the first exact definition. According to this definition plasma must fulfill three conditions [1]:

1. It must contain free charge carriers.
2. It must be quasineutral.
3. It must show collective behaviour as a response on electric and magnetic fields.

We can easily imagine plasma as hot gas. If the gas is heated above an ionization temperature, electrons detach from atoms and free charge carriers (positively charged ions and negative electrons) are created. The summation of all charges is equal to zero so the system is still electrically neutral on the macroscopic scale. If this system is subjected to an external electric and/or magnetic field, it shows a collective reaction to the field/s. If the three conditions are fulfilled then the neutral gas becomes a plasma.

In nature we can find plasma throughout the whole Universe, but on the Earth there are only few natural occurrences of plasma [1–3]. Typical examples are Earth's ionosphere or lightning discharges. More usual is to use plasmas in laboratories and in applications like fusion experiments, discharge lamps and various technologies (e. g. plasma

welding). In space there is a wide variety of plasmas: from very low dense plasma in the intergalactic medium, through hot and dense plasma in stars, to ultra-dense quantum plasma in white dwarfs. Particle density is one of the parameters with which we can categorize plasmas. The second one is the temperature and the third is magnetic field [1, 3]. The typical range of plasmas for zero magnetic field and different temperatures and densities is depicted in Fig. 1.1

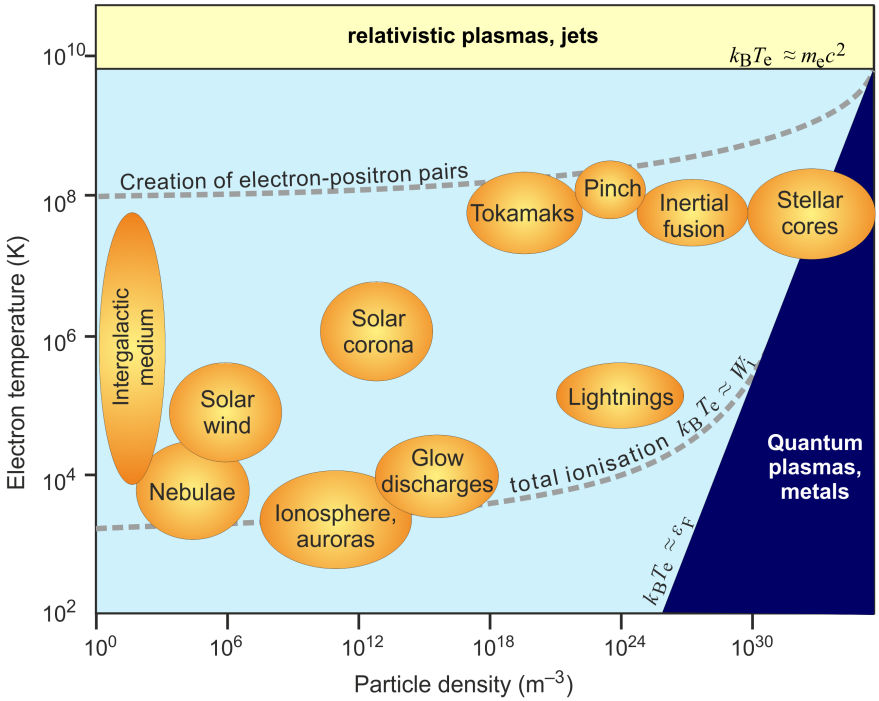

Figure 1.1. Typical range of plasmas for different particle densities and electron temperatures. Magnetic field is considered to be zero. Source: [1]

Chapter 2
Theoretical description

2.1 Single particle motion

The simplest method of how to study plasma behaviour is to address the problem of single particle motion. Unlike in neutral gases, electric and magnetic fields affect plasma particle motion which must be included in the Lagrangian and consequently in the Hamiltonian functions of the problem. Nonrelativistic Lagrangian and Hamiltonian functions are [1]:

$$\mathscr{L} = \frac{1}{2}m\mathbf{v}^2 - Q\phi + Q\mathbf{A}\cdot\mathbf{v}, \tag{2.1}$$

$$\mathscr{H} = \frac{(\mathbf{p} - Q\mathbf{A})^2}{2m} + Q\phi, \tag{2.2}$$

where $\mathbf{A}$ is vector potential and ϕ is scalar potential. The well-known Lorentz equation

$$\frac{\mathrm{d}\mathbf{v}}{\mathrm{d}t} = \frac{q}{m}(\mathbf{E} + \mathbf{v}\times\mathbf{B})$$

can be easily derived from this Lagrangian function. By solving the Hamilton equations we can investigate particle motion in particular problems.

2.1.1 Particle motion in a static magnetic field

As a first example we look on particle motion in a static magnetic field. Let us introduce a Cartesian system where a static magnetic field is oriented only in the $\hat{\mathbf{z}}$-axis and initial particle velocity is only in the $\hat{\mathbf{y}}$-axis. Then the Hamilton equations lead to the solution for particle trajectory [1–3]:

$$\mathbf{r}(t) = (R_\mathrm{L} - R_\mathrm{L}\cos\Omega_\mathrm{c}t, R_\mathrm{L}\sin\Omega_\mathrm{c}t, 0)\,, \tag{2.3}$$

where

$$R_\mathrm{L} = \frac{mv_\perp}{QB};\ \Omega_\mathrm{c} = \frac{QB}{m}$$

are Larmor radius (or gyroradius) and cyclotron frequency (or gyrofrequency), respectively.

A visualization of the particle trajectory in the system described above is depicted on the left panel of Fig. 2.1. In such cases where the initial particle velocity has also a component parallel to the magnetic field, the resulting trajectory is helical, which is shown on right panel of Fig. 2.1.

Magnetic fields cause only centripetal acceleration of the particle, thus only the direction of velocity changes, while magnitude remains at the initial value.

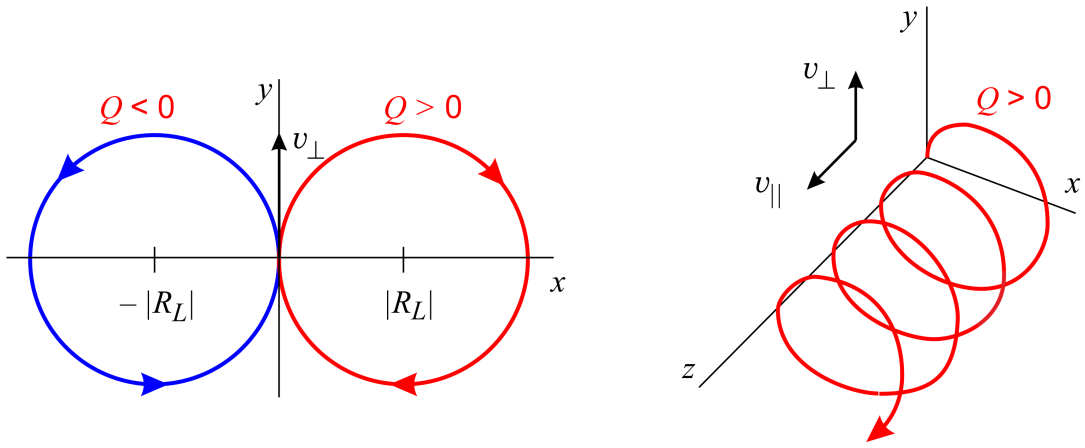

Figure 2.1. Visualization of charged particle motion in a static magnetic field. Source: [1]

2.1.2 Particle motion in E × B fields

Let us add a static electric field oriented only in the $\hat{\mathbf{y}}$-axis of the system described in the previous case and set the initial velocity to zero. Then our test particle will be exposed to both the electric and magnetic fields which are perpendicular to each other. Solving the Hamilton equation for this system we find the solution for the particle trajectory [1]:

$$\mathbf{r}(t) = (R_\mathrm{D} - R_\mathrm{D}\cos\Omega_\mathrm{c}t, R_\mathrm{D}\sin\Omega_\mathrm{c}t - v_\mathrm{D}t, 0)\,, \tag{2.4}$$

where

$$R_\mathrm{D} = \frac{mv_\mathrm{D}}{QB};\ \Omega_\mathrm{c} = \frac{QB}{m};\ v_\mathrm{D} = \frac{E}{B}$$

are drift radius, cyclotron frequency, and drift velocity, respectively.

An electric field will accelerate a particle and curve its trajectory until the particle becomes decelerated and this process repeats. The trajectory described in Eq. (2.4) is called a cycloid. In case of nonzero initial velocity of the test particle, the trajectory would be more general, the so-called trochoid. Depiction of these two types of trajectories is shown in Fig. 2.2.

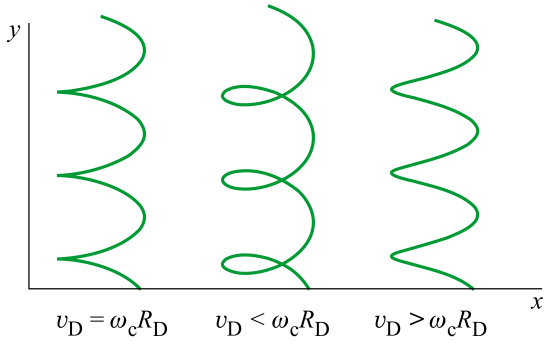

Figure 2.2. Visualization of charged particle motion in **E** × **B** fields. Left trajectory is cycloidal, middle and right trajectories are trochoidal. Source: [1]

2.1.3 Particle motion in a constant electric field

Particle motion in a static electric field (without magnetic field) has one serious problem. An electric field gives tangential acceleration to the particle which means that

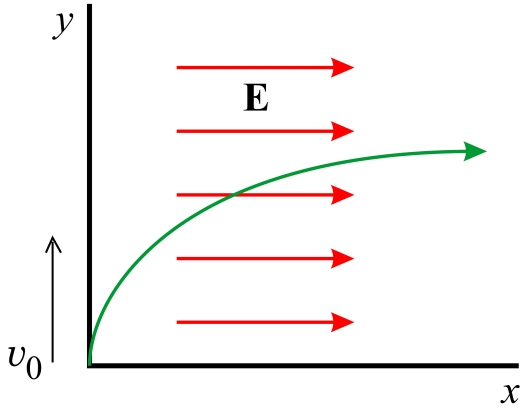

Figure 2.3. Illustration of example solution of particle motion in electric field. Source: [1]

using classical Lagrangian and Hamiltonian functions given in Eqs. (2.1),(2.2) is not possible and we must use relativistic variants [1]:

$$\mathscr{L}_\mathrm{r} = -m_0c^2\sqrt{1-\mathbf{v}^2/c^2} - Q\phi + Q\mathbf{A}\cdot\mathbf{v}, \tag{2.5}$$

$$\mathscr{H}_\mathrm{r} = c\sqrt{m_0^2c^2 + (\mathbf{p}-Q\mathbf{A})^2} + Q\phi. \tag{2.6}$$

Let us assume a system where electric field is oriented in the $\hat{\mathbf{x}}$-direction as shown in Fig. 2.3 and initial particle velocity is in the $\hat{\mathbf{y}}$-direction. Solution of the Hamilton equations using the relativistic Hamiltonian function leads to the trajectory [1]:

$$\mathbf{r}(t) = \left(\frac{\pi_0 c}{QE}\left[\sqrt{1+(QEt/\pi_0)^2}-1\right], \frac{p_0 c}{QE}\operatorname{arg\,sinh}\left[QEt/\pi_0\right], 0\right). \tag{2.7}$$

Hence,

$$x(y) = \frac{\pi_0 c}{QE}\left[\cosh\left(\frac{QE}{p_0 c}y\right)-1\right], \tag{2.8}$$

where,

$$p_0 = \frac{m_0 v_0}{\sqrt{1-v_0^2/c^2}};\ \pi_0 = \sqrt{m_0^2c^2+p_0^2}.$$

This trajectory differs from the one which would be obtained from classical Hamiltonian function because the particle velocity cannot exceed the speed of light. While the relativistic solution is $x \approx \cosh(y/y_0) - 1$ the classical theory solution would be $x \approx (y/y_0)^2/2$.

2.1.4 Adiabatic case

As an adiabatic case we consider a situation where magnetic and other fields are changing very slowly in comparison with the time of one gyroperiod [1–3]. In these cases we can average the gyromotion and then follow only the motion of the gyrocenter. The equation of the gyrocenter motion is

$$m\ddot{\mathbf{R}} = \mathbf{F}_\mathrm{ext} + Q\dot{\mathbf{R}}\times\mathbf{B} - \mu\nabla B, \tag{2.9}$$

where $\mathbf{R}$ is the position vector of the gyrocenter, dots represent time derivatives and

$$\mu = \frac{mv_\perp^2}{2B}$$

is the first adiabatic invariant. This equation leads to the drift equation which describes all kinds of drifts in plasmas [1–3].

2.2 Statistical approach

In the previous part the basics of single particle motion was introduced. As shown in Fig. 1.1 there are typically 10^6 up to 10^{24} particles per cubic meter in most types of plasmas. Thus it is impossible to calculate trajectories and velocities for each particle separately. The solution of this issue lies in the use of statistics.

Let us have a function $f = f(t, \mathbf{r}, \mathbf{v})$ which is the probability density of particle appearance in phase space. This probability density can change with particle collisions

$$\frac{\mathrm{d}}{\mathrm{d}t} f_\alpha(t, \mathbf{r}, \mathbf{v}_\alpha) = \sum_\beta \mathcal{C}_{\alpha\beta},$$

which can be rewritten as:

$$\frac{\partial}{\partial t} f_\alpha(t, \mathbf{r}, \mathbf{v}_\alpha) + (\mathbf{v}_\alpha \cdot \nabla) f_\alpha(t, \mathbf{r}, \mathbf{v}_\alpha) + \left(\frac{\mathbf{F}_\alpha}{m_\alpha} \cdot \nabla_\mathbf{v} \right) f_\alpha(t, \mathbf{r}, \mathbf{v}_\alpha) = \sum_\beta \mathcal{C}_{\alpha\beta}. \tag{2.10}$$

This is the Boltzmann equation and it is used as an initial equation for analytical studies of plasma behaviour on the microscopic scale [1–3]. The left hand side of the equation is the total time derivative of the probability density function. On the right hand side there is summation over all collisional processes. The term on the right hand side is the so-called "collision integral" and because of the difficulty (and sometimes impossibility) of its exact calculation, a lot of simplifications were established. The three most widely used approximations are:

1. *Vlasov* approach where the collisional term is

   $$\mathcal{C} = 0,$$

   because plasma can be assumed as colisionless, or sum of all collisions has negligable effect [1–2].
2. *Bhatnagar-Gross-Krook* (BGK) approach under which the collision term becomes

   $$\mathcal{C} = -\nu_\alpha (f_\alpha - f_{0\alpha}),$$

   where ν is a collisional frequency known from experiments and $f_{0\alpha}$ is local equilibrium probability density function [1–2].
3. *Fokker-Planck* (F-P) approach under which we can write the collisional term as

   $$\mathcal{C} = -\frac{1}{\Delta t} \nabla_\mathbf{v} \cdot (f \langle \Delta \mathbf{v} \rangle) + \frac{1}{2\Delta t} (\nabla_\mathbf{v} \otimes \nabla_\mathbf{v}) : (f \langle \Delta \mathbf{v} \otimes \Delta \mathbf{v} \rangle),$$

   where

   $$\langle \Delta \mathbf{v} \rangle = \int \Delta \mathbf{v} \mathscr{P} \mathrm{d}^3(\Delta \mathbf{v}), \text{ and } \langle \Delta \mathbf{v} \otimes \Delta \mathbf{v} \rangle = \int \Delta \mathbf{v} \otimes \Delta \mathbf{v} \mathscr{P} \mathrm{d}^3(\Delta \mathbf{v}),$$

   are friction term and diffusion term, respectively. These terms represent average changes in velocity due to collisions [1, 4] and $\mathscr{P}$ is given by collision type.

The usage of these collisional approximations depends on the studied system. For instance, to study basic phenomena such as Landau damping [5], the Vlasov approach is sufficient[1–2, 6–8], while the BGK equation is used for studying basic transport effects and the F-P equation can lead to more complicated solutions like a runaway particles[1, 9] In general, a statistical approach is important for calculations where we need information about velocity phase space (i. e. real dependence of collisional cross-section on velocity, relaxing times, microinstabilites etc.).

2.3 Fluid approach

For some particular problems we do not need to know the full information about phase space and in such cases we can make a shift from statistics to continuum. This can be done by calculating the moments of Boltzmann equation (2.10). Let us consider a function of velocity with which we multiply each term in Eq. (2.10) and then we integrate over velocity phase space [1–2]. This step we write as:

$$\begin{aligned}\int \psi_\alpha \frac{\partial f_\alpha}{\partial t} \mathrm{d}^3\mathbf{v}_\alpha + \int \psi_\alpha \left(\mathbf{v}_\alpha \cdot \nabla\right) f_\alpha \mathrm{d}^3\mathbf{v}_\alpha + \int \psi_\alpha \left(\frac{\mathbf{F}_\alpha}{m_\alpha} \cdot \nabla_\mathbf{v}\right) f_\alpha \mathrm{d}^3\mathbf{v}_\alpha = \\ = \int \psi_\alpha \sum_\beta \mathcal{C}_{\alpha\beta} \mathrm{d}^3\mathbf{v}_\alpha,\end{aligned} \tag{2.11}$$

where ψ_α denotes function of velocity. Hence,

$$\begin{aligned}\frac{\partial}{\partial t}\left\langle n_\alpha \psi_\alpha \right\rangle_\mathbf{v} + \nabla \cdot \left\langle n_\alpha \psi_\alpha \mathbf{v}_\alpha \right\rangle_\mathbf{v} - \frac{Q_\alpha}{m_\alpha}\left\langle n_\alpha (\mathbf{E} + \mathbf{v}_\alpha \times \mathbf{B}) \cdot \frac{\partial \psi_\alpha}{\partial \mathbf{v}_\alpha} \right\rangle_\mathbf{v} = \\ = \int \psi_\alpha \sum_\beta \mathcal{C}_{\alpha\beta} \mathrm{d}^3\mathbf{v}_\alpha.\end{aligned} \tag{2.12}$$

This is the moment equation and by substituting different powers of velocity to this equation we can calculate the moments of the Boltzman equation. Substituting a scalar summation invariant (such as 1, m_α, Q) leads to the zeroth moment which is the well known continuity equation. Substituting $\psi_\alpha = m_\alpha \mathbf{v}_\alpha$ leads to the second moment which is the momentum equation. These two fluid equations are the basis for Magnetohydrodynamis (MHD). Adding Maxwell equations and expression for fluid pressure we obtain the minimal full set of resistive MHD equations which is a non-relativistic one-fluid model without high frequency effects [1–2]. The minimal full set contains: (i) continuity equation, (ii) momentum equation, (iii) equation for magnetic field which is derived from Maxwell equations, and (iv) equation for pressure.

(i) Continuity equation:

$$\frac{\partial \rho}{\partial t} + \nabla \cdot (\rho \mathbf{u}) = 0, \tag{2.13}$$

where ρ stands for fluid density and $\mathbf{u}$ denotes fluid velocity.

(ii) Momentum equation:

$$\frac{\partial}{\partial t}(\rho \mathbf{u}) + \nabla \cdot \left(\overline{\mathbf{T}}_\mathrm{P} + \overline{\mathbf{T}}_\mathrm{M}\right) = 0, \tag{2.14}$$

where

$$\overline{\mathbf{T}}_\mathrm{P} = p\overline{\mathbf{1}} + \rho \mathbf{u} \otimes \mathbf{u} - \overline{\mathbf{V}} \text{ and } \overline{\mathbf{T}}_\mathrm{M} = \frac{\mathbf{H} \cdot \mathbf{B}}{2}\overline{\mathbf{1}} - \mathbf{H} \otimes \mathbf{B}$$

denote tensor of dynamic pressure and viscosity and tensor of magnetic pressure, respectively.

(iii) Equation for magnetic field:

$$\frac{\partial \mathbf{B}}{\partial t} = \frac{1}{\sigma\mu}\nabla^2 \mathbf{B} + \nabla \times (\mathbf{u} \times \mathbf{B}). \tag{2.15}$$

(iv) Finally the system must be closed by the appropriate equation for pressure - generally we can write

$$p = p(\rho). \tag{2.16}$$

The set of equations (i-iii) is in conservative form and can be easily transformed to the form with total time derivative, which follows in the same order as the equations listed above. To create the initial set of equations for a particular problem we can combine equations in both forms together.

$$\frac{\mathrm{d}\rho}{\mathrm{d}t} + \rho\nabla\cdot\mathbf{u} = 0, \tag{2.17}$$

$$\rho\frac{\mathrm{d}\mathbf{u}}{\mathrm{d}t} = -\nabla p - \nabla p_{\mathrm{M}} + \frac{1}{\mu}(\mathbf{B}\cdot\nabla)\mathbf{B} + \eta\nabla^2\mathbf{u} + (\zeta+\eta/3)\nabla(\nabla\cdot\mathbf{u}), \tag{2.18}$$

$$\frac{\mathrm{d}\mathbf{B}}{\mathrm{d}t} = \frac{1}{\sigma\mu}\nabla^2\mathbf{B} + (\mathbf{B}\cdot\nabla)\mathbf{u} - \mathbf{B}\left(\nabla\cdot\mathbf{u}\right). \tag{2.19}$$

These two sets of equations are the minimal variant of compressible resistive magnetohydrodynamics. There are other variants such as relativistic MHD, two (and more) fluids models, ideal incompressible MHD and so on [2]. The magnetohydrodynamics is a very useful description of plasmas in such cases, where we can neglect particle distribution in velocity phase space. It is widely used in such fields of plasma research as astrophysical plasmas (e. g. shocks [10–11], jets [12], and ionospheric instabilities [13]) or laboratory plasmas (e. g. tokamaks [14].

2.4 Instabilities

An instability is defined as a phenomenon during which the amplitude of small initial perturbation grows instead of being damped. In an unstable system there must be a source of free energy as well as positive feedback in the system.

From a mathematical point of view, with perturbation analysis we can study whether an initial perturbation causes undamped oscillations, or whether oscillations are damped or are growing [1]. We need to find the dispersion relation $F(\omega,\mathbf{k}) = 0$ and then we can find when and/or where the solution is complex. The imaginary part of $\mathbf{k}$ or ω determines if the oscillations become damped or growing (depending on the sign of imaginary part). Throughout this chapter we will work with the solution for angular frequency of a plane wave $\omega = \omega_{\mathrm{R}}(\mathbf{k}) + \mathrm{i}\gamma(\mathbf{k})$, where γ is the imaginary part of the complex solution. If the γ has positive value it is called growth rate, while if it has negative value, it is called damping rate. For an unstable solution, the initial perturbation grows exponentially.

We can divide plasma instabilities into two main categories. (i) Macroinstabilities are dominant on large scales, have long wavelengths and are caused by space configuration. (ii) Microinstabilities are usually dominant on small scales, have large wavenumbers and are driven by distortions in velocity phase space [6–7]. In principle, while kinetic and magnetohydrodynamics theories are both suitable for studying macroinstabilities, for microinstabilities only the kinetic theory is applicable.

Scalar and vector potentials are quantities of which an initial perturbation can lead to the generation of oscillations, longitudinal electric waves, or electromagnetic waves. This creates another two categories of plasma instabilities. (i) Electrostatic, where only perturbation of scalar potential plays an important role and there are no perturbations of magnetic fields. In this regime only longitudinal electric waves are present. (ii) Electromagnetic, where we cannot neglect magnetic field perturbations and we must be careful with using the Poisson equation, because for high frequency electromagnetic instabilities this equation is not applicable and one should use the d'Alembert equation for potentials [6–7].

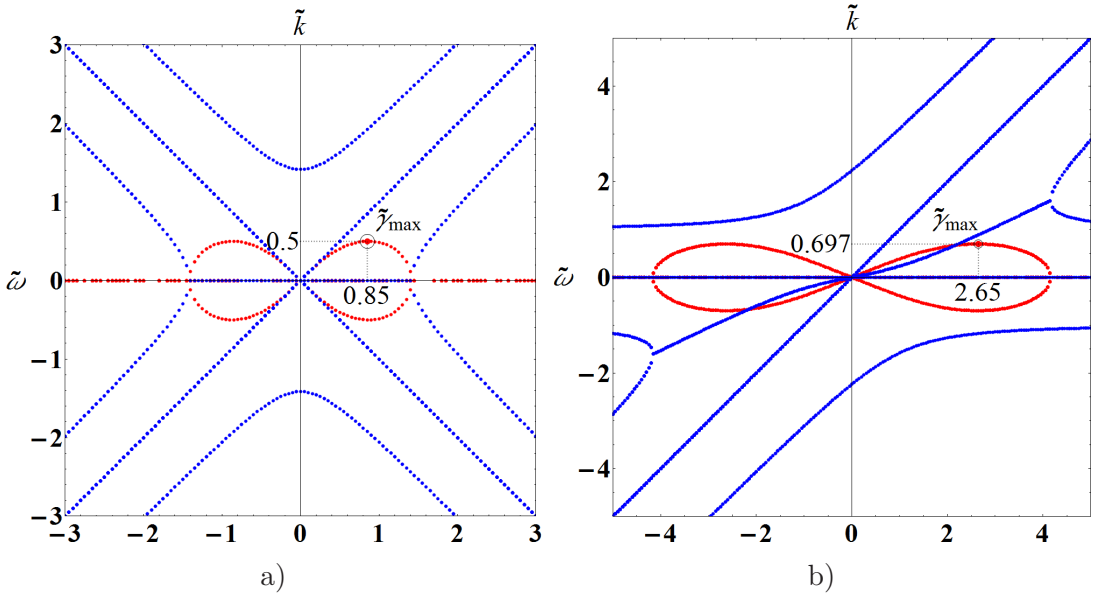

Figure 2.4. Roots of dispersion relation for Buneman instability. Blue dots represent real roots, while red dots stand for imaginary roots. Source: Author

Plasma instabilities are intensively studied both analytically (e.g. [15–17]) and numerically (e.g. [18–20]). General knowledge about plasma instabilities can be obtained from [6–8]. In next part we show typical examples of both electrostatic macro- and micro- instabilities.

2.4.1 Examples

One of the most commonly studied macroinstabilities is the Buneman instability [21] sometimes called the two-stream instability. This instability originates when two plasma beams have different velocities and flow through each other. For its derivation, the boundaries, magnetic field, and plasma temperature are neglected. For the case with two identical opposite beams the dispersion relation is

$$\sum_{\alpha} \frac{\omega_{\mathrm{p}\alpha}^2}{(\omega - \mathbf{k}\cdot\mathbf{u}_\alpha)^2} = 1, \tag{2.20}$$

where we denote plasma frequency as $\omega_{\mathrm{p}\alpha}^2 = n_{0\alpha}Q_\alpha^2/m_\alpha\varepsilon_0$. The dispersion relation (2.20) is a biquadratic equation which is analytically solvable. The dimensionless solution for two identical opposite beams is

$$\tilde{\omega}^2 = 1 + \tilde{k}^2 \pm \sqrt{1 + 4\tilde{k}^2}, \tag{2.21}$$

where $\tilde{\omega} = \omega/\omega_{\mathrm{p}}$, and $\tilde{k} = u_0 k/\omega_{\mathrm{p}}$ are dimensionless quantities. Then the solution is in the form $\tilde{\omega} = \tilde{\omega}(\tilde{k})$ where $\tilde{\omega} = \tilde{\omega}_{\mathrm{R}} + \mathrm{i}\tilde{\gamma}$. The numerical solution of this relation is depicted in Fig. 2.4 a), where blue dots represent real roots and red dots are for imaginary roots. From the analytical solution it is known that instbaility growth $\tilde{\gamma}$ reaches its maximum at $\tilde{k} = \sqrt{3}/2$ and has value $\tilde{\gamma} = 1/2$. The difference between analytical solution and numerical solution is caused by discretization of the $\tilde{k}$ axis. Sometimes the Buneman instability is described as an instability caused by electron jet flowing through an ion stationary background [2]. One solution of such a situation is depicted in Fig. 2.4 b). For simplicity, the artificial very small mass ratio between ions and electrons was used ($m_{\mathrm{i}}/m_{\mathrm{e}} = 4$). It is clearly shown, that maximal value of instability growth reaches its maximum at bigger $\tilde{k}$ and has bigger value.

As an example of microinstability we consider a gentle beam (or bump in tail instability). This instability can occur when a plasma beam interacts with a one component background plasma. The velocity distributions of background and beam are depicted in Fig. 2.5. The second peak in the velocity phase space means that fast particles will add energy to Langmuir waves - this phenomenon is called inversed Landau damping [8].

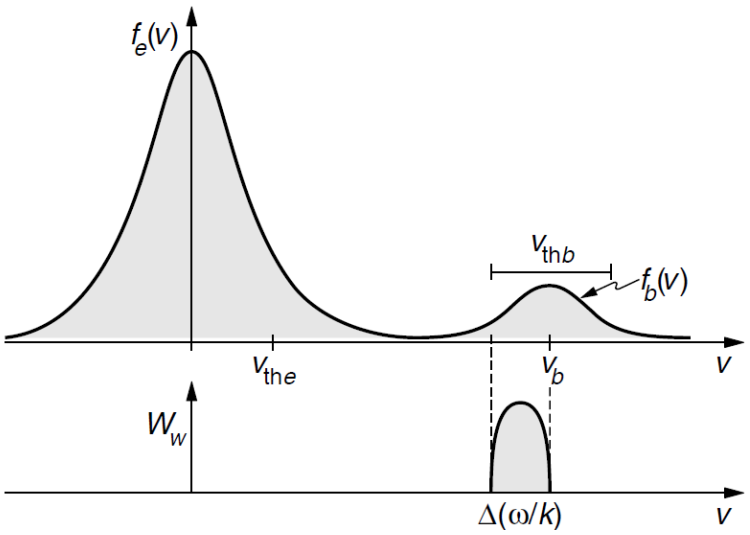

Figure 2.5. Velocity distributions of the beam and background leading to the bump in tail instability. Source: [8]

The condition needed to excite these unstable waves is

$$v_\mathrm{b} = \sqrt{3} v_\mathrm{the}. \tag{2.22}$$

In cases where this threshold is not reached, the fast particles cannot give energy to the wave. The maximal value of the instability growth rate is:

$$\gamma_\mathrm{max} = \sqrt{\frac{\pi}{2q}} \frac{n_\mathrm{b}}{n_0} \left(\frac{v_\mathrm{b}}{v_\mathrm{thb}} \right)^2 \omega_\mathrm{L}, \tag{2.23}$$

where ω_L is frequency of Langmuir waves, v_thb is thermal beam velocity, v_b. The position of these velocities in the distribution function is shown in Fig. 2.5.

These were two typical examples of plasma instabilities. Plasma instabilities can cause a lot of side effects such as turbulences, heating, magnetic reconnections, etc. These effects might be favourable or unwanted in many plasma applications. For instance in wakefield accelerators the Landau damping [5] accelerates charged particles which we can imagine as a particle "surfing" on a wave. Plasma instabilities are also a subject of studies on the Solar chromosphere heating [22]. Many studies were done on controlling and avoiding instabilities in fusion devices like tokamaks or Z-pinches [23–24].

Chapter 3
Numerical simulations

With the rapid growth of computational power in the last decades, numerical simulations have become more important in all fields of physics and nowadays are as important as theory and experiments. Numerical simulations allow us to study highly nonlinear phenomena such as instabilities, turbulences, and other nonlinear phenomena.

3.1 Essentials of numerical simulations

Since computers cannot solve derivatives analytically, the basic principle of numerical simulations is to convert differential equations (both ordinary and partial differential equations) to difference equations by discretization. Then the discretized physical problem can be solved by a computer with an accuracy given by the method of discretization and size of discrete steps. The way how to discretize an equation is given by the numerical method (sometimes called numerical scheme). Basic numerical schemes are difference schemes which we can divide into two main groups: (i) explicit, and (ii) implicit schemes. The difference between them is in the expression for the right hand side of the discretized equation and while the explicit schemes are easier to solve, the implicit schemes are more accurate. All schemes have three main parameters:

- stability - which determines the ability of a numerical scheme to damp numerical errors,
- convergence - which tells us that the scheme will reach an analytical solution, and
- order - which reflects how well the analytical solution is approximated.

Details on the theory of numerical methods can be obtained from [25]. In principle for physical numerical simulations we cannot use nonconvergent numerical method as well as an unstable method or a method with low order. In the following subsections numerical schemes for ordinary differential and partial differential equations are introduced.

3.1.1 Numerical solution of ordinary differential equations

The simplest method to solve ordinary differential equations numerically is forward Euler method. It is a convergent explicit method but its stability depends on the approximated physical problem. For instance using this method for calculating trajectory of plasma particles in a constant magnetic field will result in a linearly increasing gyroradius [1]. Let us show the principle of this method on the 1D nonrelativistic momentum equation.

The equation of motion $m(\mathrm{d}^2x/\mathrm{d}t^2) = F(t, x, v)$ can be split into two differential equations of first order

$$\frac{\mathrm{d}x}{\mathrm{d}t} = v(t), \tag{3.1}$$

$$\frac{\mathrm{d}v}{\mathrm{d}t} = \frac{F(t, x, v)}{m}. \tag{3.2}$$

After discretization of these equations we get

$$x_{n+1} \approx x_n + v_n \Delta t, \tag{3.3}$$

$$v_{n+1} \approx v_n + F(t_n, x_n, v_n)\Delta t, \tag{3.4}$$

where Δt denotes timestep and index n stands for discrete times. A numerical solution of plasma particle motion in a constant magnetic field is depicted in Fig. 3.1 (a). The figure illustrates how the error of calculation increases in each timestep.

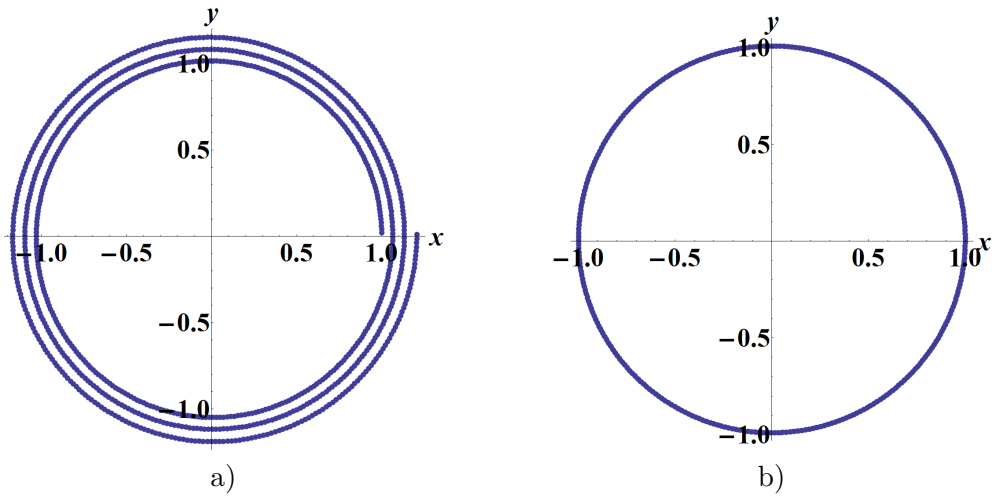

Figure 3.1. Comparison between forward Euler and Boris-Buneman algorithm used for solving the motion of a charged particle in stationary magnetic field. The result from forward Euler algorith is depicted in the left panel (a) and result from Boris-Buneman is depicted in the right panel (b). The difference in stability is clearly visible. Source: Author

Due to this issue, the forward Euler method is not good choice for plasma simulations. It is better to use a different, more accurate method. One of the methods developed mainly for plasma simulations is Boris-Buneman algorithm [1, 26] which is second order numerical scheme. This method is based on following principle. In the first step of the algorithm, the first half of acceleration due to the electric field is calculated. The second step is the calculation of rotation due to a magnetic field and the last step is the calculation of the second half of the acceleration. Let us show this scheme for the Lorentz equation. The initial set of equations is similar to the set used above

$$\frac{\mathrm{d}\mathbf{x}}{\mathrm{d}t} = \mathbf{v}, \tag{3.5}$$

$$\frac{\mathrm{d}\mathbf{v}}{\mathrm{d}t} = \frac{Q}{m}(\mathbf{E} + \mathbf{v} \times \mathbf{B}). \tag{3.6}$$

Then the consequent steps for calculation are

$$\widetilde{\mathbf{E}} = \frac{Q\Delta t}{2m}\mathbf{E} \text{ and } \widetilde{\mathbf{B}} = \frac{Q\Delta t}{2m}\mathbf{B}, \tag{3.7}$$

$$\widetilde{\mathbf{v}} = \mathbf{v}_n + \widetilde{\mathbf{E}}, \tag{3.8}$$

$$\widetilde{\widetilde{\mathbf{v}}} = \widetilde{\mathbf{v}} + 2\frac{\left(\widetilde{\mathbf{v}} + \widetilde{\mathbf{v}} \times \widetilde{\mathbf{B}}\right) \times \widetilde{\mathbf{B}}}{1 + \widetilde{\mathbf{B}}^2}, \tag{3.9}$$

$$\mathbf{v}_{n+1} = \widetilde{\widetilde{\mathbf{v}}} + \widetilde{\mathbf{E}}, \tag{3.10}$$

$$\mathbf{x}_{n+1} = \mathbf{x}_n + \mathbf{v}_{n+1}\Delta t. \tag{3.11}$$

In comparison with forward Euler method, the Boris-Buneman algorithm provides a stable solution. Fig. 3.1 shows the trajecotry for electron motion in a constant magnetic field after three gyroperiods. While in the solution of forward Euler (Fig 3.1 (a)) we see increasing Larmor radius in each step of the calculation, the trajectory calculated by the Boris-Buneman algorithm is stable and circular, in acordance with the analytical solution.

There are other methods which can be used in plasma physics simulations, for example Leap-Frog, Runge-Kutta 4$^{\text{th}}$ order etc., and more information about them can be obtained from additional literature (i. e. [1, 25–27]).

3.1.2 Numerical solution of partial differential equations

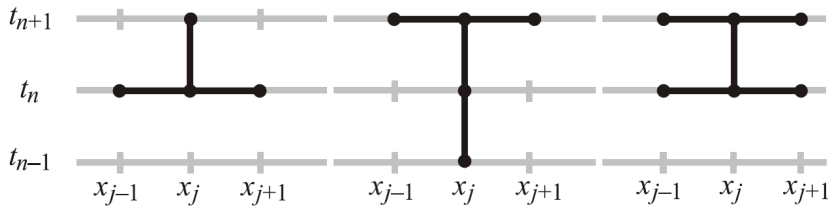

Figure 3.2. Illustration of space time discretization. Different types of numerical schemes are depicted. The left panel shows the explicit scheme while the middle and right panels show the implicit schemes. Source: [1]

In the case of partial differential equations, the situation is more complicated due to the need for discretization of both space and time, which is illustrated in Fig. 3.2. In this part we use index n to denote discrete times and index j to denote discrete step coordinates (for understandability we assume only 1D examples). The most convenient and simplest methods are finite difference methods (others are finite volume method and finite element method, which are not subject of this text). One of the simplest finite difference algorithm is the Du Fort-Frankel scheme [1]. Let us assume 1D diffusion equation

$$\frac{\partial \xi}{\partial t} = \eta \frac{\partial^2 \xi}{x^2}, \tag{3.12}$$

which can be discretized to obtain the implicit scheme

$$\frac{\xi_j^{n+1} - \xi_j^{n-1}}{2\Delta t} = \eta \frac{\xi_{j-1}^n - \left(\xi_j^n + \xi_j^{n+1}\right) + \xi_{j+1}^n}{(\Delta x)^2}, \tag{3.13}$$

which is totally stable and leads to the solution

$$\xi_j^{n+1} = \left(\frac{1-K}{1+K}\right)\xi_j^{n-1} + \left(\frac{K}{1+K}\right)\xi_{j-1}^n + \left(\frac{K}{1+K}\right)\xi_{j+1}^n; \quad K = \frac{2\eta\Delta t}{(\Delta x)^2}. \tag{3.14}$$

In plasma simulations we need to solve the Poisson equation for potentials, which is not as simple as the diffusion equation, thus different numerical methods are used. The most often used methods are multigrid method [28] and DFFT (Discrete Fast Fourier Transform) method [1, 26–27]. Numerical methods for both ordinary and partial differential equations are needed for plasma simulations.

3.2 Particle In Cell simulations

Particle In Cell (PIC) simulations represent a hybrid algorithm based on calculations of particle trajectories, while the fields are treated as continuum variables calculated at grid points only. The simulations are based on two main principles, (i) particles do not interact with each other directly but via grid points, (ii) each simulated particle represents a cloud of real particles. This method decreases computational cost from N^2 to $N \log N$ where N is number of simulated particles.

3.2.1 Principle of the algorithm

The PIC simulation algorithm consists of these steps:

1. Initialization: Particle generation according to statistical distribution, normalization of selected quantities, initial field calculations, etc.
2. Particle weighting: In this step the charge and current density from each particle is distributed to all surrounding gridpoints. The simplest type is binary weighting which assigns the whole charge/current density to the nearest gridpoint. However, it is only a rough approximation. The most usual weighting is linear weighting, of which the principle is illustrated in Fig. 3.3 (left panel). The amount of charge density distributed to each gridpoint is given by the surface of the opposite rectangle. In the case of 3D simulations it is given by the volume of the opposite prism. Quadratic, cubic, and other higher order weightings are more accurate, but they increase computational cost.
3. Poisson solver: The Poisson equation for potentials is solved for each gridpoint. The most usual methods for Poisson solver are finite difference, multigrid and DFFT methods [1, 26–28].
4. Field integrator: Electric and magnetic fields in each gridpoints are calculated from potentials. In this step an arbitrary stable convergent numerical method can be used. Usually, a finite difference method is used.
5. Fields weighting: Fields from gridpoints are redistributed to the position of each particle. The weighting of the fields should be of the same order as the weighting of particles [1]. Linear weighting is illustrated in Fig. 3.3 (right panel).
6. Particle integrator: Calculates movement of each particle according to Lorentz equation (3.6). The most widely used integrators are Leap-Frog, Boris-Buneman, Runge Kutta 4^{th} order, etc. [1, 26–27].
7. Return to point 2 until the final time is reached.

For successful numerical experiments, one should add diagnostic procedures to the appropriate place in the cycle which means saving selected datasets to output files. The basic data that are saved are information about $\mathbf{x}$–$\mathbf{v}$ phase space of simulated particles, values of potentials on gridpoints and distribution of particle density. These diagnostic routines can slow down the simulation, thus a compromise between the amount of diagnostic data and computational speed must be evaluated for each simulated problem.

Since the electrostatic collisions between simulated particles are provided through the potential distributed on a grid (so-called mean field approximation), we cannot simulate fully collisionless plasmas [1, 26]. For such simulations the Vlasov codes (i. e. [29]) are more appropriate. On the other hand, collisions provided by grid are only electrostatic and are affected by weighting, thus do not perfectly reflect the behaviour of real collisions. If we need realistic collisions or to simulate different types of collisions, a Monte Carlo collisional algorithm ([30–31]) must be implemented in the PIC code.

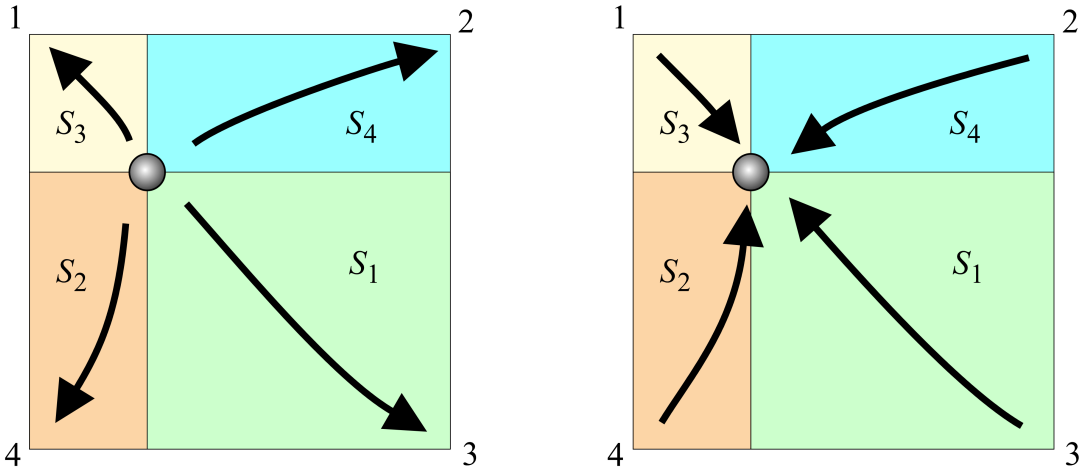

Figure 3.3. Illustration of the 1st order particle and fields weighting. Source: [1]

3.2.2 Stability and accuracy of algorithm

As it was shown, a PIC algorithm is a complex of different solvers (for both ordinary and partial differential equations) and thus assesing the numerical stability and accuracy of the whole simulation is much more complicated than in the case of separate usage of each solver. As in the separate solvers, the stability is given by size of spatial and temporal steps. It was derived ([26] and references therein) that for space discretization the resolution of Debye length is the most crucial parameter. Thus the condition for stability is $\lambda_D/\Delta x > 1$. Similarly, the timestep must be smaller than the period of plasma waves. Since in magnetized plasmas the smallest scales are not given by plasma frequency and Debye length, the effect of resolution of electron gyroradius [32] and gyroperiod [33] was also studied. The result is that resolution of these scales is not crucial for simulation stability.

Another important parameter for the result's accuracy is the number of particle per cell. The numerical noise in the potential as the function of number of particles per cell scales with $1/\sqrt{N}$. The high noise level due to this issue causes artificial fluctuations of the electric field which can cause self-heating and thermalisation of plasma particles. The numerical thermalisation due to the finite number of particles is the subject of recent studies such as [34–35].

Despite these issues, PIC codes are very useful for the numerical study of plasmas. There have been plenty of studies carried out using PIC method, for instance studies of ionospheric and space plasmas (i. e. [36–38]) or laboratory plasmas (i. e. [39–40]) and many others. PIC simulations are nowadays one of the most widely used numerical tools in plasma physics.

Chapter 4
Collection of Papers

Overview of research

Research described in the papers in this dissertation covers two main subjects. Firstly, in the beginning of my PhD study I worked on a numerical solution of the dispersion relation for a two-stream instability generalized for an arbitrary magnetic field and thermal plasma. This dispersion relation was previously derived at our university [41]. My first task was to implement an algorithm for the numerical solution of a polynomial equation of 8^{th} order [42]. The method developed by Hubbard et al. [43] was implemented in Wolfram Mathematica and used to find the solution. Then this algorithm was applied to calculate the solution of the dispersion relation corresponding to a one stream interaction with stationary background, which is quite often situation in astrophysical plasmas. A solution was found for different magnitudes of the input parameters such as plasma frequency, sound speed and cyclotron frequency (Paper I [44]). The first part of my dissertation research on dispersion relation for two-stream instabilities was concluded with solution analysis and parametric study of dependence of maximal value of instability growth rate (Paper II [45]).

The second part of my doctoral research was focused on numerical simulations of weakly collisional plasmas in $\mathbf{E} \times \mathbf{B}$ fields. This part was done in collaboration with Dr. Miloch from the University of Oslo (UiO) where I spent 142 days in total divided into three stays. For simulations we used parallelized electrostatic PIC code with collisions of plasma particles with neutral particles developed at the UiO. The code was running on the Norwegian cluster ABEL. We used two types of ion-neutral collisions (elastic and charge exchange), and the collisionless case as the reference. To analyze the results of simulations I implemented several diagnostics procedures in Wolfram Mathematica such as routines for the plotting temporal evolution of potential density, potential fluctuations, particle temperatures and so on. Beside these routines we also used previously established diagnostic procedures. Preliminary results of our simulations were presented at the 31st URSI-GASS conference (Paper III [46]) and 15th LAWPP conference (Paper IV [47]). Beside physical instabilities numerical instabilities were also identified in the preliminary results. Thus the next step was eliminating the numerical instabilities from our simulations resulting in a study of stability of weakly collisional plasmas (Paper V [48]). The numerical instabilities will be the subject of future research.

4.1 Paper I

Title: Instability Growth Rate Dependence on Input Parameters During the Beam-Target Plasma Interaction
Journal: Acta Polytechnica

This paper was submitted to the 25^{th} Symposium on Plasma Physics and Technology (2012) and covers a numerical solution of the generalized Buneman dispersion relation [41] for a problem of a plasma jet interaction with a stationary background. The main part of the paper is focused on the evolution of instability growth rate with change of several input parameters (cyclotron frequencies and sound speeds). This paper was published in a topical issue of the journal Acta Polytechnica (indexed in Scopus).
Author's contribution:

- Scientific contribution: 100 %.
- Text contribution: 100 %.

Acta Polytechnica **53**(2):174–178, 2013

© Czech Technical University in Prague, 2013
available online at `http://ctn.cvut.cz/ap/`

INSTABILITY GROWTH RATE DEPENDENCE ON INPUT PARAMETERS DURING THE BEAM–TARGET PLASMA INTERACTION

Miroslav Horký*

Department of Physics, Faculty of Electrical Engineering, Czech Technical University in Prague, Czech Republic
* corresponding author: `horkymi1@fel.cvut.cz`

Abstract. The two-stream instability without magnetic field is described by the well-known Buneman dispersion relation. For more complicated situations we need to use the Generalized Buneman Dispersion Relation derived by Kulhánek, Břeň, and Bohata in 2011, which is a polynomial equation of 8^{th} order. The maximal value of the imaginary part of the individual dispersion branches $\omega_n(k)$ is very interesting from the physical point of view. It represents the instability growth rate which is responsible for the turbulence mode onset and subsequent reconnection on the ion radius scale accompanied by strong plasma thermalization. The paper presented here is focused on the instability growth rate dependence on various input parameters, such as magnitude of a magnetic field and sound velocity. The results are presented in well-arranged plots and can be used for a survey of the plasma parameters close to which the strong energy transfer and thermalization between the beam and the target occurs.

Keywords: Buneman instability, numerical simulations, plasma, dispersion relation.

1. Introduction

Two-stream instabilities are the most common instabilities in plasmas which originate on the microscopic scale and which can develop to macroscopic phenomena like a thermal radiaton from strong thermalization or non-thermal radiaton from reconnections. If we consider that both streams have parallel direction of their velocities, we talk about Buneman instability [1] and if we consider intersecting directions of velocities and anisotropy of temperatures, we talk about Weibel instability [8]. The dispersion relation for two-stream instability without magnetic field in cold plasma is described by the relation

$$\sum_{\alpha=1}^{2} \frac{\omega_{\mathrm{p}\alpha}}{\left(\omega - \mathbf{k}\cdot\mathbf{u}_{0\alpha}\right)^2} = 1, \tag{1}$$

where ω is the wave frequency, $\omega_{\mathrm{p}\alpha}$ is the plasma frequency of the first and second stream respectively, $\mathbf{k}$ is the wave vector, and $\mathbf{u}_{0\alpha}$ is the vector of the velocity for the first and the second stream respectively.

The most simple situation, in which we can use this relation, is the interaction of two identical streams moving in opposite directions. Equation 1 has simple one dimensional form [4]

$$\frac{\omega_{\mathrm{p}}^2}{(\omega - ku_0)^2} + \frac{\omega_{\mathrm{p}}^2}{(\omega + ku_0)^2} = 1. \tag{2}$$

The two-stream instabilities are usually used for the study of the origin of the observed macroscopic phenomena (e.g. particle acceleration in relativistic plasma shocks [6]). This paper is focused on the general study of the plasma jet interaction on the microscopic scale (not only on the study of one particular phenomenon origin) and for this case the general dispersion relation is needed. Two generalizations of the two-stream instability dispersion relation were done in last years, first was done by Kulhánek, Břeň and Bohata [5] in 2011 and second was done by Pokhotelov and Balikhin [7] in 2012. In this paper we do all the calculations from [5], because the generalization is more rigorous and precise. The authors called it Generalized Buneman Dispersion Relation (GBDR) and it is described by equation

$$\begin{aligned}\prod_{\alpha=1}^{2}\Bigg\{ \Omega_\alpha^4 - \Omega_\alpha^2\left[\mathrm{i}\frac{\mathbf{F}_\alpha^{(0)}\cdot\mathbf{k}}{m_\alpha} + c_{\mathrm{s}\alpha}^2k^2 + \omega_{\mathrm{p}\alpha}^2 + \omega_{\mathrm{c}\alpha}^2\right] \\ - \frac{\Omega_\alpha\omega_{\mathrm{c}\alpha}}{m_\alpha}\left(\mathbf{F}_\alpha^{(0)}\times\mathbf{k}\right)\cdot\mathbf{e}_{\mathrm{B}} \\ + \omega_{\mathrm{c}\alpha}^2(\mathbf{k}\cdot\mathbf{e}_{\mathrm{B}})\left[\mathrm{i}\frac{\mathbf{F}_\alpha^{(0)}\cdot\mathbf{e}_{\mathrm{B}}}{m_\alpha} + \left(c_{\mathrm{s}\alpha}^2k^2 + \omega_{\mathrm{p}\alpha}^2\right)\frac{\mathbf{k}\cdot\mathbf{e}_{\mathrm{B}}}{k^2}\right]\Bigg\} \\ - \prod_{\alpha=1}^{2}\frac{\omega_{\mathrm{p}\alpha}^2}{k^2}\left[\Omega_\alpha^2k^2 - \omega_{\mathrm{c}\alpha}^2\left(\mathbf{e}_{\mathrm{B}}\cdot\mathbf{k}\right)^2\right] = 0,\end{aligned} \tag{3}$$

where

$$\Omega_\alpha = \omega - \mathbf{k}\cdot\mathbf{u}_\alpha^{(0)}, \tag{4}$$

$\omega_{\mathrm{c}\alpha}$ is the cyclotron frequency, $\mathbf{F}_\alpha^{(0)}$ is the Lorentz magnetic force, $\mathbf{e}_{\mathrm{B}}$ is the unit vector in the direction of magnetic field and $c_{\mathrm{s}\alpha}$ is the sound velocity. For $\mathbf{B} = 0$ and cold plasma limit $c_{\mathrm{s}\alpha} = 0$, the generalized relation becomes the Eq. 1.

For its analysis it is useful to convert this relation to a non-dimensional form to ensure the scale invariance of the results. The system of coordinates used in the solution is in Fig. 1.

The directions of the vectors $\mathbf{u}_\alpha$, $\mathbf{B}$ and $\mathbf{k}$ are presented in Fig. 1 in the case of our coordinates system. The wavevector can have any direction, the magnetic field is only in the (x–z) plane and the velocity vectors of the streams are only along the x-axis. These vectors have coordinates

$$\begin{aligned}\mathbf{u}_\alpha &= (u_\alpha, 0, 0),\\ \mathbf{B} &= (B\sin\theta_\mathrm{B}, 0, B\cos\theta_\mathrm{B}),\\ \mathbf{k} &= (k\cos\varphi\sin\theta_\mathrm{k}, k\sin\varphi\sin\theta_\mathrm{k}, k\cos\theta_\mathrm{k}).\end{aligned}$$

1.1. The non-dimensional form

Non-dimensional variables are defined by relations [2]

$$\begin{aligned}\overline{c}_{\mathrm{s}1} &\equiv \frac{c_{\mathrm{s}1}}{u_1}, \quad & \overline{c}_{\mathrm{s}2} &\equiv \frac{c_{\mathrm{s}2}}{u_1},\\ \overline{\omega}_{\mathrm{c}1} &\equiv \frac{\omega_{\mathrm{c}1}}{\omega_{\mathrm{p}2}}, \quad & \overline{\omega}_{\mathrm{c}2} &\equiv \frac{\omega_{\mathrm{c}2}}{\omega_{\mathrm{p}2}},\\ \overline{\omega}_{\mathrm{p}1} &\equiv \frac{\omega_{\mathrm{p}1}}{\omega_{\mathrm{p}2}}, \quad & \overline{\omega}_{\mathrm{p}2} &\equiv \frac{\omega_{\mathrm{p}2}}{\omega_{\mathrm{p}2}} = 1,\\ \overline{u}_2 &\equiv \frac{u_2}{u_1}, \quad & \overline{u}_1 &\equiv \frac{u_1}{u_1} = 1,\\ \overline{k} &\equiv \frac{k u_1}{\omega_{\mathrm{p}2}}, \quad & \overline{\omega} &\equiv \frac{\omega}{\omega_{\mathrm{p}2}},\end{aligned}$$

where index 1 denotes a jet and index 2 denotes a background. Under these definitions, we can convert Eq. 3 into a non-dimensional form [2] which will be

$$\begin{aligned}&\left[\overline{\Omega}_1^4 + \mathrm{i}\overline{\Omega}_1^2\overline{\omega}_{\mathrm{c}1}\overline{k}(G_1) - \overline{\Omega}_1^2\left(\overline{c}_{\mathrm{s}1}^2\overline{k}^2 + \overline{\omega}_{\mathrm{p}1}^2\right) - \overline{\Omega}_1^2\overline{\omega}_{\mathrm{c}1}^2\right.\\ &\quad\left. - \overline{\Omega}_1\overline{\omega}_{\mathrm{c}1}^2\overline{k}(G_3) + \left(\overline{\omega}_{\mathrm{c}1}^2\overline{k}^2\overline{c}_{\mathrm{s}1}^2 + \overline{\omega}_{\mathrm{c}1}^2\overline{\omega}_{\mathrm{p}1}^2\right)(G_2)^2\right]\\ &\cdot\left[\overline{\Omega}_2^4 + \mathrm{i}\overline{\Omega}_2^2\overline{\omega}_{\mathrm{c}2}\overline{k}\overline{u}_2(G_1) - \overline{\Omega}_2^2\left(\overline{c}_{\mathrm{s}2}^2\overline{k}^2 + 1\right) - \overline{\Omega}_2^2\overline{\omega}_{\mathrm{c}2}^2\right.\\ &\quad\left. - \overline{\Omega}_2\overline{\omega}_{\mathrm{c}2}^2\overline{k}\overline{u}_2(G_3) + \left(\overline{\omega}_{\mathrm{c}2}^2\overline{k}^2\overline{c}_{\mathrm{s}2}^2 + \overline{\omega}_{\mathrm{c}2}^2\right)(G_2)^2\right]\\ &- \left[\overline{\omega}_{\mathrm{p}1}^2\left(\overline{\Omega}_1^2 - \overline{\omega}_{\mathrm{c}1}^2(G_2)^2\right)\right]\cdot\left[\overline{\Omega}_2^2 - \overline{\omega}_{\mathrm{c}2}^2(G_2)^2\right] = 0,\end{aligned} \tag{5}$$

where we denoted

$$\begin{aligned}G_1 &= (\cos\theta_\mathrm{B}\sin\varphi\sin\theta_\mathrm{k}),\\ G_2 &= (\cos\varphi\sin\theta_\mathrm{k}\sin\theta_\mathrm{B} + \cos\theta_\mathrm{k}\cos\theta_\mathrm{B}),\\ G_3 &= (\cos^2\theta_\mathrm{B}\cos\varphi\sin\theta_\mathrm{k} - \cos\theta_\mathrm{B}\cos\theta_\mathrm{k}\sin\theta_\mathrm{B}),\\ \overline{\Omega}_1 &= \overline{\omega} - \overline{k}\cos\varphi\sin\theta_\mathrm{k},\\ \overline{\Omega}_2 &= \overline{\omega} - \overline{k}\overline{u}_2\cos\varphi\sin\theta_\mathrm{k}.\end{aligned}$$

The main goal is to find the solution for the $\overline{\omega}$ dependence on $\overline{k}$. Equation 5 is a polynomial equation of 8^{th} order.

2. Numerical Solution

A classical Newton's algorithm for finding the roots of polynomial equations has one big disadvantage. It does not specify the initial points (points where an algorithm starts the iterations) so it does not guarantee the finding of all the roots. In 2001 Hubbard, Schleicher and Sutherland published the article "*How to Find All Roots of Complex Polynomials With Newton's Method*", where they demonstrated how to determine the initial points to find all the roots of polynomial equation [3].

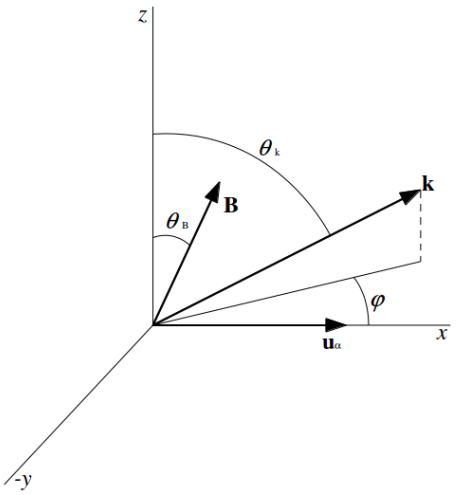

Figure 1. System of coordinates used in the simulations.

2.1. Principle of the algorithm fundamentals

Basic principles are described in [4]. For each $\overline{k}$ we have a polynomial equation of a type

$$\begin{aligned}c_0 + c_1\overline{\omega} + c_2\overline{\omega}^2 + c_3\overline{\omega}^3 + c_4\overline{\omega}^4 + c_5\overline{\omega}^5 + c_6\overline{\omega}^6\\ + c_7\overline{\omega}^7 + c_8\overline{\omega}^8 = 0.\end{aligned} \tag{6}$$

At first we must rescale the polynom, so we have to find

$$A_{\max} = 1 + \max_k\left\{\left|\frac{c_k}{c_N}\right|\right\}. \tag{7}$$

From now we will work with the polynomial

$$Q(z) \equiv \sum_{k=0}^{N}\overline{c}_k z^k, \tag{8}$$

where

$$z \equiv \frac{\overline{\omega}}{A_{\max}}, \qquad \overline{c}_k \equiv c_k A_{\max}^k. \tag{9}$$

The second step is to determine the initial points where the algorithm will start the iterations. The net of initial points is determined by radii and angles in the complex plane:

$$r_l \equiv \left(1+\sqrt{2}\right)\left(\frac{N-1}{N}\right)^{(2l-1)/4L}, \tag{10}$$

$$l = 1, \ldots, L, \tag{11}$$

$$L \equiv \lceil 0.26632\ln N\rceil, \tag{12}$$

$$\xi_m \equiv \frac{2\pi m}{M}, \tag{13}$$
$$m = 0, \ldots, M-1, \tag{14}$$
$$M \equiv \lceil 8.32547 N \ln N \rceil . \tag{15}$$

Then the net of initial points is

$$z_{lm} = r_l \exp(\mathrm{i}\xi_m), \tag{16}$$
$$l = 1, \ldots, L, \tag{17}$$
$$m = 0, \ldots, M-1. \tag{18}$$

The initial net of points has definitely LM numbers. From these numbers the algorithm starts the iterations. A number of iterations O is defined by accuracy ε by the definition

$$O \equiv \left\lceil \frac{\ln(1+\sqrt{2}) - \ln\varepsilon}{\ln N - \ln(N-1)} \right\rceil . \tag{19}$$

The bracket $\lceil x \rceil$ means the ceiling function (first integer number which is higher or equal to x). Solutions which do not accomplish $|Q(z_\mathrm{o}) < \varepsilon|$ are not the roots of the polynomial.

After finding all the roots in the rescaled polynomial we have to do the backscaling

$$\overline{\omega}_\mathrm{o} = A_\mathrm{max} z_\mathrm{o}. \tag{20}$$

2.2. Example of the solution

The first numerical solution was made in [5] for the situation of two identical opposite plasma beams in a magnetic field. This example of dispersion branches is for more complicated situation – one plasma beam penetrates into the plasma background and magnetic field has both perpendicular and parallel components. The parameters of this simulation are in Tab. 1 and graphical result is in Fig. 2.

The result is depicted in well arranged plot where blue dots represent real branches and red dots imaginary branches of the solution. Also maximal value of the imaginary branch which is so called Plasma Instability Growth Rate (PIGR) is depicted with sign "Max".

Parameter	Value
$\overline{\omega}_{\mathrm{c}1} = \overline{\omega}_{\mathrm{c}2}$	0.5
$\overline{c}_{\mathrm{s}1} = \overline{c}_{\mathrm{s}2}$	0.1
$\overline{u}_2$	0
$\overline{\omega}_{\mathrm{p}1}$	1
θ_k	$\pi/2$
φ	0
θ_B	$\pi/4$

Table 1. Parameters used in example of the solution.

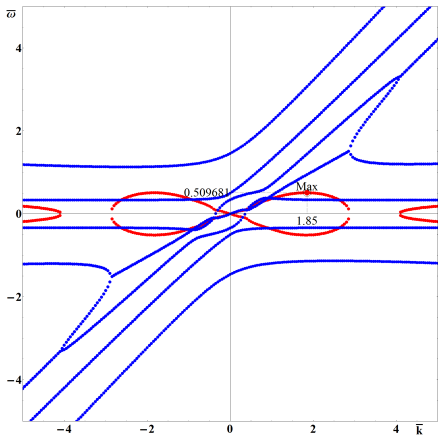

Figure 2. Example of solution of the GBDR with marked maximal value of imaginary part.

3. PIGR dependence on various input parameters

3.1. Dependence on cyclotron frequencies

At first the PIGR dependence on both jet and the background cyclotron frequencies was found.

3.1.1. Results for $\overline{\omega}_{\mathrm{c}1}$

The parameters used in the simulations are presented in Tab. 2 and the results are depicted in Fig. 3. It is obvious that the PIGR grows linearly from the value $\overline{\omega}_{\mathrm{c}1} = 0.6$.

Parameter	Value
$\overline{\omega}_{\mathrm{c}1}$	$\langle 0.5, 3 \rangle$
$\overline{\omega}_{\mathrm{c}2}$	0.5
$\overline{c}_{\mathrm{s}1} = \overline{c}_{\mathrm{s}2}$	0.1
$\overline{u}_2$	0
$\overline{\omega}_{\mathrm{p}1}$	1
θ_k	$\pi/2$
φ	0
θ_B	$\pi/4$

Table 2. Parameters used in the simulations with various parameter $\overline{\omega}_{\mathrm{c}1}$.

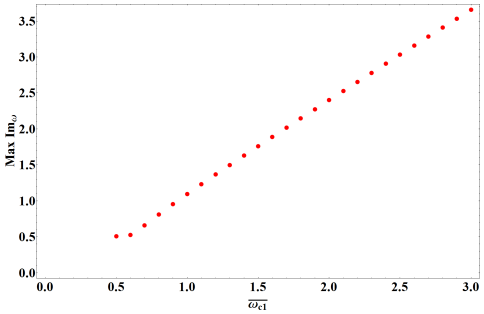

Figure 3. The PIGR dependence on $\overline{\omega}_{\mathrm{c}1}$.

3.1.2. Results for $\overline{\omega}_{c2}$

The parameters used in the simulations are presented in Tab. 3 and the results are shown in Fig. 4.

From these results we can see the local minimum of PIGR which origins due to the bifurcation of the solution. The bifurcation is depicted in three dimensional plot where the first axis is $\overline{k}$, second is $\overline{\omega}$ and third is $\overline{\omega}_{c2}$ (see the Fig. 5).

Parameter	Value
$\overline{\omega}_{c1}$	0.5
$\overline{\omega}_{c2}$	$\langle 0.5, 3\rangle$
$\overline{c}_{s1} = \overline{c}_{s2}$	0.1
$\overline{u}_2$	0
$\overline{\omega}_{p1}$	1
θ_k	$\pi/2$
φ	0
θ_B	$\pi/4$

Table 3. Parameters used in the simulations with various parameter $\overline{\omega}_{c2}$.

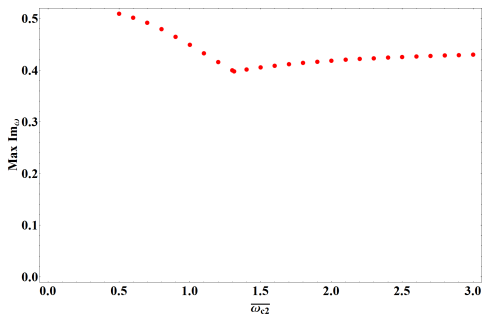

Figure 4. The PIGR dependence on $\overline{\omega}_{c2}$.

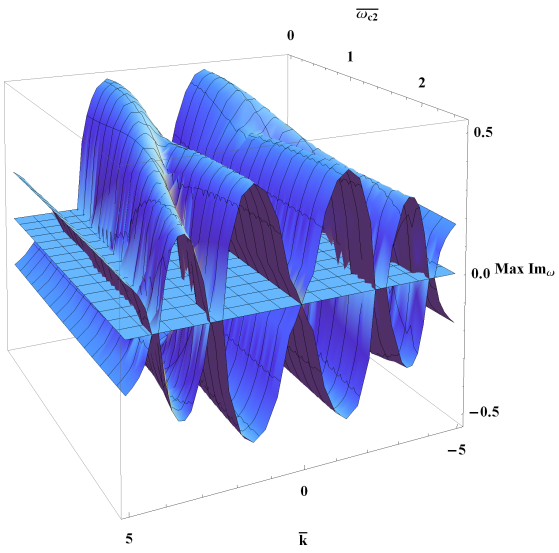

Figure 5. Imaginary part of the solution in three dimensions with an observable bifurcation.

3.2. Dependence on sound velocities

Subsequently the PIGR dependence on both jet and the background sound velocities was found.

3.2.1. Results for $\overline{c}_{s1}$

The parameters used in the simulations are presented in Tab. 4 and the results are depicted in Fig. 6.

Parameter	Value
$\overline{\omega}_{c1}$	0.5
$\overline{\omega}_{c2}$	0.5
$\overline{c}_{s1}$	$\langle 0.1, 2\rangle$
$\overline{c}_{s2}$	0.1
$\overline{u}_2$	0
$\overline{\omega}_{p1}$	1
θ_k	$\pi/2$
φ	0
θ_B	$\pi/4$

Table 4. Parameters used in the simulations with various parameter $\overline{c}_{s1}$.

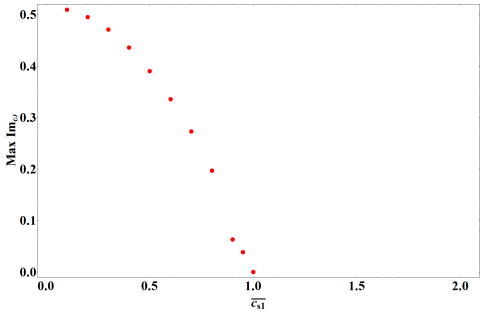

Figure 6. The PIGR dependence on $\overline{c}_{s1}$.

It is obvious that after value $\overline{c}_{s1} = 1$, there is no imaginary branch of the solution, so there are not any instabilities.

3.2.2. Results for $\overline{c}_{s2}$

The parameters used in the simulations are presented in Tab. 5 and the results are depicted in Fig. 7.

Figure 7 presents a similiar bifurcation point like in Fig. 4.

Parameter	Value
$\overline{\omega}_{c1}$	0.5
$\overline{\omega}_{c2}$	0.5
$\overline{c}_{s1}$	0.1
$\overline{c}_{s2}$	$\langle 0.1, 1.5\rangle$
$\overline{u}_2$	0
$\overline{\omega}_{p1}$	1
θ_k	$\pi/2$
φ	0
θ_B	$\pi/4$

Table 5. Parameters used in the simulations with various parameter $\overline{c}_{s2}$.

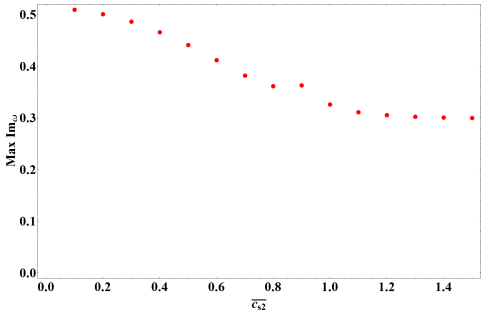

Figure 7. The PIGR dependence on $\overline{c}_{s2}$.

3.3. Results overview

We found the PIGR dependence on four parameters $\overline{\omega}_{c1}$, $\overline{\omega}_{c2}$, $\overline{c}_{s1}$, and $\overline{c}_{s2}$. The main dissimilarity between the dependencies on the cyclotron frequencies is caused by zero velocity of the background. Since the jet has non-zero velocity with a component perpendicular to the magnetic field, the jet particles react to the change of the magnetic field more strongly than the background particles. The dissimilarity between the dependencies on the sound velocities has the same origin. Beause of the non-zero velocity of the jet, the jet could be subsonic and therefore it could be in the state with no instabilities.

4. Conclusions and future work

First of all, the GBDR was converted into a non-dimensional form which ensures the scale invariance of the problem, which means that the results can be used both for the laboratory and astrophysical plasmas. Afterwards the dispersion relation had been solved for the angular frequency via the algorithm suggested by Hubbard, Schleicher, and Sutherland. In every solution branch there were separated real and imaginary parts and subsequently found plasma instability growth rate numerically. Finally, the PIGR dependence on four input parameters $\overline{\omega}_{c1}$, $\overline{\omega}_{c2}$, $\overline{c}_{s1}$ and $\overline{c}_{s2}$ was found. All these numerical calculations were done on microscopic scale and in the linear approximation. These results can be used for lookup of the plasma parameters close to which the strong energy transfer and thermalization between the beam and the target occurs which will be the first part of the future work. Another part will be Particle In Cell simulations of plasma turbulences origin in the vicinity of PIGR maximum.

Acknowledgements

Research described in the paper was supervised by Prof. P. Kulhánek from the FEE CTU in Prague and supported by the CTU grants SGS10/266/OHK3/3T/13, SGS12/181/OHK3/3T/13.

References

[1] O. Buneman. Dissipation of currents in ionized media. *Phys Rev* **115**(3):503–517, 1959.

[2] M. Horky. Numerical solution of the generalized Buneman dispersion relation. In *Proceedings of Poster 2012*. Prague, 2012.

[3] J. Hubbard, D. Schleicher, S. Sutherland. How to find all roots of complex polynomials with Newton's method. *Inventiones Mathematicae* **146**:1–33, 2001.

[4] P. Kulhanek. *Uvod to teorie plazmatu*. AGA, Prague, 1st edn., 2011. (in Czech).

[5] P. Kulhanek, D. Bren, M. Bohata. Generalized Buneman dispersion relation in longitudinally dominated magnetic field. *ISRN Condensed Matter Physics* **2011**, 2011. Article id 896321.

[6] I. Nishikawa, K., P. Hardee, B. Hededal, C., et al. Particle acceleration, magnetic field generation, and emission in relativistic shocks. *Advances in Space Research* **38**:1316–1319, 2006.

[7] A. Pokhotelov, O., A. Balikhin, M. Weibel instability in a plasma with nonzero external magnetic field. *Ann Geophys* **30**:1051–1054, 2012.

[8] E. S. Weibel. Spontaneously growing transverse waves in a plasma due to an anisotropic velocity distribution. *Phys Rev Lett* **2**(3):83–84, 1959.

4.2 Paper II

Title: Analysis of the instability growth rate during the jet-background interaction in a magnetic field
Coauthor: Petr Kulhánek
Journal: Research in Astronomy and Astrophysics

Research described in this paper follows the previous one. The dependencies of plasma instability growth rate was completed by calculating the evolution of the growth rate with the rest of input parameters (plasma frequency and orientation of wave vector and magnetic field) and all the results were analyzed. The paper was submitted to the journal Research in Astronomy and Astrophysics (IF 1.516) in the last quarter of 2012 and was published in June 2013.
Author's contribution:

- Scientific contribution: 50 %.
- Text contribution: 50 %.

Research in Astron. Astrophys. **2013** Vol. **13** No. **6**, 687–694
http://www.raa-journal.org *http://www.iop.org/journals/raa*

***R**esearch in*
***A**stronomy and*
***A**strophysics*

Analysis of the instability growth rate during the jet–background interaction in a magnetic field

Miroslav Horký[1,2] and Petr Kulhánek[1]

[1] Czech Technical University in Prague, Faculty of Electrical Engineering, Department of Physics, Technická 2, 166 27 Prague, Czech Republic; *horkymi1@fel.cvut.cz*
[2] Astronomical Institute of the Academy of Sciences of the Czech Republic, Boční II 1401/1a, 141 31 Prague 4, Czech Republic

Received 2012 October 31; accepted 2013 February 13

Abstract The two-stream instability is common, responsible for many observed phenomena in nature, especially the interaction of jets of various origins with the background plasma (e.g. extragalactic jet interacting with the cosmic background). The dispersion relation that does not consider magnetic fields is described by the well-known Buneman relation. In 2011, Bohata, Břeň and Kulhánek derived the relation for the two-stream instability without the cold limit, with the general orientation of a magnetic field, and arbitrary stream directions. The maximum value of the imaginary part of the individual dispersion branches $\omega_n(k)$ is of interest from a physical point of view. It represents the instability growth rate which is responsible for the onset of turbulence mode and subsequent reconnection on the scale of the ion radius accompanied by a strong plasma thermalization. The paper presented here is focused on the non-relativistic instability growth rate and its dependence on various input parameters, such as magnitude and direction of magnetic field, sound velocity, plasma frequency of the jet and direction of the wave vector during the jet – intergalactic medium interaction. The results are presented in plots and can be used for determination of the plasma parameter values close to which the strong energy transfer and thermalization between the jet and the background plasma occur.

Key words: plasmas — methods: numerical — instabilities — turbulence — waves — MHD

1 INTRODUCTION

The most common plasma instabilities are the two-stream instabilities, which can occur during a plasma jet interaction with the plasma background. Such situations are observed in astrophysical processes, e.g. interaction of galactic jets with the intergalactic medium (e.g. Silk et al. 2012, and references therein) or interaction of star jets with the interstellar medium (Murphy et al. 2008). Oscar Buneman derived the basic dispersion relation describing such instabilities in the late 1950s for cold unmagnetized plasmas (Buneman 1959). The magnetohydrodynamic instabilities in an ideal plasma are discussed in Bonanno & Urpin (2011). Magnetic fields are crucial for the phenomena taking place in jets (Urpin 2006). In 2011, Bohata et al. published a paper containing the derivation of the non-relativistic dispersion relation for magnetized plasmas without the cold limit restriction (Bohata

et al. 2012). It is called the Generalized Buneman Dispersion Relation (GBDR) and is described by the equation

$$\prod_{\alpha=1}^{2}\left\{\Omega_\alpha^4-\Omega_\alpha^2\left[\mathrm{i}\frac{\boldsymbol{F}_\alpha^{(0)}\cdot\boldsymbol{k}}{m_\alpha}+c_{\mathrm{s}\alpha}^2k^2+\omega_{\mathrm{p}\alpha}^2+\omega_{\mathrm{c}\alpha}^2\right]-\frac{\Omega_\alpha\omega_{\mathrm{c}\alpha}}{m_\alpha}\left(\boldsymbol{F}_\alpha^{(0)}\times\boldsymbol{k}\right)\cdot\boldsymbol{e}_{\mathrm{B}}\right.$$
$$\left.+\ \omega_{\mathrm{c}\alpha}^2(\boldsymbol{k}\cdot\boldsymbol{e}_{\mathrm{B}})\left[\mathrm{i}\frac{\boldsymbol{F}_\alpha^{(0)}\cdot\boldsymbol{e}_{\mathrm{B}}}{m_\alpha}+\left(c_{\mathrm{s}\alpha}^2k^2+\omega_{\mathrm{p}\alpha}^2\right)\frac{\boldsymbol{k}\cdot\boldsymbol{e}_{\mathrm{B}}}{k^2}\right]\right\}-\prod_{\alpha=1}^{2}\frac{\omega_{\mathrm{p}\alpha}^2}{k^2}\left[\Omega_\alpha^2k^2-\omega_{\mathrm{c}\alpha}^2\left(\boldsymbol{e}_{\mathrm{B}}\cdot\boldsymbol{k}\right)^2\right]=0, \tag{1}$$

where $\Omega_\alpha=\omega-\boldsymbol{k}\cdot\boldsymbol{u}_\alpha^{(0)}$ is the Doppler shifted frequency, $\omega_{\mathrm{c}\alpha}$ is the cyclotron frequency, $\omega_{\mathrm{p}\alpha}$ is the plasma frequency, $\boldsymbol{F}_\alpha^{(0)}$ is the Lorentz force, $\boldsymbol{e}_{\mathrm{B}}$ is the unit vector in the direction of the magnetic field and $c_{\mathrm{s}\alpha}$ is the sound velocity. Index α denotes the corresponding media (jet or background).

In the previous work of Bohata et al. (2012), the numerical solution for the case of two identical plasma beams with the same velocities, but opposite directions, was found for various input parameters. The situation of the plasma jet interaction with the plasma background was studied as well and the numerical solution for this problem was found by Horký (2012, 2013).

The maximum of the imaginary part of the solution is denoted as the Plasma Instability Growth Rate (PIGR). This paper is focused on finding the plasma parameters for which this maximum occurs (the non-relativistic case and the plasma jet interaction with the plasma background are assumed). The calculations are performed on a microscopic level using the linear approximation. For the plasma parameters leading to the maximum of the imaginary part of the dispersion relation, the instability arises and amplitudes of all variables grow exponentially. In such a situation, the linear approximation is no longer valid, and other methods for modeling of the physical phenomena must be introduced. One of the possibilities is the Particle in Cell (PIC) simulation (e.g. Stockem et al. 2008). The results of these calculations can therefore be applied to: 1) The search for the instability regimes in which strong thermalization, turbulence, micro-reconnections on ion radius, non-thermal radiation, shock onset and other interesting phenomena can occur. The subsequent PIC simulations of the plasma behavior leading to significant phenomena seem to be the most reasonable next step for research in this regime. 2) The tests for the acceptance of the PIC codes (the PIC code must lead to an onset of instability for the parameters calculated by the method proposed in the next paragraph). Section 2 gives a short description of the algorithm used for calculation of complex roots of the GBDR relation. Section 3 discusses PIGR value dependences on various input parameters and geometrical situations.

2 METHOD

The following indices were designated in our analysis: “j” for parameters of the jet and “b” for parameters of the background. It is beneficial to transform the variables and the whole GBDR relation to a dimensionless form. After this step the relation is simply scalable and the equations are covariant in this transformation, which implies that the results can be used for both space and laboratory plasmas, such as thermalization in astrophysical jets or in fusion experiments. The relations for the dimensionless form were chosen with regard to the zero background velocity as in Horký (2012, 2013):

$$\begin{gathered}\overline{c}_{\mathrm{sj}}\equiv\frac{c_{\mathrm{sj}}}{u_{\mathrm{j}}}\,,\qquad\overline{c}_{\mathrm{sb}}\equiv\frac{c_{\mathrm{sb}}}{u_{\mathrm{j}}}\,,\quad\overline{\omega}_{\mathrm{cj}}\equiv\frac{\omega_{\mathrm{cj}}}{\omega_{\mathrm{pb}}}\,,\quad\overline{\omega}_{\mathrm{cb}}\equiv\frac{\omega_{\mathrm{cb}}}{\omega_{\mathrm{pb}}}\,,\ \overline{\omega}_{\mathrm{pj}}\equiv\frac{\omega_{\mathrm{pj}}}{\omega_{\mathrm{pb}}}\,,\\ \overline{\omega}_{\mathrm{pb}}\equiv\frac{\omega_{\mathrm{pb}}}{\omega_{\mathrm{pb}}}=1\,,\ \overline{u}_{\mathrm{b}}\equiv\frac{u_{\mathrm{b}}}{u_{\mathrm{j}}}\,,\ \overline{u}_{\mathrm{j}}\equiv\frac{u_{\mathrm{j}}}{u_{\mathrm{j}}}=1\,,\quad\overline{k}\equiv\frac{ku_{\mathrm{j}}}{\omega_{\mathrm{pb}}}\,,\quad\overline{\omega}\equiv\frac{\omega}{\omega_{\mathrm{pb}}}\,,\\ \overline{\Omega}_{\mathrm{j}}=\overline{\omega}-\overline{k}\cos\varphi\sin\theta_{\mathrm{k}}\,,\qquad\overline{\Omega}_{\mathrm{b}}=\overline{\omega}-\overline{k}\overline{u}_2\cos\varphi\sin\theta_{\mathrm{k}}\,.\end{gathered} \tag{2}$$

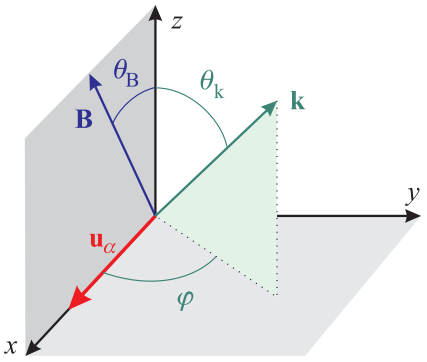

Fig. 1 The system of coordinates used in calculations.

The reference system was set according to Figure 1, in which the directions of the respective vectors $\boldsymbol{u}_\alpha$, $\boldsymbol{B}$ and $\boldsymbol{k}$ are drawn. The wave vector can point in any direction, the magnetic field vector lies in the (x-z) plane and the jet is directed along the x-axis. The vector coordinates are

$$\begin{aligned} \boldsymbol{u}_\alpha &= (u_\alpha, 0, 0)\,, \\ \boldsymbol{B} &= (B\sin\theta_\mathrm{B}, 0, B\cos\theta_\mathrm{B})\,, \\ \boldsymbol{k} &= (k\cos\varphi\sin\theta_\mathrm{k}, k\sin\varphi\sin\theta_\mathrm{k}, k\cos\theta_\mathrm{k})\,. \end{aligned} \tag{3}$$

After simple manipulation, the dimensionless form of the dispersion relation becomes (Horký 2012, 2013)

$$\begin{aligned} &\left[\overline{\Omega}_\mathrm{j}^4 + \mathrm{i}\overline{\Omega}_\mathrm{j}^2\overline{\omega}_\mathrm{cj}\overline{k}(G_1) - \overline{\Omega}_\mathrm{j}^2\left(\overline{c}_\mathrm{sj}^2\overline{k}^2 + \overline{\omega}_\mathrm{pj}^2\right) - \overline{\Omega}_\mathrm{j}^2\overline{\omega}_\mathrm{cj}^2\right. \\ &\quad \left. - \overline{\Omega}_\mathrm{j}\overline{\omega}_\mathrm{cj}^2\overline{k}(G_3) + \left(\overline{\omega}_\mathrm{cj}^2\overline{k}^2\overline{c}_\mathrm{sj}^2 + \overline{\omega}_\mathrm{cj}^2\overline{\omega}_\mathrm{pj}^2\right)(G_2)^2\right] \\ &\cdot \left[\overline{\Omega}_\mathrm{b}^4 + \mathrm{i}\overline{\Omega}_\mathrm{b}^2\overline{\omega}_\mathrm{cb}\overline{k}\overline{u}_\mathrm{b}(G_1) - \overline{\Omega}_\mathrm{b}^2\left(\overline{c}_\mathrm{sb}^2\overline{k}^2 + 1\right) - \overline{\Omega}_\mathrm{b}^2\overline{\omega}_\mathrm{cb}^2\right. \\ &\quad \left. - \overline{\Omega}_\mathrm{b}\overline{\omega}_\mathrm{cb}^2\overline{k}\overline{u}_\mathrm{b}(G_3) + \left(\overline{\omega}_\mathrm{cb}^2\overline{k}^2\overline{c}_\mathrm{sb}^2 + \overline{\omega}_\mathrm{cb}^2\right)(G_2)^2\right] \\ &- \left[\overline{\omega}_\mathrm{pj}^2\left(\overline{\Omega}_\mathrm{j}^2 - \overline{\omega}_\mathrm{cj}^2(G_2)^2\right)\right]\cdot\left[\overline{\Omega}_\mathrm{b}^2 - \overline{\omega}_\mathrm{cb}^2(G_2)^2\right] = 0\,, \end{aligned} \tag{4}$$

where the geometrical terms are denoted as

$$\begin{aligned} G_1 &= (\cos\theta_\mathrm{B}\sin\varphi\sin\theta_\mathrm{k})\,, \\ G_2 &= (\cos\varphi\sin\theta_\mathrm{k}\sin\theta_\mathrm{B} + \cos\theta_\mathrm{k}\cos\theta_\mathrm{B})\,, \\ G_3 &= (\cos^2\theta_\mathrm{B}\cos\varphi\sin\theta_\mathrm{k} - \cos\theta_\mathrm{B}\cos\theta_\mathrm{k}\sin\theta_\mathrm{B})\,. \end{aligned} \tag{5}$$

This dimensionless relation is a polynomial equation with complex roots of the 8^{th} order. The algorithm developed by Hubbard, Shleicher and Sutherland (Hubbard et al. 2001) was used to find the solution. The algorithm was implemented in the Wolfram commercial software package Mathematica 8.0.1. Unlike the Newton-Raphson method, this algorithm can select seed values that later converge to solutions. The results are arranged into plots in which the real branches of the solution have a different style than the imaginary branches, and the maximum imaginary value that determines the PIGR value is highlighted. An example of the program's output is shown in Figure 2.

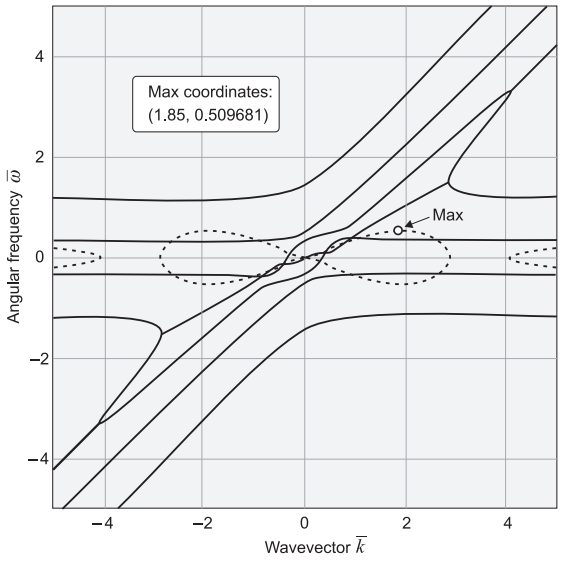

Fig. 2 Real (*solid*) and imaginary (*dashed*) branches of the GBDR dispersion relation and PIGR value (denoted as Max) for $\overline{\omega}_{\mathrm{cj}} = \overline{\omega}_{\mathrm{cb}} = 0.5$, $\overline{c}_{\mathrm{sj}} = \overline{c}_{\mathrm{sb}} = 0.1$, $\overline{\omega}_{\mathrm{pj}} = 1$, $\theta_{\mathrm{k}} = \pi/2$, $\varphi = 0$ and $\theta_{\mathrm{B}} = \pi/4$. These values were used as initial values for the calculations, see Table 1 for details.

In the next step, the dependence of the PIGR value on various parameters of the dimensionless GBDR (such as cyclotron frequencies of the jet and the background, the sound velocities of the jet and the background, the plasma frequency of the jet and the directions of the magnetic field and of the wave vector) is found.

3 RESULTS

The PIGR value was calculated during the program cycle running from the minimum to the maximum value of the tracked parameter while other parameters were fixed at their initial values. Intervals of these parameters are shown in Table 1. It was not necessary to change the jet velocity, because its dimensionless value was fixed at 1.

Table 1 Parameters used for the numerical solution. The dispersion relation for the initial values is depicted in Fig. 1.

Parameter	Initial value	Minimum value	Maximum value
$\overline{\omega}_{\mathrm{cj}}$, $\overline{\omega}_{\mathrm{cb}}$	0.5	0.1	3.0
$\overline{c}_{\mathrm{sj}}$, $\overline{c}_{\mathrm{sb}}$	0.1	0.1	1.5
$\overline{\omega}_{\mathrm{pj}}$	1	1	5
θ_{k}	$\pi/2$	0	$\pi/2$
φ	0	0	$\pi/2$
θ_{B}	$\pi/4$	0	$\pi/2$

3.1 The Dependence of the PIGR Value on the Cyclotron Frequencies

The cyclotron frequency of the jet and the cyclotron frequency of the background were increased from the minimum value of 0.1 to the final value of 3.0 with a step size of 0.1. The cyclotron

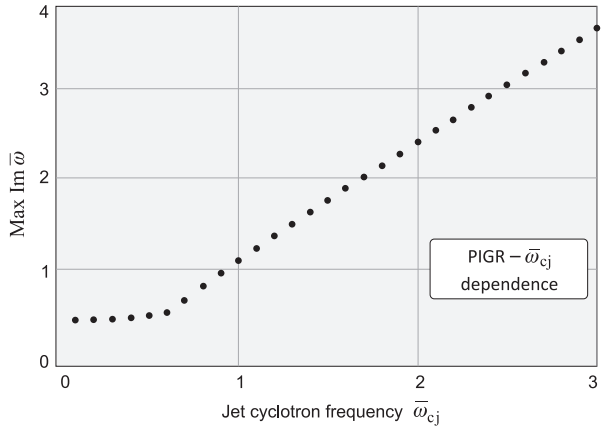

Fig. 3 The dependence of the PIGR value on the jet cyclotron frequency.

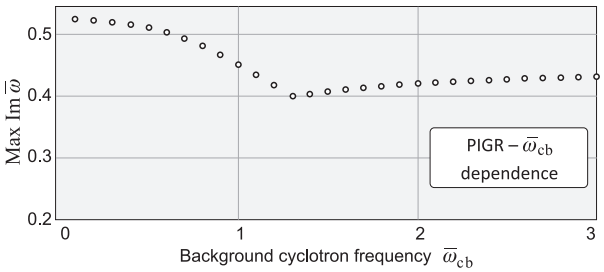

Fig. 4 The dependence of the PIGR value on the background cyclotron frequency.

frequency is proportional to the magnetic field intensity influencing the charged particles. The dependence of the PIGR value on the cyclotron frequency of the jet is depicted in Figure 3, where the almost linear increase of this relation for $\overline{\omega}_{\mathrm{cj}} > 0.6$ is noticeable. The change of the slope at this point ($\overline{\omega}_{\mathrm{cj}} = 0.6$) corresponds to the location of the minimum for the two different imaginary branches of the dispersion relation. The dependence of the PIGR value on the cyclotron frequency of the background is more complicated than the case of jet cyclotron frequency. In Figure 4, the decrease of lower frequency values is visible. The curve reaches a minimum and then it rises to an asymptote. The minimum is numerically determined to be $\overline{\omega}_{\mathrm{cb}} = 1.313$ and the corresponding PIGR value is equal to 0.39795. This effect is caused by the fact that the solution has two imaginary branches in this area and while the value of $\overline{\omega}_{\mathrm{cb}}$ is increasing, the first branch is descending and the second is rising. At the minimum both branches have equal PIGR values.

3.2 The Dependence of PIGR Value on the Sound Velocities

Sound velocity is proportional to $(T_\alpha/m_\alpha)^{1/2}$, where T_α is the plasma temperature, and m_α is the mass of the jet or of the background particles (electrons or ions). The index α labels the corresponding media (jet or background). Modification of the original Buneman dispersion relation by addition of the sound velocities of both media is a result of the calculation with non-zero pressure gradient, i.e. without the cold limit. The dimensionless parameter $\overline{c}_{\mathrm{s}}$ involves the plasma jet velocity, see

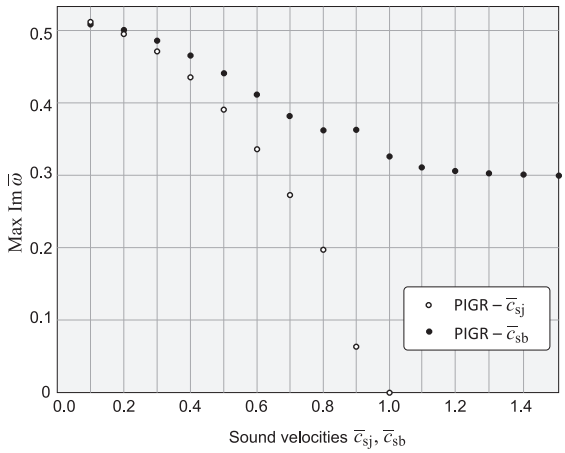

Fig. 5 The dependence of the PIGR value on the sound velocities.

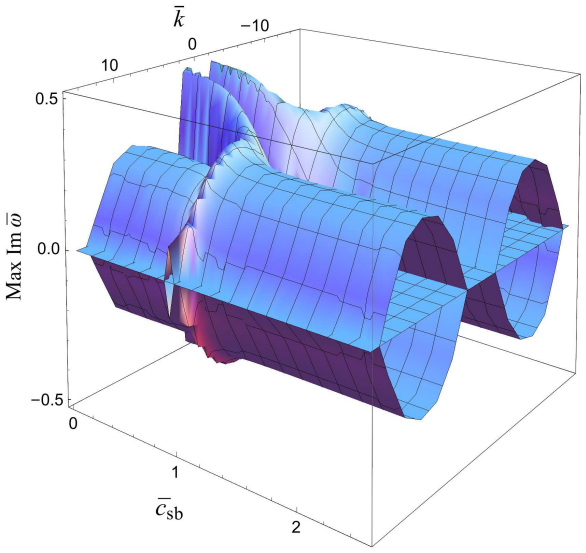

Fig. 6 The dependence of the imaginary branches on $\overline{c}_{\mathrm{sb}}$.

Equation (2), and $\overline{c}_{\mathrm{sj}} > 1$ indicates a subsonic jet while $\overline{c}_{\mathrm{sj}} < 1$ denotes a supersonic one. Both the sound velocity of the jet and the sound velocity of the background were increased from the initial value 0.1 to the final value 1.5 with a step size of 0.1. The dependence of the PIGR value on the sound velocities of both jet and background is depicted in Figure 5. The jet dependence (unfilled circles) shows a decreasing trend and the PIGR value is zero, while $\overline{c}_{\mathrm{sj}} \geq 1$. This implies that for a subsonic jet (in dimensionless form the sound velocity equals 1) the GBDR relation has no imaginary branch and therefore the PIGR value is zero and no instabilities occur. The dependence of the PIGR value on the sound velocity of the background (filled circles) is more complicated. An interesting peak is located at the value $\overline{c}_{\mathrm{sb}} \doteq 0.9$. We made a three-dimensional plot of the imaginary

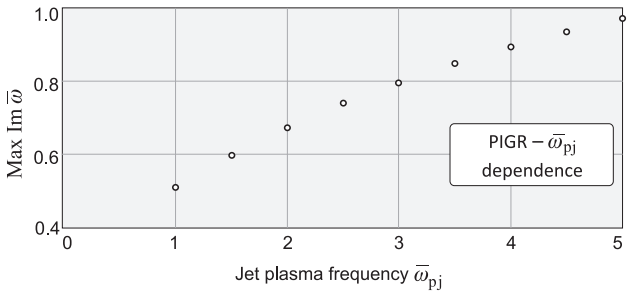

Fig. 7 The dependence of the PIGR value on $\overline{\omega}_{\mathrm{pj}}$.

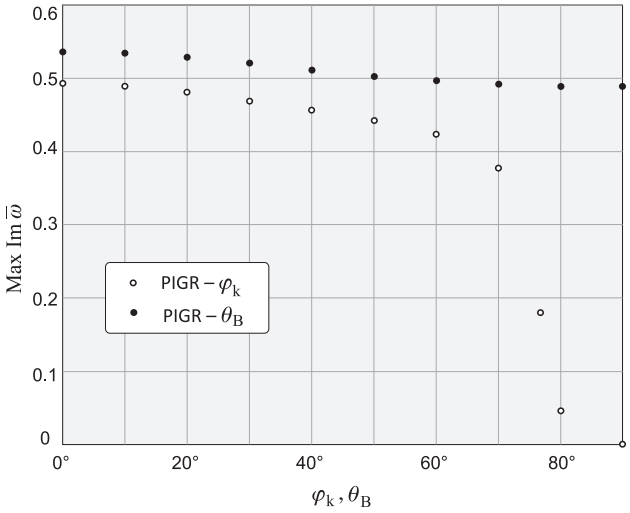

Fig. 8 The dependence of the PIGR value on the magnetic field direction (*filled circles*) and on the wave vector direction (*unfilled circles*).

branches of the GBDR solution to uncover the origin of this local maximum. The result can be seen in Figure 6. The first axis corresponds to $\overline{c}_{\mathrm{sb}}$, the second to $\overline{k}$, and the vertical axis to the value of the imaginary branch of the PIGR coefficient. This clearly shows that the peak originates from the ridge present in the solution of the dispersion relation.

3.3 The Dependence of the PIGR Value on the Plasma Frequency of the Jet

All dimensionless frequencies in the system are related to the background plasma frequency, see Equation (2). This means that the dimensionless plasma frequency of the background $\overline{\omega}_{\mathrm{pb}}$ is always equal to 1, see Equation (2). The dimensionless plasma frequency of the jet $\overline{\omega}_{\mathrm{pj}}$ is in fact the ratio of the jet to the background plasma frequencies. This parameter is therefore proportional to $(n_{\mathrm{ej}}/n_{\mathrm{eb}})^{1/2}$. During the numerical calculation it was increased from the initial value 1 to the final value 5 with a step size of 0.5. It is a rather big step, but as can be seen in Figure 7, the dependence is very simple and does not have any discontinuities or local maxima or minima.

3.4 The Dependencies of the Directional PIGR Value

The dependence of the PIGR value on the magnetic field direction is simply predictable from the Lorentz equation of motion. A longitudinal magnetic field will evoke less disturbances than a perpendicular one. As can be seen in Figure 8, the PIGR value has a maximum at $\theta_{\mathrm{B}} = 0$ (perpendicular direction) and decreases for increasing θ_{B}. The dependence of PIGR value on the direction of the wave vector is also predictable due to the dot product between $\boldsymbol{k}$ and $\boldsymbol{u}_\alpha$ in the GBDR relation, so if the angle between the wave vector and the velocity equals $90°$, the PIGR value should be zero.

In Figure 8, the dependence shows a decreasing trend and it is zero at the angle $90°$. Because of the cylindrical symmetry, both angles φ_{k} and θ_{B} were only varied from $0°$ to $90°$ with a step size of $10°$.

4 CONCLUSIONS

Plasma jets from black holes and other types of astronomical objects are driven by magnetic fields, and classical Buneman instability analysis (without magnetic fields) is inapplicable. All calculations must be performed using the GBDR with nonzero pressure gradient and nonzero magnetic fields. The PIGR as the maximum of the imaginary parts of the GBDR relation was numerically calculated in this paper. The PIGR value is responsible for a strong thermalization during the jet-background interaction and these calculations can be useful for understanding the underlying processes. Furthermore, the known PIGR value can be used as a simple test of PIC numerical methods frequently used for plasma jet simulations. It is an interesting but still an open question as to whether the PIGR value could be analytically directly calculated from the dimensionless GBDR relation. The dispersion relation is not anisotropic in velocity space. This possibility can cause other phenomena, e.g. particle acceleration, shock origin, etc. (Nishikawa et al. 2005; Mizuno et al. 2009, and references therein), which will be the topic of detailed PIC simulations.

Acknowledgements Research described in this paper was supported by the Czech Technical University in Prague with grants SGS10/266/OHK3/3T/13 (Electric discharges, basic research and application), SGS12/181/OHK3/3T/13 (Plasma instabilities and plasma-particle interactions) and by the Grant Agency of the Czech Republic with grant GD205/09/H033 (General relativity and its applications in astrophysics and cosmology).

References

Bohata, M., Břen, D., & Kulhánek, P. 2012, ISRN Condensed Matter Physics, 2011, 896321
Bonanno, A., & Urpin, V. 2011, A&A, 525, A100
Buneman, O. 1959, Physical Review, 115, 503
Horký, M. 2012, Numerical Solution of the Generalized Buneman Dispersion Relation, Proceedings of Poster 2012, Prague, 2012
Horký, M. 2013, Instability Growth Rate Dependence on Input Parameters During the Beam–Target Plasma Interaction, Acta Polytechnica 53(2), 174
Hubbard, J., Schleicher, D., & Sutherland, S. 2001, Inventiones Mathematicae, 146, 1
Mizuno, Y., Zhang, B., Giacomazzo, B., et al. 2009, ApJ, 690, L47
Murphy, G. C., Lery, T., O'Sullivan, S., et al. 2008, A&A, 478, 453
Nishikawa, K.-I., Hardee, P., Richardson, G., et al. 2005, ApJ, 622, 927
Silk, J., Antonuccio-Delogu, V., Dubois, Y., et al. 2012, A&A, 545, L11
Stockem, A., Dieckmann, M. E., & Schlickeiser, R. 2008, Plasma Physics and Controlled Fusion, 50, 025002
Urpin, V. 2006, A&A, 455, 779

4.3 Paper III

Title: Kinetic plasma instabilities due to charge exchange and elastic collisions
Coauthor: Wojciech Jacek Miloch
Journal: Journal of Physics: Conference Series

This paper was submitted to the 15$^{\text{th}}$ Latin American Workshop on Plasma Physics (2014) and covers numerical simulations of magnetized weakly collisional plasmas in $\mathbf{E} \times \mathbf{B}$ fields. The presenting author on the conference was W. J. Miloch. Numerical simulations were performed using electrostatic PIC code developed at the University of Oslo. The research described in the paper focuses on the study of temporal evolution of electrostatic potential fluctuations and potential density for two different ion-neutral collisional regimes (charge exchange and elastic). The research was linked to previous research at the University of Oslo [49]. The paper was published in Journal of Physics: Conference Series in March 2015.
Author's contribution:

- Scientific contribution: 67 %.
- Text contribution: 67 %.

15th Latin American Workshop on Plasma Physics (LAWPP2014) IOP Publishing
Journal of Physics: Conference Series **591** (2015) 012034 doi:10.1088/1742-6596/591/1/012034

Kinetic plasma instabilities due to charge exchange and elastic collisions

M. Horký[1,2], **W. J. Miloch**[3]

[1] Department of Physics, Faculty of Electrical Engineering, Czech Technical University in Prague, Technická 2, 166 27 Prague, Czech Republic
[2] Astronomical Institute, Czech Academy of Sciences, Boční II 1401/1a, 141 00 Prague, Czech Republic
[3] Department of Physics, Univeristy of Oslo, P. O. Box 1048 Blindern, N-0316 Oslo, Norway

E-mail: horkymi1@fel.cvut.cz; w.j.miloch@fys.uio.no

Abstract.
With numerical particle-in-cell simulations, we study kinetic plasma instabilities induced by collisions between plasma particles and neutral background in magnetized drifting plasmas. We consider the role of charge exchange as well as elastic collisions in the evolution of the system. Charge exchange collisions can give rise to velocity distributions in the form of loss-cone or ring shaped distributions that can become linearly unstable. Elastic collisions also lead to the instability, but in this case the principal mechanism may be attributed to the generalized two-stream instability. We investigate the growth rates and saturation levels for instabilities associated with these collisional processes, and find higher saturation levels and stronger fluctuations for the case with charge exchange collisions. Characteristics of the studied system are similar to the E- and F-regions of the Earth's ionosphere. Our results are relevant for explaining some of the low frequency oscillations observed in the lower parts of the Earth's ionosphere, and are also relevant for some laboratory experiments.

1. Introduction

In the lower parts of the Earth's ionosphere, the plasma collisional processes can dominate the plasma dynamics. In those regions, the collision rates between the charged particles and neutrals can surpass the rates of collisions between charged particles [1]. In general, the frequency of collisions with neutrals strongly depends on the altitude, and this process is mostly relevant for the ionospheric E-region, which extends above ca. 100 km. In the lower E-region, the ions can become effectively unmagnetized, which can give rise to the two-stream like instabilities [1, 2]. In the upper E-region and lower F-region, all charged particles are magnetized, and the plasma is weakly collisional, and is in general drifting due to external electric and magnetic fields in the $\mathbf{E} \times \mathbf{B}$ direction. In those regions, the collisions may significantly modify the ion velocity distribution functions. Similar conditions can be found in dedicated laboratory experiments [3, 4].

Distorted ion velocity distribution functions can lead to different kinetic microinstabilities. For example, charge-exchange collisions can give rise to loss-cone or ring shaped velocity distribution functions that can become linearly unstable. These distributions will generally not be cylindrically symmetric [5, 6]. Elastic collisions can, on the other hand, distort the $\mathbf{E} \times \mathbf{B}$

Content from this work may be used under the terms of the Creative Commons Attribution 3.0 licence. Any further distribution of this work must maintain attribution to the author(s) and the title of the work, journal citation and DOI.
Published under licence by IOP Publishing Ltd

15th Latin American Workshop on Plasma Physics (LAWPP2014) IOP Publishing
Journal of Physics: Conference Series **591** (2015) 012034 doi:10.1088/1742-6596/591/1/012034

drift of the ions, and in a limiting case, give rise to a generalized two-stream instability [7]. Since the instability origin is often due to distorted velocity distribution functions, one should use a kinetic approach or first-principle particle simulations to address this problem.

Different ion-neutral collision types can thus lead to distinct instability regimes. In this paper, we focus on two limiting cases, where we consider charge exchange or alternatively elastic scattering for ions in two-component plasmas. We address the problem with a self-consistent particle-in-cell code that accounts for collisions. By simulating weakly collisional plasmas, we investigate nonlinear plasma dynamics with the emphasis on the question on how the collision type affects instability characteristics such as the instability growth, level of the electrostatic potential fluctuations, and the potential distribution.

2. Numerical Model

Our analysis is carried out with a three-dimensional, electrostatic particle-in-cell (PIC) code. We simulate the dynamics of electrons and ions in self-consistent fields in a periodic system, and account also for external electric and magnetic fields, as well as collisions with a neutral background gas. The code is based on our previous PIC codes, with details on its numerical implementation given in earlier works [5, 8]. Collisions between plasma particles and neutral background are implemented with the null-collision method, which allows for arbitrary, energy dependent collision cross-sections. In the present work, however, we choose to use a constant collision frequency ν in order to focus on the basic physical mechanisms associated with a given collision type. We account for charge exchange collisions or alternatively elastic collisions for ions. In both cases the electrons experience elastic collisions.

The simulated system is a box of size of 0.5 m in each direction, and spatial grid resolution of 0.7 cm. Initially, the system is spatially homogeneous. The plasma density is $n = 10^{12}$ m^{-3}, with the electron temperature $T_e = 8.6$ eV, and the electron to ion temperature ratio $T_e/T_i = 4$. The external magnetic and electric fields are $B_0 = 0.005$ T and $E_0 = 550$ Vm^{-1}. The $\mathbf{E} \times \mathbf{B}/B^2$ drift v_d is supersonic, with $v_d = 2\sqrt{T_e/M}$, where M is the ion mass. The ion collision frequency is $\nu_{in} = 3.52 \cdot 10^5$ s^{-1}, which is lower than the ion gyrofrequency Ω_{ci}, $\nu_{in} = \Omega_{ci}/5$, while the electron collision frequency is given by $\nu_{en} = \nu_{in}\sqrt{M/m}$, where m is the electron mass. For computational reasons, we use the reduced mass ratio $M/m = 500$, while keeping the electron mass realistic, and the mass of cold neutral species $m_n = M$. This reduced mass ratio speeds up the simulations, while it still gives credible results [9]. We typically run large-scale simulations for times up to $t = 95000\Delta t$, which corresponds to 19 ion gyroperiods with a timestep Δt being a fraction of the electron gyroperiod.

The simulated plasma parameters can be related to scaled conditions in the upper parts of the ionospheric E-region, where the plasma is only weakly collisional [1, 2, 5]. However, while the respective ratios of the parameters are within the relevant range, the one-to-one correspondence is not maintained; rather the scaled system is simulated. Thus, while we expect that the main phenomena will be present in the simulations, some of the ionospheric processes might be not well represented.

3. Results and Discussion

In the simulated system, the charge exchange collisions lead to an asymmetric ring distribution function for ion velocities, which after one ion gyroperiod, when the full ring shape velocity is formed, becomes unstable and triggers the instability [5]. This instability mechanism is equivalent to the loss-cone instability discussed in the context of fusion research [2, 10]. The instability grows during a few ion gyroperiods until the ring in the distribution function is filled-in in the velocity phase-space. It is characterized by an enhanced level of fluctuations in the electrostatic potential distribution, and the growth of harmonics in the wave spectra. A partially filled ion velocity distribution at a later stage is shown in Figure 1(a). In Figure 2 we

15th Latin American Workshop on Plasma Physics (LAWPP2014) IOP Publishing
Journal of Physics: Conference Series **591** (2015) 012034 doi:10.1088/1742-6596/591/1/012034

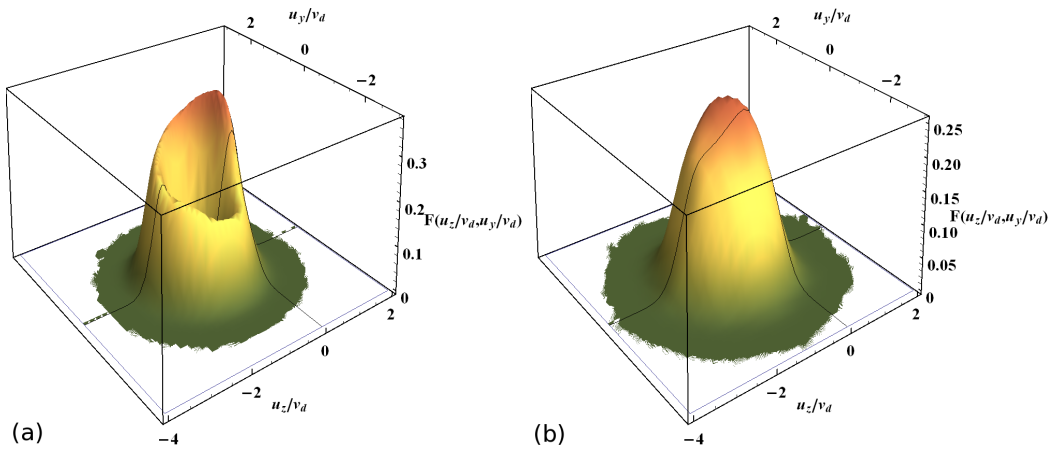

Figure 1. Ion velocity distribution function for the charge exchange (a) and elastic (b) collisions at $t = 4 \cdot 2\pi/\Omega_i$.

show the absolute value of potential fluctuations as a function of time for different collision types averaged over a chosen subset of grid points in the simulated system. The average amplitude of potential fluctuations in the case of charge exchange collisions increases by a factor of three during the simulation, and is characterized by strong fluctuations in the saturated stage with amplitudes up to seven times the initial value. For elastic scattering the growth rate is similar as in the charge-exchange case, while the saturation level is lower, being characterized by much smaller fluctuations. We observe that the elastic scattering modifies the ion-velocity distribution function by strongly broadening the distribution, see Figure 1(b). Thus, the mechanism for the instability will be different than in the case of charge exchange collisions, where the typical loss-cone instability due to non-Maxwellian distribution can be expected [6]. Moreover, in this nonlinear regime there may also be a competition between several other instabilities, thus the instability due to collisions might act to only modulate other instabilities present in the system [1, 11].

The potential structures in the saturated stage of instability are strongly aligned with the **B**-field. The long wavelengths along **B** can be crucial for the dynamics of the system [1, 12]. However, to study waves at small wavelengths, it suffices to consider only the plane perpendicular to the **B**-field direction. In Figure 3, the potential distribution in the plane perpendicular to the direction of magnetic field is shown for charge exchange collisions, together with the corresponding potential distribution at the beginning of the simulations and at the onset and saturated stage of instability. Initially, the potential distribution is normal, with the maximum values of ± 5 V, and there are no coherent structures observed, see Figure 3(a). Coherent structures start forming during the onset of the instability, and in the saturated stage large, coherent structures propagating in the $\mathbf{E} \times \mathbf{B}$ direction are observed (i.e., in the negative $\hat{z}$ direction, see Figures 3b-c). The angle of propagation of these structures with respect to the $\mathbf{E} \times \mathbf{B}$ direction can be related to the supersonic drift regime. As the amplitudes of the fluctuations increase, the potential distribution becomes more shallow, but can still be approximated by a normal distribution.

15th Latin American Workshop on Plasma Physics (LAWPP2014) IOP Publishing
Journal of Physics: Conference Series **591** (2015) 012034 doi:10.1088/1742-6596/591/1/012034

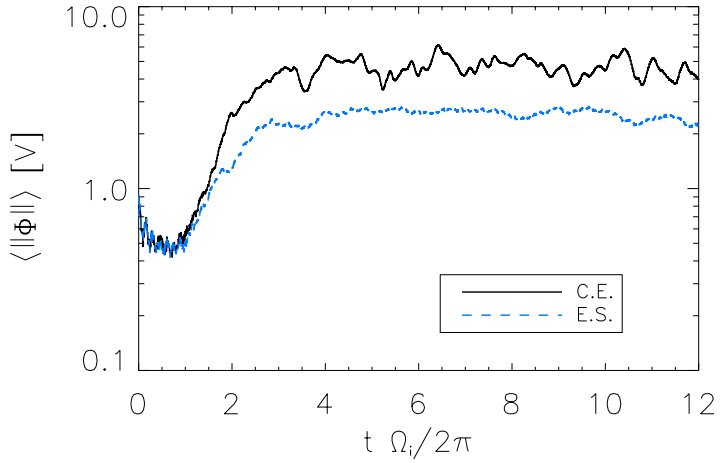

Figure 2. The amplitude of the potential fluctuations $\|\Phi\|$ averaged over a part of the simulation box as a function of time for elastic (dashed line), and for charge exchange (full line) ion-neutral collisions. Time is normalized to the ion gyroperiod.

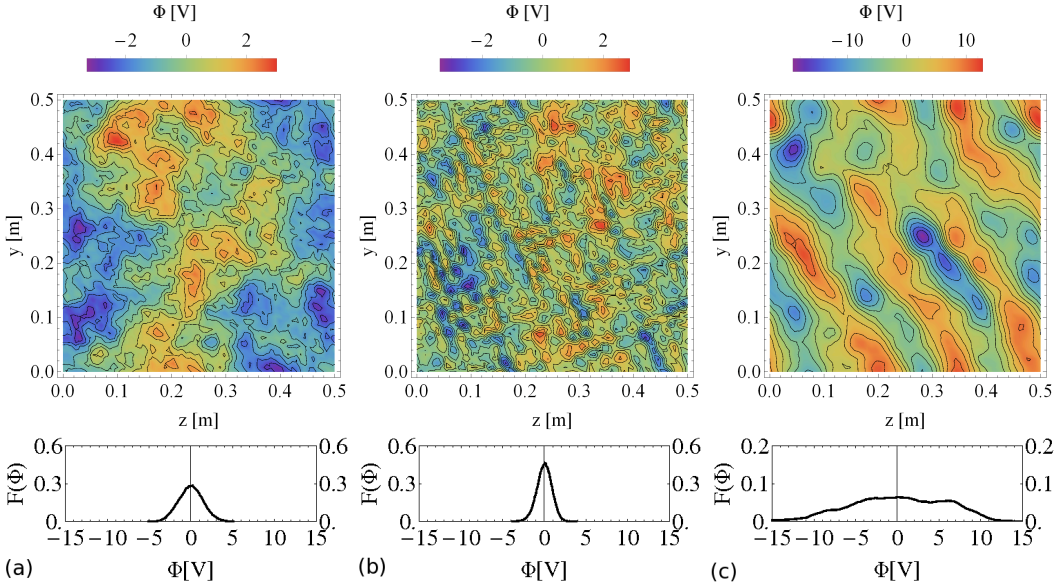

Figure 3. The potential distribution in the plane perpendicular to the direction of the magnetic field in the middle of the box together with the corresponding distribution of potential fluctuations in the whole system. The $\mathbf{E} \times \mathbf{B}$-drift is in the negative $\hat{z}$-direction. The results shown are for charge exchange collisions in the beginning of the simulations (a), at the onset of instability (b), and for the developed stage of the instability (c). Note that the range of the $F(\Phi)$-axis in (c) is reduced.

15th Latin American Workshop on Plasma Physics (LAWPP2014) IOP Publishing
Journal of Physics: Conference Series **591** (2015) 012034 doi:10.1088/1742-6596/591/1/012034

4. Conclusions

With numerical PIC simulations, we have studied the kinetic plasma instabilities in the $\mathbf{E} \times \mathbf{B}/B^2$-drifting weakly collisional plasma, with the parameter regime that can be relevant for ionospheric conditions. Two limiting cases have been considered: charge exchange and elastic collisions. For the case with charge exchange collisions, a significant saturation level for the amplitudes in the potential fluctuations is reached after a few ion gyroperiods. Elastic collisions give rise to much smaller potential fluctuations and a lower saturation level. While the ion velocity distributions are different for these two collision types, the instability growth rate is the same for both cases. It is expected that in this nonlinear regime there is a competition between several instabilities, and thus further detailed analytical and numerical studies are required to identify different competing and dominant processes in the evolution of this system.

Acknowledgments

M.H. acknowledges support by the CTU grants SGS12/181/OHK3/3T/13 and SGS13/194/OHK3/3T/13 that allowed him to carry out this research during his stay at the University of Oslo. This work is also a part of the 4DSpace Strategic Research Initiative at the University of Oslo.

References

[1] Kelley M C 2009 *The Earth's Ionosphere: Plasma Physics and Electrodynamics* (Amsterdam: Elsevier)
[2] Treumann R A and Baumjohann W 2001 *Advanced Space Plasma Physics* (London: Imperial College Press)
[3] Saito S, Sato N and Hatta Y 1964 *Appl. Phys. Lett.* **5** 467
[4] Mikkelsen T, Pécseli H L 1980 *Phys. Lett. A* **77** 15962
[5] Miloch W J, Pécseli H L and Trulsen J K 2013 *Plasma Phys. Control. Fusion* **55** 124006
[6] St-Maurice J-P and Schunk R W 1979 *Rev. Geophys.* **17** 99134
[7] Farley D T 1963 *J. Geophys. Res.* **68** 60836097
[8] Miloch W J, Kroll M and Block D 2012 *Phys. Plasmas* **17** 103703
[9] Miloch W J, Pécseli H L and Trulsen J 2007 *Nonlin. Processes Geophys.* **14** 575
[10] Teller E 1981 *Fusion Vol 1, Magnetic Confinement Part A* (New York: Academic Press)
[11] Hasegawa A 1975 *Plasma Instabilities and Nonlinear Effects* (Berlin: Springer-Verlag)
[12] Dimant Y S and Milikh G M 2003 *J. Geophys. Res.* **108** 1350

4.4 Paper IV

Title: Numerical Simulations of Weakly Collisional Plasmas in $\mathbf{E} \times \mathbf{B}$ Fields
Coauthor: Wojciech Jacek Miloch
Proceedings: 31st URSI-GASS (published online at IEEExplore)

This paper was submitted to the 31st URSI-GASS conference (2014) and also covers numerical simulations of magnetized weakly collisional plasmas in $\mathbf{E} \times \mathbf{B}$ fields. The presenting author on the conference was W. J. Miloch. Numerical simulations were again performed using electrostatic PIC code developed at the University of Oslo. Beside the temporal evolution of electrostatic potential fluctuations, the research described in the paper focuses also on the study of temporal evolution of ion velocity phase space. The paper was published in proceedings of the conference on the IEEExplore webpage.
Author's contribution:

- Scientific contribution: 67 %.
- Text contribution: 67 %.

Numerical Simulations of Weakly Collisional Plasmas in ExB Fields

*Miroslav Horký[1,2] and Wojciech J. Miloch *[3]*

[1]Department of Physics, Faculty of Electrical Engineering, Czech Technical University in Prague, Technická 2, 166 27 Prague, Czech Republic
e-mail: horkymi1@fel.cvut.cz

[2]Astronomical Institute, Czech Academy of Sciences, Boční II 1401/1a, 141 00 Prague, Czech Republic

[3]Department of Physics, University of Oslo, P.O. Boks 1048 Blindern, N-0316 Oslo, Norway
e-mail: w.j.miloch@fys.uio.no

Abstract

We study the stability of weakly collisional, magnetized plasmas in the presence of the $\vec{E} \times \vec{B}$ fields with self-consistent particle-in-cell simulations. Collisional interactions with a neutral background can lead to distorted, unstable velocity distributions. In the case of charge-exchange collisions, we observe the formation of a ring-shape velocity distribution for ions. For elastic ion-neutral collisions the ion velocity distribution is distorted and broadened. In both cases, after one gyroperiod, we observe a significant increase in the fluctuations in potential, which can be related to the instability growth. In the saturated frequency-wavenumber spectrum, nonlinear three-wave interaction is observed.

1. Introduction

In the presence of external electric and magnetic fields, the plasma will drift with the $\vec{E} \times \vec{B}/B^2$ velocity. In the collisionless case, electrons and ions will drift with the same velocity in the same direction. Thus, there will be no net current through the plasma. However, the situation can change significantly, when one or both of the species experience collisions with neutrals. If one of the species becomes unmagnetized due to collisions, a net current will be present. Above a certain threshold, this can lead to instabilities and an exponential growth of fluctuations in potential and electric fields [1]. In the ionosphere, enhanced fluctuation levels can have implications for the scintillations of for instance Global Navigation Satellite System signals, such as GPS signals. Thus their understanding is also important for the assessment of space weather effects [2]. A typical example of an unstable plasma configuration for ionospheric plasmas is the well known Farley-Buneman instability, for which the ions are effectively unmagnetized [3]. In the present work, we focus on a different regime, in which the ions are magnetized, but the collisions are frequent enough to induce significant changes in the ion velocity distributions.

It is known that in the ionospheric E region, a collisional regime exists where $\omega_{ce} >> \nu_{en}$, while $\Omega_{ci} \leq \nu_{in}$, in terms of electron and ion cyclotron frequencies ω_{ce}, Ω_{ci}, and collision frequencies ν_{en}, ν_{in} between charged particles and neutrals. This regime is relevant for the Farley-Buneman instability, which has been studied extensively in the past [4]. At higher altitudes, however, the regime may exist where $\Omega_{ci} \geq \nu_{in}$, while electrons are still collisionless. Under these conditions, it has been shown that a ring-shaped velocity distribution may form for ions with charge-exchange collisions [5]. Such distribution will generally be unstable, but other instabilities may also be excited [1,6], before the fully shaped ring velocity distribution is even established. Thus, the nonlinear situation will be a competition between several instabilities, which are characterized by different ranges in frequencies and wave numbers. Studies of such a regime may be important for comprehensive knowledge of ionospheric processes at different altitudes. Of particular interest is the role of different collision types for the dynamics of the system. While charge-exchange collisions could give rise to unstable ring-shaped velocity distributions, the relative importance of charge exchange and elastic ion collisions is not clear.

Weakly collisional plasmas in the $\vec{E} \times \vec{B}$ fields can form highly nonlinear systems, and thus analytical studies can be difficult [6]. A natural choice for studies of such systems will be by using first principle numerical simulations that account for nonlinear plasma dynamics. In this study, we employ the particle-in-cell (PIC) numerical code to carry out self-consistent simulations and address the problem of the role of collisions for the plasma stability in weakly collisional plasmas.

2. Numerical simulation

Our analysis is carried out with a three-dimensional, electrostatic PIC code. The dynamics of electrons and ions is simulated in self-consistent electrostatic fields in a periodic system. We account for external electric and magnetic fields, and collisions with a neutral background gas. This new code is based on our previous PIC codes, with details of numerical implementation given in earlier works [7,8]. The underlying principles of the code are standard, with the grid being used for field calculations to reduce the numerical complexity of simulations of a large number of plasma particles, and the leap-frog method and Boris algorithm used for advancing particle trajectories [9]. Collisions between plasma particles and neutral background are implemented with the null-collision method [10]. This method is an efficient algorithm for plasma-neutral collisions, and it allows for arbitrary collision cross-sections σ. In particular we can simulate real, energy dependent collision cross-sections. However, to have a control over the dynamics of the system and to allow for systematic studies, in the present work we choose to use a constant collision frequency v. In our simulations, we allow for charge exchange collisions for ions, and elastic collisions for electrons and for ions.

We use the box size of 0.5 m in each direction, with the spatial grid resolution of 0.7 cm. The plasma density in the simulation is $n = 10^{12}$ m^{-3}, with the initial electron temperature $T_e = 8.6$ eV, and the electron to ion temperature ratio $T_e/T_i = 4$. External magnetic and electric fields are $B_0 = 0.005$ T and $E_0 = 550$ Vm^{-1}, respectively. For these parameters, the $\vec{E} \times \vec{B}/B^2$ drift will be supersonic, i.e., $v_d = 2\sqrt{T_e/M}$, where M is the ion mass. The ion collision frequency is $v_{in} = 3.52 \cdot 10^5$ s^{-1}. This frequency is lower than the ion gyrofrequency, $v_{in} = \Omega_{ci}/5$, while the electron collision frequency is given by $v_{en} = v_{in}\sqrt{M/m}$, where m is the electron mass. To speed-up the simulations we simulate the reduced mass ratio $M/m = 500$, while keeping the electron mass realistic. We set mass of neutral species $m_n = M$, and assume neutrals to be cold, $T_n = 0$. The plasma parameters can be related to the scaled conditions in the upper parts of E-region of ionosphere. However, while the respective ratios of the parameters are within the relevant range, the one-to-one correspondence is not maintained. Thus, while we expect that the main phenomena will be present in the simulations, some of ionospheric processes might be not well represented.

With a timestep of $\Delta t \approx 0.1 \cdot 2\pi/\Omega_{ce}$ we can resolve also the electron gyromotion. With these parameters, we can also resolve the smallest scales in the system, i.e., the Debye length and electron gyroperiod, which is necessary for the stability and reliability of the simulations [9]. We typically run the code for about $t = 95000\Delta t$ which corresponds to 19 ion gyroperiods, and simulate 10^7 plasma particles using the Message-Passing-Interface (MPI) for the parallel computing environment.

3. Results

During the course of the simulation we observe the effects of collisions on the ion velocity distribution function. The initially Maxwellian distribution (see Figure 1a) rotates in the u_y-u_z velocity phase space for velocity components perpendicular to the magnetic field direction, where $\vec{B} = B_0\hat{x}$. For the charge exchange collisions, the gyrorotating bi-Maxwellian cone becomes narrower in time, as the colliding ions move to the origin in the velocity phase space. Thus, ions that have collided, give rise to the ring shape of the velocity distribution function. After one ion gyroperiod the full ring distribution is formed. We observe that after several ion gyroperiods the ring distribution fills in, indicating the saturation of the instability. The resulting distribution is characterized by a peak close to the origin, which is due to charge exchange collisions, see Figure 1(b). On the other hand, ion-neutral elastic collisions lead to diffusion in the velocity phase-space and give rise to a broad distribution function, which center is shifted by the drift velocity, as shown in Figure 1(c).

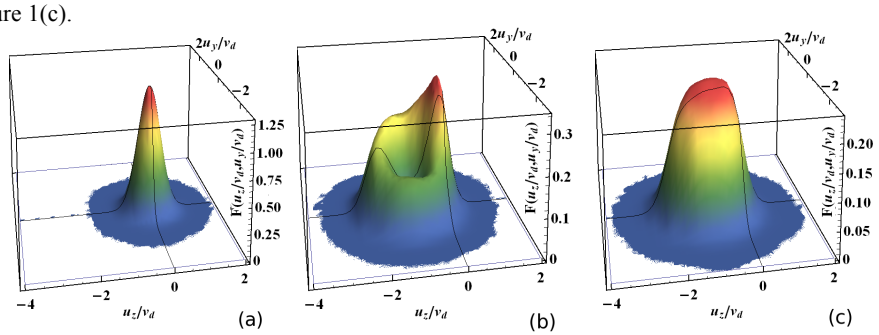

Figure 1. Ion velocity distributions for the velocity components perpendicular to the magnetic field direction at the beginning of simulations (a), and after four ion gyroperiods for charge exchange collisions (b) and elastic collisions (c).

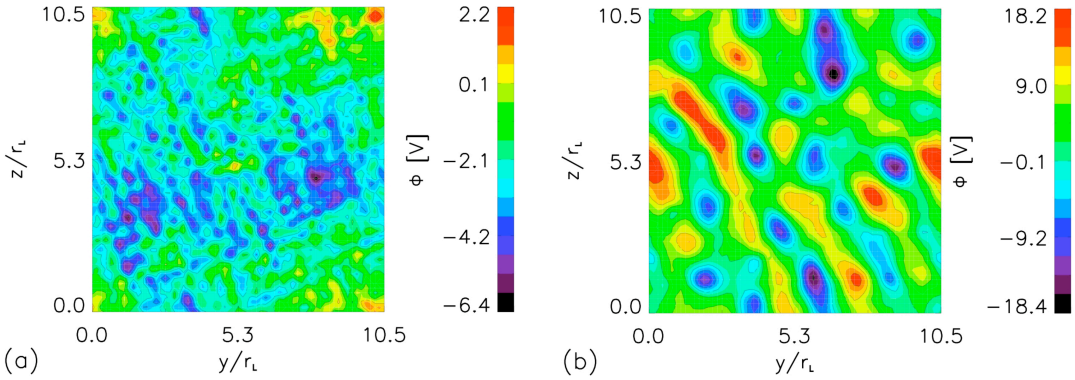

Figure 2: Electrostatic potential distribution in the plane perpendicular to the magnetic field direction for charge-exchange collisions, at time t=1.2·2π/Ω_{ci} in the growing phase of the instability (a), and for the saturated stage at t=3·2π/Ω_{ci} (b).

The evolution in the ion velocity distribution function is accompanied by the growth of the amplitude of the potential and electric field fluctuations. The fluctuation level growth occurs after the first ion gyroperiod, and saturates after several gyroperiods. The growth is by approximately one order of magnitude. There is little difference between the growth rate for the elastic and charge exchange collisions. However the saturation level is higher for the charge exchange collisions. In this case, the fluctuation level remains high at the saturation stage, suggesting strong nonlinear interactions between different wave modes generated in the system. For elastic collisions, the saturation is lower by a factor of two for the considered parameters. The evolution of the potential distribution in the plane perpendicular to the magnetic field is illustrated in Figure 2 for the case with charge exchange collisions, where one can observe a development of coherent structures during the growth phase (Figure 2a), and propagation of such structures in the $\vec{E} \times \vec{B}$ direction the at the saturated stage (Figure 2b).

With the frequency-wavenumber spectral analysis of the electrostatic potential fluctuations, we observe that the number of harmonics increases during the growing phase of the instability. Because of the assumed vanishing neutral temperature and distorted velocity distributions, we have a rapid initial growth of wave amplitudes, with amplitudes increasing by a factor 2 within approximately one ion gyroperiod after the onset of instability. The dominant component of the fluctuations propagates at an angle to the $\vec{E} \times \vec{B}$ direction and $\omega/k_z \approx E/B$, while $k_x \approx 0$. We find the dominant wave-numbers in the saturated spectrum to be $|k| \approx \Omega_{ci}/C_s$ within a factor 2. At the saturated stage, the growth of modes at low frequencies is observed, and their relations indicate nonlinear three-wave interactions. For charge-exchange collisions we also observe the presence of half-harmonics of the ion cyclotron frequency. Furthermore, in the spectra we identify possible resonances between the wave and electrons corresponding to their thermal velocities.

4. Conclusions

With numerical simulations we have studied the relative role of charge exchange and elastic ion collisions with neutrals on the evolution of the weakly collisional plasma in the $\vec{E} \times \vec{B}$ fields. We have observed significant distortions of the ion velocity distributions that highly depend on the type of collisions. Such distorted distributions may be kinetically unstable. Indeed, we observe diffusion in the velocity phase space in the case of the charge exchange collisions. The simulations considered cold neutral background, but in reality, neutrals will be thermalized in the charge exchange events, and the ring-shaped distributions for ions will be slightly more diffuse already in the initial phase. For both cases, there is a growth of amplitude of the field fluctuations, and larger coherent structures propagating in the $\vec{E} \times \vec{B}$ direction are observed. In the frequency-wavenumber spectra we observe a number of harmonics during the growth phase, including modes at half-harmonics of the cyclotrone frequency. Note, that narrow frequency-band oscillations near half of the cyclotron frequency of hydrogen have at times been observed in the lower parts of the ionospheric F-region [11]. In the saturated phase, we see the growth of three main modes, reflecting the nonlinear three-wave interaction [12]. Since we expect that in this nonlinear regime there is a competition between several instabilities,

further detailed studies are required to indentify different competing and dominant processes in the evolution of this system.

4. Acknowledgments

M.H. acknowledges support by the CTU grants SGS12/181/OHK3/3T/13 and SGS13/194/OHK3/3T/13 that allowed him to carry out this research during his stay the University of Oslo. This work is also a part of the 4DSpace initiative at the University of Oslo.

5. References

1. H. L. Pécseli, *Waves and Oscillations in Plasmas*, CRC Press, 2013.

2. V. Bothmer, and I. A. Daglis, *Space Weather - Physics and Effects*, New York, Springer, 2007.

3. D. T. Farley, "A Plasma Instability Resulting in Field-Aligned Irregularities in the Ionosphere", *J. Geophys. Res.*, **68**, 1963, pp. 6083–6097.

4. M. C. Kelley, *The Earth's Ionosphere Plasma Physics and Electrodynamics*, Amsterdam, Elsevier, 2009.

5. J-P. St-Maurice and R. W. Schunk, "Ion velocity distributions in the high latitude ionosphere", *Rev. Geophys.* **17**, 1979, pp. 99–134.

6. W. J. Miloch, H. L. Pécseli, and J. K. Trulsen, "Unstable ring-shaped ion distribution functions induced by charge–exchange collisions", *Plasma Phys. Control. Fusion,* **55**, (2013), 124006.

7. W. J. Miloch, M. Kroll, and D. Block, "Charging and dynamics of a dust grain in the wakefield of other grain", *Phys. Plasmas,* **17**, 2012, p. 103703.

8. W. J. Miloch, S. R. Habbal, and R. Esser, "Plasma dynamics at the prominence-corona interface", Astrophys. J., **752**, 2012, p. 85.

9. C. K. Birdsall, and A. B. Langdon *Plasma Physics via Computer Simulation*, Bristol, Adam Hilger,1991.

10. V. Vahedi, and M. Surendra, "Monte Carlo collision model for the particle-in-cell method: applications to argon and oxygen discharges", *Comput. Phys. Commun.* **87,** 1995, pp.179–98.

11. K. Iranpour, et al., "Propagation and dispersion of electrostatic waves in the ionospheric E region", *Ann. Geophys.* **15,** 1997, pp. 878-889.

12. A. Hasegawa, *Plasma Instabilities and Nonlinear Effects*, Springer-Verlag, 1975.

4.5 Paper V

Title: Numerical study on the stability of weakly collisional plasma in $\mathbf{E} \times \mathbf{B}$ fields
Coauthor: Wojciech Jacek Miloch
Journal: Physics of Plasmas

Research described in this paper follows research in tho two previous conference papers. It summarises all the results such as time evolution of ion velocity phase space, potential fluctuations, potential density, and wave spectra for two different collisional regimes and compares them with the reference collisionless case. While for the collisionless case and the case with ion-neutral elastic collisions we found the system stable, for ion-neutral charge exchange collisions we observed an instability growth rate and the creation of coherent structures in potential density corresponding to electrostatic waves. The paper was published in the journal Physics of Plasmas (IF 2.249) in February 2015.
Author's contribution:

- Scientific contribution: 75 %.
- Text contribution: 75 %.

PHYSICS OF PLASMAS 22, 022109 (2015)

Numerical study on the stability of weakly collisional plasma in E×B fields

M. Horký[1,2,a] and W. J. Miloch[3]
[1]Department of Physics, Faculty of Electrical Engineering, Czech Technical University in Prague, Technická 2, 166 27 Prague, Czech Republic
[2]Astronomical Institute, Czech Academy of Sciences, Boční II 1401/1a, 141 00 Prague, Czech Republic
[3]Department of Physics, University of Oslo, P.O. Box 1048 Blindern, N-0316 Oslo, Norway

(Received 8 December 2014; accepted 9 January 2015; published online 4 February 2015)

Plasma stability in weakly collisional plasmas in the presence of $\mathbf{E} \times \mathbf{B}$ fields is studied with numerical simulations. Different types of ion-neutral collisions are considered in a fully magnetized regime. We study the influence of ion-neutral collisions and the role of collision types on the stability of plasma. It is found that the stability of plasma depends on the type of ion-neutral collisions, with the plasma being unstable for charge exchange collisions, and stable for the elastic scattering. The analysis focuses on the temporal evolution of the velocity phase space, RMS values of the potential fluctuations, and coherent structures in potential densities. For the unstable case, we observe growth and propagation of electrostatic waves. Simulations are performed with a three-dimensional electrostatic particle in cell code. © *2015 AIP Publishing LLC*. [http://dx.doi.org/10.1063/1.4906887]

I. INTRODUCTION

In nature, an initial perturbation of a physical system is usually damped and the system reaches new equilibrium state. Otherwise, under specific conditions the amplitude of initial perturbation can grow because of a positive feedback in the system. This phenomenon is called instability. In plasmas, instabilities are mostly connected with perturbations in potentials which give rise to electrostatic and/or electromagnetic waves. Instabilities are ubiquitous in both naturally occurring plasmas, such as space and ionospheric plasmas,[1] and in laboratory plasma experiments, where they may be a subject of a specific study or an unwanted contribution.[2]

For theoretical description of plasma instabilities, one should use the magnetohydrodynamics (MHD) or kinetic approaches. MHD is applicable for macroscopic problems where instabilities can grow due to configuration in space. These macroinstabilities grow predominantly at large wavelengths. While macroinstabilities can also be addressed with the kinetic theory, the main importance of the kinetic approach is in describing instabilities at a microscopic level. These so-called microinstabilities can rise due to distortions in the velocity phase-space and grow at small wavelengths.[3]

Microinstabilites in collisionless plasmas were well studied in the past and a good overview can be found in several textbooks.[1–3] A typical example of microinstability in a collisionless magnetized plasma is the component/component instability, like electron/ion cyclotron instability,[3] where the instability growth depends on the relative drift speed between plasma species. There are different criteria for the plasma stability.[2] An example is the Penrose criterion that is used at kinetic scales for electrostatic wave modes in plasmas with multi-peaked velocity distribution functions: $\int_{-\infty}^{\infty} F(v_0) - F(v)/(v - v_0)^2 \mathrm{d}v < 0$, where v_0 is a value of the minimum between two peaks in the velocity distribution function $F(v)$.[4] A crucial parameter for the stability of collisionless, magnetized plasmas is the relative drift between plasma species. Under realistic conditions, because of different inertia of plasma species, the difference in drift speed can occur even in case of the $\mathbf{E} \times \mathbf{B}$ drift.[3]

In case of collisional plasmas, the problem is more complex, in particular, in $\mathbf{E} \times \mathbf{B}$ fields. Collisions between charged particles and neutrals can provide damping as well as growth of an initial fluctuation. Collisions can effectively demagnetize plasma particles, if the collision frequency is much larger then the relevant gyrofrequency. In $\mathbf{E} \times \mathbf{B}$ fields, this may lead to the well-known Farley-Buneman instability that can occur in lower parts of the E-region ionosphere, where there is a relative flow between electrons and unmagnetized ions, due to high collision frequency.[5,6] Ott and Farley[7] studied microinstabilites in weakly collisional plasmas ($\nu_{in}/\Omega_i \ll 1$) which can result in the Post-Rosenbluth instability[8,9] or electrostatic flutelike ion cyclotron mode.[10] In recent years, Perron *et al.*[11] studied the effects of temperature anisotropy on the dispersion relation in the ionospheric F-region and found that temperature anisotropy lowers the instability threshold. Miloch *et al.*[12] studied stability of the ring shaped velocity distribution functions induced by charge exchange collisions and the dynamics of unstable waves. Ring shaped velocity distribution functions can be found in magnetized plasmas at low collisional frequency for ions, thus when ions are still magnetized.[7,13,14]

Nowadays, both micro- and macroinstabilities in $\mathbf{E} \times \mathbf{B}$ fields are mostly studied numerically. Due to the importance of collisions, it is advisable to use particle simulations, or hybrid (particle-fluid) simulations. There have been a number of numerical studies in 2-D and 3-D, but most of them focused on the highly collisional regime, and many considered, just as in theoretical works, the relative drift speeds between plasma species.[15–17]

In the view of previous works, the question arises if there is any unstable regime for perfectly magnetized and weakly collisional plasmas in $\mathbf{E} \times \mathbf{B}$ fields. In such systems, it is necessary to distinguish between different collisional

[a]Electronic mail: miroslav.horky@fel.cvut.cz

 © 2015 AIP Publishing LLC

This article is copyrighted as indicated in the article. Reuse of AIP content is subject to the terms at: http://scitation.aip.org/termsconditions. Downloaded to IP: 185.47.220.152 On: Wed, 04 Feb 2015 23:03:32

mechanisms, where elastic and inelastic collisions can each have different effects on the velocity phase-space of the plasma in question. For ionized atoms, there are in practice two main types of collisions that need to be considered first due to their large collision cross-sections: charge exchange and elastic collisions.[18] Thus, it is a question what is the effect of those different collision types on the plasma stability, and which collision type could provide favorable conditions for the instability growth?

In this study, we focus on the role of the collision type on the stability of the plasma in $\mathbf{E} \times \mathbf{B}$ fields in a weakly collisional regime, i.e., when both species remain magnetized. We address this question by 3D electrostatic Particle-In-Cell (PIC) numerical simulations. We have simulated weakly collisional plasma in $\mathbf{E} \times \mathbf{B}$ fields, and consider elastic collisions or charge exchange collisions for ions, i.e., collision types with largest collision cross-sections, and elastic collisions for electrons. The results are analyzed in terms of velocity distribution functions, amplitudes of potential fluctuations, and electrostatic wave spectra. We show that the type of ion-neutral collisions plays a substantial role in the plasma stability.

II. NUMERICAL SIMULATIONS

For our studies, we use the self-consistent PIC numerical simulations. We employ a three-dimensional, electrostatic code with periodic boundary conditions, in which the dynamics of electrons and ions are simulated in self-consistent fields. In addition, we apply external static magnetic and electric fields, and also account for collisions of plasma particles with a neutral background gas. The code is based on our previous PIC codes, with the details of numerical implementation given in previous works,[19–21] and with the present version we can simulate fully periodic systems in all directions for both particles and fields.[12]

We use the Cartesian coordinate system, and set the external magnetic field $\mathbf{B}$ in the $\hat{\mathbf{x}}$-direction and external electric field $\mathbf{E}$ in the $\hat{\mathbf{y}}$-direction, thus having the $\mathbf{v}_\mathrm{d} = \mathbf{E} \times \mathbf{B}/B^2$ drift in the negative $\hat{\mathbf{z}}$-direction. The plasma particle trajectories are advanced with the leap-frog method combined with the Boris algorithm.[20] During each time-step, a given number of randomly chosen plasma particles collide with neutral atoms. These collisions are implemented with the null-collision method,[18,22] which is an efficient algorithm allowing for arbitrary collision cross-sections σ that can also be energy dependent. However, to have better control over the dynamics of the system and to allow for systematic studies, in the present work we choose to use a constant collision frequency ν.

We consider the charge exchange collisions for ions, and elastic collisions for electrons and for ions. The neutrals have the same mass as ions. For simplicity and clarity of presentation, we assume the neutrals to be cold, with vanishing temperature $T_\mathrm{n} \approx 0$. However, we have performed control simulations, in which neutrals have finite, realistic temperatures to assure that the main physical processes in the cold neutral limit remain unchanged.

In our simulations, we use the box size of $L = 0.5\,\mathrm{m}$ in each direction, with the spatial grid resolution of $\Delta x = 3.9\,\mathrm{mm}$. With a time-step of $\Delta t \approx 0.04\tau_\mathrm{Le}$, where $\tau_\mathrm{Le} = 2\pi/\Omega_\mathrm{e}$ is the electron gyroperiod and Ω_e is the electron gyrofrequency, we can resolve well the electron gyromotion, and thus the smallest timescales in the system. The grid spacing is chosen to resolve the electron gyroradius r_Le, which is the smallest characteristic scale in the system (for the chosen parameters $r_\mathrm{Le} < \lambda_\mathrm{De}$, where λ_De is the electron Debye length). To speed-up the simulations, we use the reduced mass ratio $m_\mathrm{i}/m_\mathrm{e} = 500$, which is still large enough to well separate the ion and electron timescales. The plasma density is $n = 4.3 \times 10^{13}\,\mathrm{m}^{-3}$, the initial electron temperature $T_\mathrm{e} = 74.1\,\mathrm{eV}$, and the electron to ion temperature ratio $T_\mathrm{e}/T_\mathrm{i} = 4$. For these parameters, the $\mathbf{E} \times \mathbf{B}$ drift is subsonic, i.e., $v_\mathrm{d} = 0.58\sqrt{T_\mathrm{e}/m_\mathrm{i}}$. The relatively high electron temperature as well as the size of the simulation box is the result of compromise between the accuracy and numerical stability of simulations. The summary of simulation parameters is given in Table I. While the parameters are chosen predominantly according to numerical stability and performance, their characteristic ratios (e.g., temperature, frequencies, and velocities) can be related to realistic values, such as those in the lower regions of the ionospheric F-layer or laboratory plasma.

The simulations are run until almost 4 ion gyroperiods. We find this time long enough to reach the new equilibrium in the system. This has been confirmed by longer test simulations for smaller systems with reduced number of particles. In this study, we simulate 4×10^7 particles per plasma specie, and use the Message-Passing-Interface (MPI) for the parallel computing environment. The finite number of particles in the simulations leads to increased fluctuation level which scales with $1/\sqrt{N}$, where N is the average number of particles per simulation cell. We have verified our results by varying the number of particles per cell, and found that the further increase of N will not affect the evolution of the system. Note that due to a finite number of the simulated particles, even in the collisionless case, we are not in the Vlasov limit, and thus there will be effective collisions between charged particles due to fluctuations in the electrostatic potential. This feature is typical for all PIC simulations.

The ion collision frequency is $\nu_\mathrm{i} = 3.52 \times 10^5\,\mathrm{s}^{-1}$. This frequency is lower than the ion gyrofrequency, $\nu_\mathrm{i} = \Omega_\mathrm{ci}/5$.

TABLE I. Parameters used in simulations.

Parameter	Value	Units
Grid	$128 \times 128 \times 128$	—
Box size, L	$0.5 \times 0.5 \times 0.5$	m
Δt	2.5×10^{-10}	s
$\mathbf{B}_0$	$0.005\hat{x}$	T
$\mathbf{E}_0$	$550\hat{y}$	$\mathrm{V\,m^{-1}}$
$n_\mathrm{i}, n_\mathrm{e}$	4.3×10^{13}	$\mathrm{m^{-3}}$
$N_\mathrm{i}, N_\mathrm{e}$	4×10^7	—
ν_i	3.52×10^5	$\mathrm{s^{-1}}$
$\nu_\mathrm{i}/\Omega_\mathrm{i}$	1/5	—
$v_\mathrm{d}/c_\mathrm{s}$	0.57	—
$T_\mathrm{e}/T_\mathrm{i}$	4	—
$m_\mathrm{i}/m_\mathrm{e}$	500	—

This article is copyrighted as indicated in the article. Reuse of AIP content is subject to the terms at: http://scitation.aip.org/termsconditions. Downloaded to IP: 185.47.220.152 On: Wed, 04 Feb 2015 23:03:32

In this regime, the ion gyromotion is resolved and both species remain to be magnetized.[12] Thus, it is expected that different collision types will lead to different evolution of the velocity distributions.

To study the effects of collision types on the evolution of the simulated system, we consider three limiting cases: (E.S.) ion-neutral and electron-neutral collisions are elastic; (C.E.) ion-neutral collisions are charge-exchange and electron-neutral collisions are elastic; and (N.C.) no collisions are considered as a control case.

III. RESULTS

In this section, we present the results from numerical studies on the influence of collision types on the plasma stability in $\mathbf{E} \times \mathbf{B}$ fields. We consider three limiting cases: (i) no collisions between charged particles and neutrals (N.C.), (ii) charge exchange collisions for ions and elastic collisions for electrons (C.E.), and (iii) elastic collisions for both species (E.S.).

Effects of different ion-neutral collisions are clearly visible in the evolution of ion velocity distribution functions. Examples of ion velocity distribution functions for v_z and v_y components obtained in our simulations are shown in Fig. 1 for different time instances: half of the ion gyroperiod ($t \approx 0.5\tau_{Li}$, left panels) and approximately three ion gyroperiods ($t \approx 2.8\tau_{Li}$, right panels). In all cases, the initial bi-Maxwellian distributions for the v_z and v_y components are gyrorotating in the v_z–v_y plane that is perpendicular to the external magnetic field. The center of gyrorotation is thus at

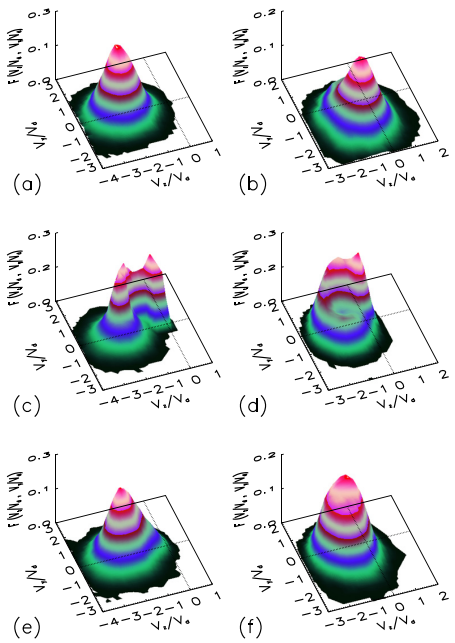

FIG. 1. Velocity distribution functions in the v_y–v_z velocity components for different types of ion collisions. (a) and (b) for the case with no collisions (N.C.); (c) and (d) for the charge exchange collisions (C.E.), and (e) and (f) for the elastic collisions (E.S.). Results in the left panels (a), (c), (e) are for $t \approx 0.5\tau_{Li}$ and in the right panels (b), (d), (f) for $t \approx 2.8\tau_{Li}$. Velocity axes are normalized to drift velocity.

$v_z/v_d = -1$, $v_y = 0$. This rotation is due to the low collisional regime for which ions remain magnetized. Thus, in Fig. 1, the peak of the distribution function in the v_z component is at $v_z/v_d = -1$ after half of the gyroperiod.

For the N.C. case (with no charged particle-neutral collisions, Figs. 1(a) and 1(b)), the distributions in all directions remain Maxwellian-like during the whole simulation. There are only small disturbances caused by weak electrostatic scattering between particles due to potential fluctuations originating from a finite number of simulation particles.

The charge exchange collisions, in the C.E. case, give rise to distinct evolution of the velocity distribution function, see Figs. 1(c) and 1(d). Due to the charge exchange, the gyrorotating bi-Maxwellian cone becomes narrower in time, while the new, cold ions originating from collisions with neutrals start at the origin in the v_z–v_y plane. Thus, the new ions follow the gyroorbit giving rise to a ring shape velocity distribution function, which is formed after one gyroperiod. After several gyroperiods the ring distribution fills in due to instability, and is centered to drift velocity with a peak close to origin. This peak is due to on-going charge exchange collisions. While in this study we consider cold neutrals, we observed similar evolution for finite neutral temperatures in control simulations.

Effects of ion-neutral elastic collisions, i.e., the E.S. case, are already visible after one gyroperiod, see Figs. 1(e) and 1(f), and are manifested by a skewness of the distribution for the v_y component. At a later stage, $t \approx 2.8\tau_{Li}$ the elastic collisions eventually lead to the spread of distribution and centering it to the value of the drift velocity in the v_z direction. The resulting distribution function is again Maxwellian-like but with a significant skewness in the v_y component. However, it is a single peak distribution which can be well approximated by a Maxwellian.

As seen in Fig. 1, different types of collisions give rise to distinct velocity distribution functions for ions, which suggests different dynamical properties of plasma in each of the cases. Thus, we can expect the instability growth for the C.E. case, while other cases are expected to be more stable. Since electrostatic instabilities are characterized by the growth of electrostatic waves, it can be instructive to look at the RMS values of the fluctuations in the electrostatic potential Φ for different collision types. We obtain RMS value as $\Phi_{RMS} = \sqrt{1/n \sum_{i=1}^{n} \Phi_i^2}$, where the sum is over a representative subset of the simulation grid. The time evolution of the potential fluctuations for three different cases is shown in Fig. 2. The significant growth of RMS values is present only for the C.E. case. This growth starts after the first gyroperiod. Note that a logarithmic scale is used for the vertical axis, so that the growth is exponential as it is expected for plasma instabilities. The growth is estimated to be $2.5/\tau_{Li}$ [V/s], which corresponds to the growth rate $\gamma/\omega_{pi} = 0.096$. The growth rate γ generally depends on wide variety of parameters, and the estimated value corresponds to usual values for electrostatic instabilities.[2,3]

For the E.S. case, one can observe an initial damping of fluctuations up to time corresponding to 1.5 ion gyroperiods and a subsequent increase back to the initial level of fluctuations. Therefore, we further investigated ion velocity

This article is copyrighted as indicated in the article. Reuse of AIP content is subject to the terms at: http://scitation.aip.org/termsconditions. Downloaded to IP: 185.47.220.152 On: Wed, 04 Feb 2015 23:03:32

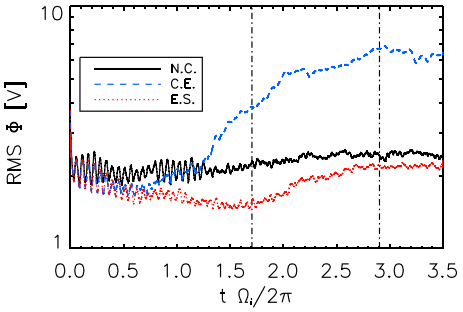

FIG. 2. Time evolution of potential fluctuations for three different ion collisional regimes: collisionless plasma (N.C.), charge exchange (C.E.), and elastic scattering (E.S.). Vertical lines indicate times for potential densities shown in Fig. 3 and also time interval for calculating spectra shown in Fig. 4.

distributions between one and three ion gyroperiods. The velocity distribution in the v_y direction becomes skewed while Φ_{RMS} decreases. After $t \approx 3\tau_{Li}$, the distribution returns to the initial (unskewed) state when the RMS of potential fluctuations increases again.

In the collisionless case (N.C.), the initial oscillations of the fluctuation level are damped in time. In spite of no RMS growth above the initial values in the N.C. and E.S., one can still expect that stable or weakly damped waves are present in plasmas in these both cases. Note that all three considered cases have similar evolution until the end of the first ion gyroperiod, and that after the third gyroperiod they reach new equilibrium-like states. We confirm the stability of these new states by longer simulations with reduced number of particles and resolution.

The two vertical lines in Fig. 2 indicate time instances for which the further analysis is done. We choose these time instances since the first one corresponds to the growth phase in the C.E. case, and the second one relates to time when the new equilibrium is being reached. Since the electrostatic waves form well organized structures in potential, it can be instructive to study the potential density in the plane perpendicular to magnetic field which is also a plane for which we can expect the development of waves in the $\mathbf{E} \times \mathbf{B}$ drift.

Fig. 3 shows electrostatic potential distribution in the y–z plane at $x = 1/2L_x$ at two different time instances, so that it gives idea on spatio-temporal evolution of the potential. Left panels correspond to time $t_1 \approx 1.7\tau_{Li}$ (indicated by the first vertical line in Fig. 2) and right panels correspond to time $t_2 \approx 2.9\tau_{Li}$ (marked by the second vertical line in Fig. 2). Note that while in Fig. 2 we presented RMS values of the potential fluctuations, now in Fig. 3 the color bar values correspond to the normalized potential amplitudes.

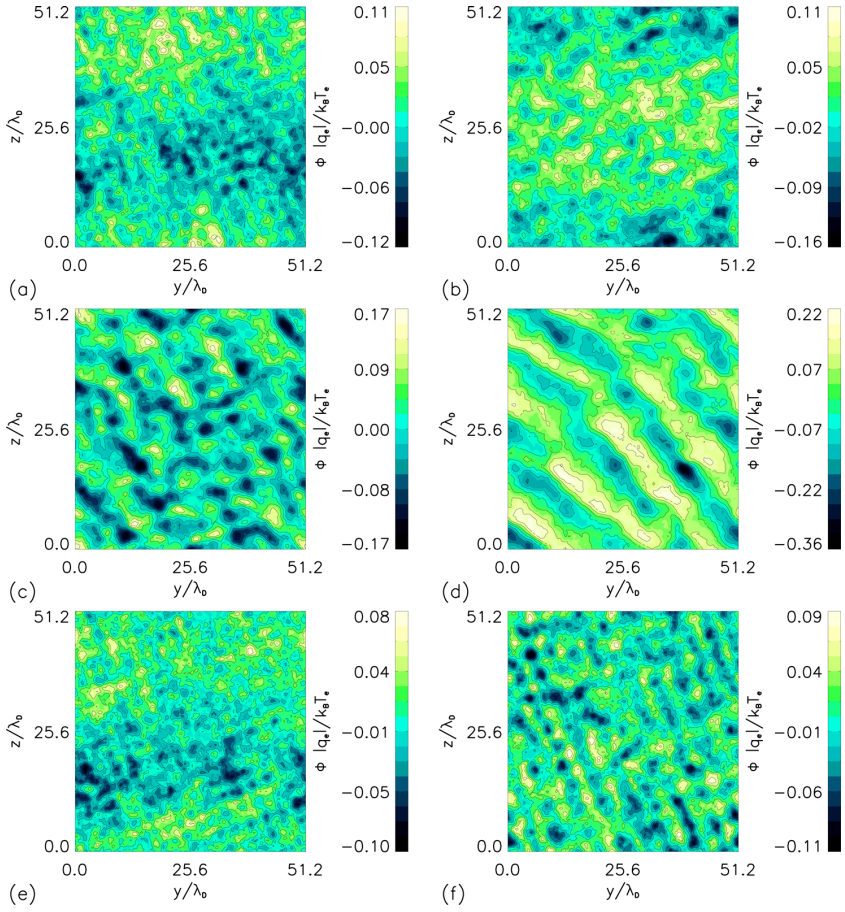

FIG. 3. Potential densities at different time instances for different ion collision types: (a) and (b) N.C., (c) and (d) C.E., (e) and (f) E.S. left panels correspond to time $t_1 \approx 1.7\tau_{Li}$, and panels correspond to time $t_2 \approx 2.9\tau_{Li}$.

This article is copyrighted as indicated in the article. Reuse of AIP content is subject to the terms at: http://scitation.aip.org/termsconditions. Downloaded to IP: 185.47.220.152 On: Wed, 04 Feb 2015 23:03:32

For the N.C. case, we do not observe any significant development of coherent structures throughout the simulation (see Figs. 3(a) and 3(b)), and also the scale corresponds to only relatively small fluctuations. However, for the C.E. case there is a clear growth of wavefronts propagating in both, y and z directions. The wavefront formation is visible already at an earlier time corresponding to the growth phase (see Fig. 3(c)), where areas with low and high potential start to form coherent structures. These structures are at the same angle with respect to the $\mathbf{E} \times \mathbf{B}$-direction, as the angle they have at a later time corresponding to the saturation. We estimate the angle as $\alpha \approx \pi/2$, so that the waves propagate at the same velocity in both z and y directions. The distance between wavefronts perfectly fits to the wavelength calculated from the wave spectra. At saturation, there is a noticeable increase in amplitudes, which is also expected from the time evolution of RMS fluctuations.

In the E.S. case, the propagating structures have smaller dimensions and shorter wavelength than in the C.E. case. The propagation angle is also different, and we estimate it to be $\alpha \approx \pi/3$ measured from y-direction, so that in the drift direction the wave propagates faster than in the direction of electric field. Even if the structures are less pronounced and less organized, we can still identify their time evolution. The wave amplitudes, just as RMS values, are lower than in the N.C. and C.E. cases.

Finally, to study the wave dynamics we analyze the ω–k spectra of electrostatic waves in the system. The spectra are calculated with the Fourier transform in space and in time in all three directions and time interval which corresponds to the growth phase in C.E. case, allowing to study the wave dynamics during this particular time period.

In Fig. 4, we present wave spectra for all three cases in directions perpendicular to magnetic field ($\hat{\mathbf{y}}, \hat{\mathbf{z}}$). We observe

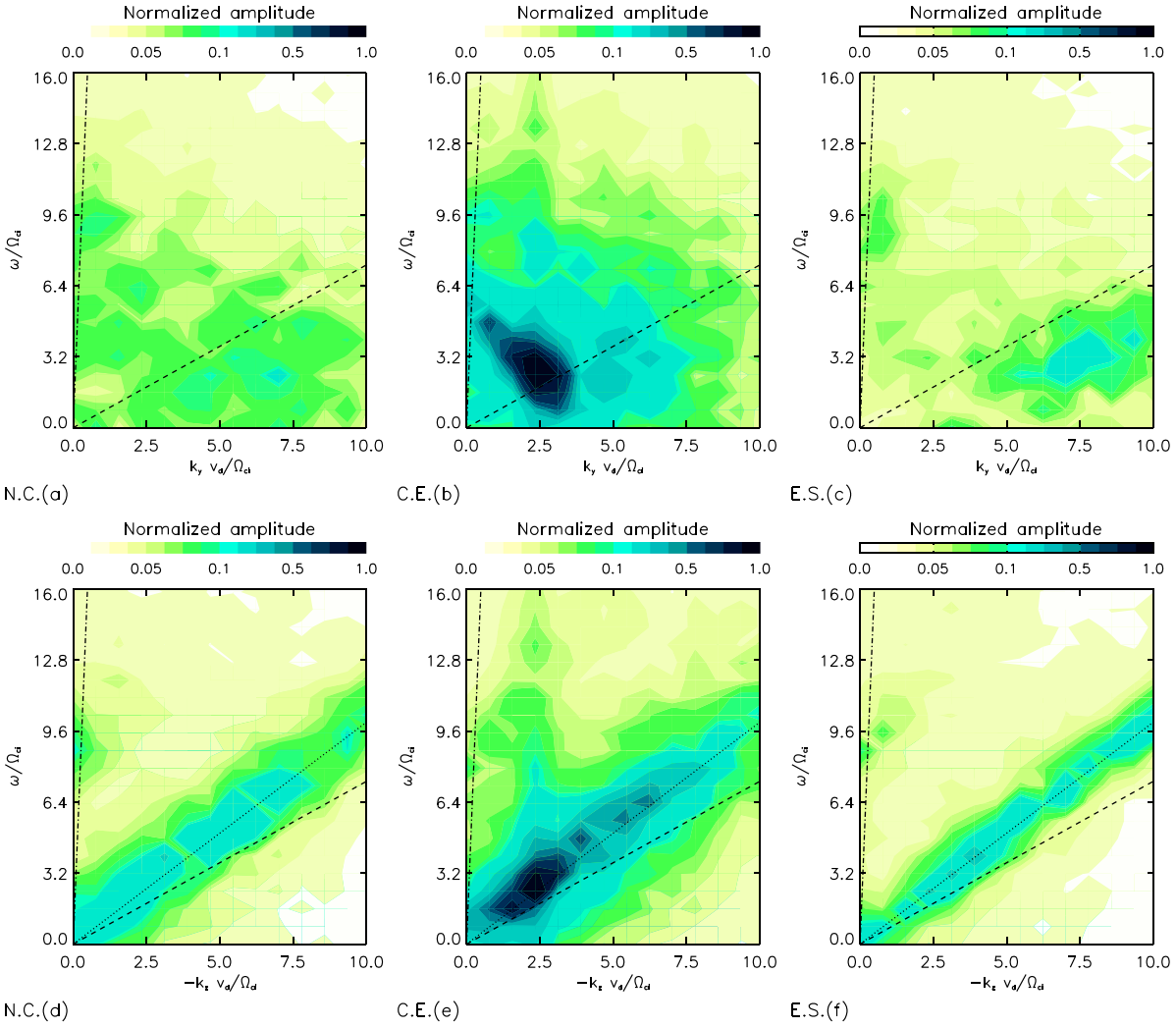

FIG. 4. Examples of spectra taken from the time period $t \in (1.7 - 2.9)\tau_{\mathrm{Li}}$ taken in the directions perpendicular to the magnetic field. Panels (a) and (d) show spectra for the N.C. case, (b) and (e) for the C.E. case, and panels (c) and (f) to the E.S. case. Upper row shows spectra in the $\hat{\mathbf{y}}$-direction, while lower rows shows spectra in the $\hat{\mathbf{z}}$-direction. Dotted-dashed line corresponds to the electron thermal velocity, dashed line is for the ion thermal velocity, and dotted line represents drift velocity (shown in spectra from the drift direction).

This article is copyrighted as indicated in the article. Reuse of AIP content is subject to the terms at: http://scitation.aip.org/termsconditions. Downloaded to IP: 185.47.220.152 On: Wed, 04 Feb 2015 23:03:32

little dynamical activity and basically no propagating waves in the $\hat{\mathbf{x}}$-direction (parallel to the magnetic field). The spectra correspond to time interval of 1.2 gyroperiods taken between approximately 1.7 and $2.9\tau_{\mathrm{Li}}$ (depicted in Fig. 2 by vertical lines). The ω and k axes are normalized to Ω_{i} and $\Omega_{\mathrm{i}}/v_{\mathrm{d}}$, respectively. We also plot lines corresponding to electron thermal velocity (dotted-dashed), ion thermal velocity (dashed), and $\mathbf{E}\times\mathbf{B}$ drift velocity (dotted). Figs. 4(a) and 4(d), correspond to the N.C. case, Figs. 4(b) and 4(e) to the C.E. case and Figs. 4(c) and 4(f) to the E.S. case. All the spectra have the same scaling and can be directly compared. Note that the color scale is nonlinear.

While in general we observe different wave behaviours in each direction, some aspects of wave evolution are the same for all runs. In the $\hat{\mathbf{y}}$-direction (parallel to the electric field, upper row in Fig. 4), the spectrum is symmetric around ω axis (we therefore show only a half of the spectrum), and in the $\hat{\mathbf{z}}$-axis ($\mathbf{E}\times\mathbf{B}$ drift direction) there is asymmetry due to the drift (there is little activity on the not-shown part of the spectrum). In the latter direction, we observe harmonics of modes with phase velocity equal to drift velocity in all the cases. These harmonic modes propagate in general with the $\mathbf{E}\times\mathbf{B}/B^2$ drift velocity in the $-\hat{\mathbf{z}}$ drift direction.

For the collisionless N.C. case, there is only propagation of waves in directions perpendicular to magnetic field. There is also a weak signature of oscillations at ion plasma frequency, $\omega_{\mathrm{pi}}\approx 9.4\Omega_{\mathrm{i}}$. In other cases, there are also present waves with several harmonics. In the C.E. case, we can see that harmonics can be related as $\omega_3=\omega_2+\omega_1$ and $k_3=k_2+k_1$. Our estimate from the spectrum is

$$\omega_3\approx 4\Omega_{\mathrm{ci}},\quad \omega_2\approx 3\Omega_{\mathrm{ci}},\quad \omega_1\approx 1\Omega_{\mathrm{ci}}$$

and

$$k_3\approx 4\Omega_{\mathrm{ci}}/v_{\mathrm{d}},\quad k_2\approx 2.5\Omega_{\mathrm{ci}}/v_{\mathrm{d}},\quad k_1\approx 1.5\Omega_{\mathrm{ci}}/v_{\mathrm{d}},$$

which indicates the possibility of the nonlinear three wave interaction[23,24] in the growing phase. Moreover, in this case the harmonics propagate in the $-\hat{\mathbf{z}}$ direction slightly faster than the $\mathbf{E}\times\mathbf{B}/B^2$ drift velocity. In this case, the amplitudes of wave modes are significantly larger than in the E.S. case, which we relate to the growth of amplitude of potential fluctuations.

IV. DISCUSSION

Results from our self-consistent numerical simulations show that there is a strong dependence of dynamic parameters (such as electrostatic potential fluctuations or wave spectra) on the type of ion-neutral collisions. Initially, in all our simulations the plasma is Maxwellian, but ion-neutral collisions lead to distortions in the ion velocity distributions, which are significant already after one ion gyroperiod. Thus, the plasma stability should be studied in the context of the actual form of the ion velocity distribution function.

We observed the growth of electrostatic wave amplitude only in the C.E. case, where the growth starts after the first ion gyroperiod, during which the initially bi-Maxwellian distribution function gyrorotates in the v_z–v_y phase space. This leads to the formation of a ring-shaped velocity distribution function, which thickness in general can depend on the temperature of neutrals.[13] During following gyroperiods, the central region of the ring becomes filled in due to quasilinear diffusion.[12,14] The ring-shaped distribution is unstable[12] and is the most probable trigger of the observed instability. While this is the dominant mechanism, another processes, such as electrostatic approximation of lower-hybrid drift waves, which can be excited by ring shape velocity distribution function,[25] can also be considered.

For N.C. and E.S. cases, the initial bi-Maxwellian cone rotates just as in the C.E. case, but the evolution of distribution is totally different. Since for the N.C. case we simulate almost Vlasov plasma (only weak electrostatic scattering is present due to potential fluctuations), there is only very light distortion, and the distribution rotates almost unchanged. For the E.S. case, elastic collisions between ions and neutrals lead to distribution that is centered to the drift velocity and at later time of the simulations becomes wider and skewed. However, it still has the Maxwellian-like shape which provides the stabilizing mechanism.[7]

The stability of plasma is reflected in the time evolution of the RMS of potential fluctuations. From Fig. 2, it is clear that amplitude grows only in the C.E. case, while in two other cases it is damped. This is in accordance with presumption that Maxwellian-like distributions are stable even if they rotate or are displaced.[7] In the C.E. case, the instability starts after the first ion gyroperiod when the ring shape distribution is formed.[12] We estimate here the growth rate as $\gamma/\omega_{\mathrm{pi}}=0.096$. This order of magnitude of the growth rate is usual for component-component electrostatic instabilities in unmagnetized plasmas.[3] It looks like that this can also apply to the magnetized regime. In addition, the growth rate depends on the strength of the external electric field, which is substantial in our simulations (to speed up the evolution of the system). The increase of the growth rate with increasing electric field was also demonstrated by Miloch *et al.*[12]

Even though there have been some attempts to use the Penrose criterion to magnetized plasma,[26] this criterion has been derived for unmagnetized plasma.[4] Thus, it is hardly applicable for our simulations. However, it can partially explain the growth of electrostatic modes related to double peaked distribution, such as the ring shape, in magnetized plasma. For the N.C. case, the plasma is stable and only some initial oscillations in the potential are present, which are damped in time. At earlier stages, the frequency and "modulation like" shape of oscillations indicate possible interaction between the cyclotron and plasma oscillations. For the E.S. case, it is clear that damping of oscillations in the beginning of simulation is stronger than in the N.C. case which can be related to collisional processes.[27]

In the E.S. case, the damping of the amplitude of fluctuations is up to the end of second ion gyroperiod and then the amplitude returns to the initial level. This transition regime might be caused by elastic collisions with gyrorotating ions. Initially, the distribution is clearly Maxwellian, so the decrease of fluctuations seems to be a transient to new equilibrium. Due to collisions, the transient distribution is not clearly Maxwellian and the presence of a distortion may

This article is copyrighted as indicated in the article. Reuse of AIP content is subject to the terms at: http://scitation.aip.org/termsconditions. Downloaded to IP: 185.47.220.152 On: Wed, 04 Feb 2015 23:03:32

cause a growth. At later times, the distribution does not rotate in velocity phase space and it is centered to the drift velocity to become again Maxwellian-like which stabilizes the system.

Potential densities correspond to the amplitudes of potential fluctuations, as it is shown in Fig. 3. For the C.E. case, it is obvious development of wavefronts with wavelengths corresponding to that obtained from spectra. The wavefronts propagate in both directions in the plane perpendicular to magnetic field with roughly the same speed and are inclined by $\alpha = \pi/4$ to both the electric field and the $\mathbf{E} \times \mathbf{B}$ direction. In case of symmetric ring distribution in the v_y–v_z plane, one would expect a more isotropic propagation in the y-z plane. However, in the presence of charge-exchange collisions, the ring distribution is asymmetric, with a peak close to the origin and more particles in the $v_y > 0$ part of the distribution. We attribute the inclination and tilt of the wavefronts to the shape of the ion velocity distribution as well as the strength of the external electric field. We have verified that with increasing electric field the angle α (with respect to the $\hat{\mathbf{y}}$-axis) decreases. Furthermore, with the increase of the collision frequency the peak close to the origin in the distribution function starts to dominate, and the distribution becomes effectively symmetric centered around the origin, which leads to the destruction of the wave pattern due to more isotropic propagation.

In two other cases, the situation is different. While for the N.C. case the potential density is random, for the E.S. case there is a visible formation of structures propagating again in the plane perpendicular to magnetic field, but the amplitude of fluctuations remains in the scale of an initial amplitude. However, in this case the wavefronts are not fully developed and the velocity distribution returns to the Maxwellian-like after the transient period. The final propagation has some tilt, but is much more isotropic.

The wave spectra match perfectly the other results: the angles of propagation and distance between wavefronts in Fig. 3 correspond to wavenumbers and wavelength, respectively. A very little activity along magnetic fieldlines (in our simulations $\hat{\mathbf{x}}$-direction) can be expected in a fully magnetized drifting plasma. In all collisional cases, we observe waves in the two directions perpendicular to magnetic field. From the spectra it is also clear that only in the C.E. case the amplitudes are significantly higher, and that for the E.S. case the amplitude is more damped than for the N.C. case. What is interesting in the C.E. case is the presence of several modes around the drift velocity in the $\mathbf{E} \times \mathbf{B}$ direction, but only one clear mode in the $\hat{\mathbf{y}}$-direction, i.e., the $\mathbf{E}$-direction. The modes might be higher harmonics (or half-harmonics) or the result of three wave interaction.[23,24] We also note that during the time evolution of the modes around drift velocity, the one mode corresponding to ion plasma oscillations became damped.

From all the results, we conclude that in C.E. we see, most probably electrostatic ion acoustic modes in the plane perpendicular to magnetic field that become unstable due to the ion velocity distribution function. Here, the propagation of the waves is slightly faster than the drift velocity, see again Fig. 4(e), but slower than the speed of sound. We have verified that the propagation gets closer to the sound speed with increasing collision frequency, i.e., when the peak in the distribution function becomes dominant so that the resulting electron-ion distributions remind the ion-beam that can trigger the ion-acoustic instability.[1] The free energy source in our system is the electric field, and its magnitude is a crucial parameter for the system stability in the C.E. case.[12] There were several analytical studies of the ring shape distributions,[13,14] but focused only on particular ionospheric plasma conditions. Thus, such a more general analytical study is required to compare the analytical theory with our numerical results.

Due to the low collisional regime, these results may be important for ionospheric research related to regions between the E and F-layers, as well as for laboratory experiments with partially ionized strongly magnetized plasmas (i.e., gas discharges in strong magnetic field). We expect that with changing system parameters, the results will also be slightly affected. We have already mentioned effect of electric field, while another aspect is that collisions can effectively demagnetize plasma particles, so by increasing collision frequency for ions up to the limit $\nu_i \gg \Omega_i$ we would shift our system to the Farley-Buneman limit.[5,6]

Finally, one should consider the limitations of our study. We have simulated only three extreme cases (N.C., E.S., and C.E.), and there are many types of collisions in real physical systems, and the probability of these collision events is given by relevant collisional cross-sections. For example, in ionosphere the charge exchange and elastic collisions have the biggest collisional cross-sections, meaning that they will both dominate and compete in a real system. Another constraint is the finite size of simulated box, which puts limits on the length of waves that can be resolved in the simulation. The long wavelengths that are not accommodated in the present box could affect the dynamics of instability and its characteristics. Furthermore, the PIC simulations are burden with a finite noise due to a finite number of particles. The particles interact electrostatically via grid points and this interaction provides electrostatic scattering, which can be regarded as effective collisions between charged particles. Thus, we were not able to set a completely collisionless regime in the cases with zero collision frequency $\nu = 0$.

Since our simulations have been performed for the low collisional conditions, our results cannot be directly related to and compared with the results of past numerical simulations which are focused on the ionospheric highly collisional regime.[15–17] However, due to the exponential decrease of neutral particle density in the ionosphere, one can find low collisional conditions in the upper part of the ionospheric E-region or in F-region. Similar conditions can also be set in experimental devices (e.g., discharges at low pressure). Thus, the parameter regime considered in this study may also play an important role in the dynamics of the ionospheric plasmas. Note that we used increased amplitudes of some parameters, but we still keep characteristic ratios like v_d/c_s or Ω_α/ν_α (where α denotes plasma species) close to realistic ones. For completeness, the transition between different regimes should also be addressed.

This article is copyrighted as indicated in the article. Reuse of AIP content is subject to the terms at: http://scitation.aip.org/termsconditions. Downloaded to IP: 185.47.220.152 On: Wed, 04 Feb 2015 23:03:32

V. CONCLUSIONS

We have studied the role of ion-neutral collision types on the plasma stability in the $\mathbf{E} \times \mathbf{B}$ fields, and focused on the electrostatic potential fluctuations, and wave dynamics of plasma for weakly collisional regimes. We considered only the weakly collisional regime and fully magnetized plasmas, and found that the ion-neutral collision type is an important parameter for plasma stability. While for elastic scattering or no collisions between ions and neutrals, the plasma is stable for charge exchange collisions even the fully magnetized plasma becomes unstable. We find that the calculated instability growth corresponds well to the growth rates of electrostatic instabilities. The formation and growth of coherent structures in potential density is observed in the plane perpendicular to the external magnetic field. We conclude that triggering of this instability is caused by a specific distortion of the ion velocity distribution function due to charge exchange collisions. Under such conditions, in the plane perpendicular to the external magnetic field a ring-shaped or loss cone ion velocity distribution function is established, which can trigger ion acoustic-like waves. Under elastic collisions and in the collisionless case, the distortions of velocity distribution functions are weak and we do not observed any significant growth but still we detected stable waves and their harmonics. Since there is no theoretical research on weakly collisional regime in fully magnetized plasmas, performing of at least linear analysis is needed. Thus, precise derivation of dispersion relation from the kinetic theory, linear, and nonlinear study of simulated regimes are topics of our future research.

ACKNOWLEDGMENTS

Research presented in this paper was carried out during three M.H.'s research visits at the Department of Physics, University of Oslo which was supported by the CTU Grant Nos. SGS12/181/OHK3/3T/13, SGS13/194/OHK3/3T/13, and the Czech Science Foundation grant GAČR 14-37086G—Albert Einstein Center for Gravitation and Astrophysics. The last stay was primarily supported by the Norway grant NF-CZ07-INS-3-002-2014. The authors thank Professors H. L. Pécseli and J. Trulsen for useful discussions. This study is a part of 4DSpace Strategic Research Initiative at the University of Oslo.

[1]R. A. Treumann and W. Baumjohann, *Advanced Space Plasma Physics*, 1st ed. (Imperial College Press, 2001).
[2]D. B. Melrose, *Instabilities in Space and Laboratory Plasmas* (Cambridge University Press, 1989).
[3]S. P. Gary, *Theory of Space Plasma Microinstabilities*, 1st ed. (Cambridge University Press, 2005).
[4]H. L. Pécseli, *Waves and Oscillations in Plasmas*, 1st ed. (CRC Press, 2013).
[5]O. Buneman, "Excitation of field aligned sound waves by electron streams," Phys. Rev. Lett. **10**(7), 285–287 (1963).
[6]D. T. Farley, "Two-stream plasma instability as a source of irregularities in the ionosphere," Phys. Rev. Lett. **10**(7), 279–282 (1963).
[7]E. Ott and D. T. Farley, "Microinstabilities and the production of short-wavelength irregularities in the auroral F region," J. Geophys. Res. **80**(34), 4599–4602, doi:10.1029/JA080i034p04599 (1975).
[8]R. F. Post and M. N. Rosenbluth, "Electrostatic instabilities in finite mirror-confined plasmas," Phys. Fluids **9**(4), 730–749 (1966).
[9]M. N. Rosenbluth and R. F. Post, "High-frequency electrostatic plasma instability inherent to 'loss-cone' particle distributions," Phys. Fluids **8**(3), 547–550 (1966).
[10]E. G. Harris, "Unstable plasma oscillations in a magnetic field," Phys. Rev. Lett. **2**, 34–36 (1959).
[11]P. J. G. Perron, J.-M. Noël, J.-P. St.-Maurice, and K. Kabin, "Ion temperature anisotropy effects on the dispersion relation and threshold conditions of a sheared current-driven electrostatic ion-acoustic instability with applications to the collisional high-latitude F-region," J. Plasma Phys. (in press).
[12]W. J. Miloch, H. L. Pécseli, and J. K. Trulsen, "Unstable ring-shaped ion distribution functions induced by charge-exchange collisions," Plasma Phys. Control. Fusion **55**, 124006 (2013).
[13]J.-P. St.-Maurice and R. W. Schunk, "Ion velocity distributions in the high-latitude ionosphere," Rev. Geophys. Space Phys. **17**(1), 99–134, doi:10.1029/RG017i001p00099 (1979).
[14]J.-P. St.-Maurice, "On a mechanism for the formation of VLF electrostatic emission in the high latitude F region," Planet. Space Sci. **26**, 801–816 (1978).
[15]D. V. Kovalev, A. P. Smirnov, and Y. S. Dimant, "Modelling of the Farley-Buneman instability in the E-region ionosphere: A new hybrid approach," Ann. Geophys. **26**(9), 2853–2870 (2008).
[16]M. M. Oppenheim, N. Otani, and C. Ronchi, "Hybrid simulations of the saturated Farley-Buneman instability in the ionosphere," Geophys. Res. Lett. **22**(4), 353–356, doi:10.1029/94GL03277 (1995).
[17]M. M. Oppenheim, Y. S. Dimant, and L. P. Dyrud, "Large-scale simulations of 2-D fully kinetic Farley-Buneman turbulence," Ann. Geophys. **26**(3), 543–553 (2008).
[18]V. Vahedi and M. Surendra, "A Monte Carlo collision model for the particle-in-cell method: Applications to argon and oxygen discharges," Comput. Phys. Commun. **87**(1–2), 179–198 (1995).
[19]D. Block and W. J. Miloch, "Charging of multiple grains in subsonic and supersonic plasma flows," Plasma Phys. Controlled Fusion **57**, 014019 (2015).
[20]W. J. Miloch, S. R. Habbal, and R. Esser, "Plasma dynamics at the prominence-corona interface," Astrophys. J. **752**(2), 85 (2012).
[21]W. J. Miloch, M. Kroll, and D. Block, "Charging and dynamics of a dust grain in the wakefield of other grain," Phys. Plasmas **17**, 103703 (2010).
[22]H. R. Skullerud, "The stochastic computer simulation of ion motion in a gas subjected to a constant electric field," J. Phys. D: Appl. Phys. **1**, 1567–1569 (1968).
[23]A. Hasegawa, *Plasma Instabilities and Nonlinear Effects*, 1st ed. (Springer-Verlag, 1975).
[24]A. S. Volokitin and B. Atamaniuk, "Nonlinear regimes of Farley–Buneman instability," Plasma Phys. Rep. **36**(5), 390–402 (2010).
[25]D. Winske and W. Daughton, "Generation of lower hybrid and whistler waves by an ion velocity ring distribution," Phys. Plasmas **19**, 072109 (2012).
[26]I. H. Hutchinson, "Electron velocity distribution instability in magnetized plasma wakes and artificial electron mass," J. Geophys. Res. **117**, A03101, doi:10.1029/2011JA017119 (2012).
[27]E. W. McDaniel, *Atomic Collisions*, 1st ed. (Wiley, 1989).

This article is copyrighted as indicated in the article. Reuse of AIP content is subject to the terms at: http://scitation.aip.org/termsconditions. Downloaded to IP: 185.47.220.152 On: Wed, 04 Feb 2015 23:03:32

Chapter 5
Conclusions and future work

During my doctoral studies I have worked on two major topics. The first one was the analysis of the generalized Buneman dispersion relation for the problem of plasma jet interaction with a stationary plasma background. Such situations are usual in astrophysical plasmas. I found how the instability growth rate changes with change of input parameters like the plasma frequency of the jet, cyclotron frequency of jet and background, sound speed of jet and background and the spatial orientation of magnetic field and wave vector. Knowledge of these dependencies allows finding conditions with maximal growth rate. This research will continue in the future by performing MHD simulations of highly unstable situations. The algorithm that I developed also allows study of different situations (i. e. two opposite streams, two streams with the same direction but different velocities etc.), which means applicability to a wide variety of real physical problems.

The second part of my doctoral training was a project carried out in collaboration with the Department of Physics at the University of Oslo. This project was focused on electrostatic Particle-In-Cell simulations of magnetized weakly collisional plasmas. Parameters used in simulations can be related to the ionospheric F-layer parameters, because typical ratios like a Ω_α/ν_α remained close to the natural ones. Using the numerical simulations we studied the dependence of plasma stability on the type of ion-neutral collisions. Different types of collisions give rise to different evolution of ion velocity phase space. The ion-neutral charge exchange collisions lead to formation of a ring shape velocity distribution which can cause microinstabilities. In contrast, elastic ion-neutral collisions have a stabilizing effect. In real plasmas, these two collision types have the largest collisional cross-sections and it can be expected that both of them are present. Thus in real plasmas we can expect competition between instability growth originating from charge exchange collisions and a stabilizing effect due to elastic collisions. This project creates a basis for future work focusing on two subjects: (i) numerical instabilities that probably arose from not resolving electron Larmor radius (these numerical instabilities were observed during our simulations and were avoided by using the finer numerical grid), and (ii) analytical solution of the simulated system. Although the analytical solution is nontrivial due to the character of collisions and parameter range, it will allow for a better understanding the problem.

References

[1] P. Kulhánek. *Úvod do teorie plazmatu*. AGA, 1st. edition, 2011. In Czech languge only.

[2] H. L. Pécseli. *Waves and Oscillations in Plasmas*. CRC Press, 1st. edition, 2013.

[3] W. Baumjohann, R. A. Treumann. *Basic Space Plasma Physics*. Imperial College Press, 1st. edition, 1996.

[4] M. N. Rosenbluth, W. M. MacDonald, D. L. Judd. Fokker-Planck Equation for an Inverse-Square Force. *Physical Review*, **107**(1), pp. 1–6, 1957.

[5] L. Landau. On the vibration of the electronic plasma. *Journal of Experimental and Tehoretical Physics*, **10**, 1946.

[6] S. P. Gary. *Theory of Space Plasma Microinstabilities*. Cambridge University Press, 1st. pbk. edition, 2005.

[7] D. B. Melrose. *Instabilities in Space and Laboratory Plasmas*. Cambridge University Press, reprint edition, 1989.

[8] R. A. Treumann, W. Baumjohann. *Advanced Space Plasma Physics*. Imperial College Press, revised 1st. edition, 2001.

[9] T. Fülöp, M. Landreman. Ion Runaway in Lightning Discharges. *Physical Review Letters*, **111**, p. 015006, 2013.

[10] Y. Mizuno, B. Zhang, B. Giacomazzo, K.-I. Nishikawa, P. E. Hardee, S. Nagataki, D. H. Hartmann. Magnetohydrodynamic Effects in Propagating Relativistic Jets: Reverse Shock and Magnetic Acceleration. *Astrophysical Journal*, **690**, p. L47, 2009.

[11] K.-I. Nishikawaa, P. Hardee, C. B. Hededalc, G. Richardsond, R. Preecee, H. Solf, G. J. Fishman. Particle acceleration, magnetic field generation, and emission in relativistic shocks. *Advances in Space Research*, **38**(7), 2006.

[12] V. Urpin. Generation of the magnetic fields in jets. *Astronomy and Astrophysics*, **455**, 2006. Page no. 779.

[13] O. Buneman. Excitation of Field Aligned Sound Waves by Electron Streams. *Physical Review Letters*, **10**(7), pp. 285–287, 1963.

[14] D. P. Brennan, J. M. Finn. Control of linear modes in cylindrical resistive magnetohydrodynamics with a resistive wall, plasma rotation, and complex gain. *Physics of Plasmas*, **21**(10), p. 102507, 2014.

[15] D. T. Farley. Two-Stream Plasma Instability as a Source of Irregularities in the Ionosphere. *Physical Review Letters*, **10**(7), pp. 279–282, 1963.

[16] E. Ott, D. T. Farley. Microinstabilities and the Production of Short-Wavelength Irregularities in the Auroral F Region. *Journal of Geophysical Research*, **80**(34), pp. 4599–4602, 1975.

[17] M. N. Rosenbluth, R. F. Post. High-Frequency Electrostatic Plasma Instability Inherent to Loss-Cone Particle Distributions. *Physics of Fluids*, **8**(3), pp. 730–749, 1966.

[18] H. R. Skullerud. The stochastic computer simulation of ion motion in a gas subjected to a constant electric field. *J. Phys. D: Appl. Phys.*, **1**, pp. 1567–1569, 1968.

[19] M. M. Oppenheim, N. Otani, C. Ronchi. Hybrid Simulations of the Saturated Farley-Buneman Instability in the Ionosphere. *Geophysical Research Letters*, **22**(4), pp. 353–356, 1995.

[20] D. V. Kovalev, A. P. Smirnov, Y. S. Dimant. Modelling of the Farley-Buneman Instability in the E-Region Ionosphere: A New Hybrid Approach. *Annales Geophysicae*, **26**(9), pp. 2853–2870, 2008.

[21] O. Buneman. Dissipation of Currents in Ionized Media. *Physical Review*, **115**(3), pp. 503–517, 1959.

[22] G. Gogoberidze, Y. Voitenko, S. Poedts, M. Goossens. Farley-Buneman Instability in the Solar Chromosphere. *Astrophysical Journal Letters*, **706**(1), pp. L12–L16, 2009.

[23] E. J. Strait. Magnetic control of magnetohydrodynamic instabilities in tokamaks. *Physics of Plasmas*, **22**(2), p. 021803, 2015.

[24] L. F. Wanex, V. I. Sotnikov, J. N. Leboeuf. Linear analysis of magnetic and flow shear stabilization of Z-pinch instabilities. *Physics of Plasmas*, **12**(4), p. 042101, 2005.

[25] R. W. Hamming. *Numerical Methods for Scientists and Engineers*. McGraw-Hill Book Company, 2nd. edition, 1973.

[26] C. K. Birdsall, A. B. Langdon. *Plasma Physics via Computer Simulations*. McGraw-Hill Book Company, 1st. edition, 1985.

[27] R. W. Hockney, J. W. Eastwood. *Computer Simulation Using Particles*. IOP Publishing, 1st. edition, 1988.

[28] W. L. Briggs, V. E. Henson, S. F. McCormick. *A Multigrid Tutorial*. Society for Industrial and Applied Mathematics, 2nd. edition, 2000.

[29] B. Eliasson. Numerical simulations of the Fourier transformed Vlasov-Maxwell system in higher dimensions – Theory and applications. *Transport Theory and Statistical Physics*, **39**(5&7), pp. 387–465, 2010.

[30] V. Vahedi, M. Surendra. A Monte Carlo Collision Model for the Particle-In-Cell Method: Applications to Argon and Oxygen Discharges. *Computer Physics Communications*, **87**(1–2), pp. 179–198, 1995.

[31] E. W. McDaniel. *Atomic Collisions*. Wiley, 1st. edition, 1989.

[32] M. Melzani, C. Winisdoerffer, R. Walder, D. Folini, J. M. Favre, S. Krastanov, P. Messmer. Apar-T: code, validation, and physical interpretation of particle-in-cell results. *Astronomy and Astrophysics*, **558**, 2013. A133.

[33] S. E. Parker, C. K. Birdsall. Numerical Error in Electron Orbits with Large $\omega_c \Delta t$. *Journal of Computational Physics*, **96**(17), pp. 91–102, 1991.

[34] V. Tarjáni, J. D. Skalný. Investigation of numerical thermalization in particle-in-cell simulations. In *PLASMA 2007: Proceedings of the International Conference on Research and Applications of Plasmas; 4th German-Polish Conference on*

Plasma Diagnostics for Fusion and Applications; 6th French-Polish Seminar on Thermal Plasma in Space and Laboratory. 2008.

[35] P. Y. Lai, T. Y. Lin, Y. R. Lin-Liu, S. H. Chen. Numerical thermalization in particle-in-cell simulations with Monte-Carlo collisions. *Physics of Plasmas*, **21**(12), p. 122111, 2014.

[36] M. M. Oppenheim, Y. S. Dimant, L. P. Dyrud. Large-Scale Simulations of 2-D Fully Kinetic Farley-Buneman Turbulence. *Annales Geophysicae*, **26**(3), pp. 543–553, 2008.

[37] M. M. Oppenheim, Y. S. Dimant. Kinetic Simulations of 3-D Farley-Buneman Turbulence and Anomalous Electron Heating. *Journal of Geophysical Research: Space Physics*, **118**(3), pp. 1306–1318, 2013.

[38] D. Winske, W. Daughton. Influence of plasma beta on the generation of lower hybrid and whistler waves by an ion velocity ring distribution. *Physics of Plasmas*, **22**(2), p. 022102, 2015.

[39] R. Dejarnac, A. Podolník, M. Komm, G. Arnoux, J. W. Coenen, S. Devaux, L. Frassinetti, J. P. Gunn, G. F. Matthews, R. A. Pitts. Numerical evaluation of heat flux and surface temperature on a misaligned JET divertor W lamella during ELMs. *Nuclear Fusion*, **54**(12), p. 123011, 2014.

[40] J. Psikal, O. Klimo, J. Limpouch. 2D particle-in-cell simulations of ion acceleration in laser irradiated submicron clusters including field ionization. *Physics of Plasmas*, **19**(4), p. 043107, 2012.

[41] M. Bohata, D. Břeň, P. Kulhánek. Generalized Buneman Dispersion Relation in Longitudinally Dominated Magnetic Field. *ISRN Condensed Matter Physics*, **1**, p. Article ID 896321, 2011.

[42] M. Horký. Numerical Solution of the Generalized Buneman Dispersion Relation. In *Proceedings of Poster 2012*. 2012.

[43] J. Hubbard, D. Schleicher, S. Sutherland. How to Find All Roots of Complex Polynomials With Newton's Method. *Inventiones Mathematicae*, **146**, pp. 1–33, 2001.

[44] M. Horký. Instability Growth Rate Dependence on Input Parameters During the Beam-Target Plasma Interaction. *Acta Polytechnica*, **53**(2), pp. 174–178, 2013.

[45] M. Horký, P. Kulhánek. Analysis of the instability growth rate during the jet-background interaction in a magnetic field. *Research in Astronomy and Astrophysics*, **13**(6), pp. 687–694, 2013.

[46] M. Horký, W. J. Miloch. Numerical simulations of weakly collisional plasmas in $\mathbf{E} \times \mathbf{B}$ fields. In *Proceedings of 31st General Assembly and Scientific Symposium (URSI GASS)*. IEEExplore, 2014.

[47] M. Horký, W. J. Miloch. Kinetic plasma instabilities due to charge exchange and elastic collisions. *Journal of Physic: Conference Series*, **591**, p. 012034, 2015.

[48] M. Horký, W. J. Miloch. Numerical study on the stability of weakly collisional plasma in $\mathbf{E} \times \mathbf{B}$ fields. *Physics of Plasmas*, **22**(2), p. 022109, 2015.

[49] W. J. Miloch, H. L. Pécseli, J. K. Trulsen. Unstable Ring-Shaped Ion Distribution Functions Induced by Charge-Exchange Collisions. *Plasma Physics and Controlled Fusion*, **55**, 2013.

Appendix A
List of publications and grants

A.1 Scientific papers

Papers in impacted journals

- M. Horký, W. J. Miloch, Numerical study on the stability of weakly collisional plasma in $\mathbf{E} \times \mathbf{B}$ fields, *Physics of Plasmas*, **22**, 2, 022109, 2015 (contribution of Miroslav Horký - 75 %),
- M. Horký and P. Kulhánek, Analysis of the instability growth rate during the jet-background interaction in a magnetic field, *Research in Astronomy and Astrophysics*, **13**, 6, 687–694, 2013 (contribution of Miroslav Horký - 50 %).

Papers in other journals and conference proceedings

- M. Horký, W. J. Miloch, Numerical instability in PIC simulations of weakly collisional magnetized plasmas. Accepted paper for 32^{nd} International Conference on Phenomena in Ionized Gases (ICPIG), 2015.
- M. Horký, W. J. Miloch, Kinetic plasma instabilities due to charge exchange and elastic collisions, *Journal of Physics: Conference Series*, **591**, 012034, 2015.
- M. Horký, W. J. Miloch, Numerical simulations of weakly collisional plasmas in $\mathbf{E} \times \mathbf{B}$ fields, *Proceedings of 31^{st} General Assembly and Scientific Symposium (URSI-GASS)*, 2014.
- M. Horký, Dispersion relation for magnetically aligned electrostatic waves in weakly collisional plasmas, *Proceedings of 18^{th} international student conference Poster*, 2014.
- M. Horký, Instability Growth Rate Dependence on Input Parameters During the Beam-Target Plasma Interaction, *Acta Polytechnica*, **53**, 2, 174–178, 2013.
- M. Horký, Numerical Solution of the Generalized Buneman Dispersion Relation, *Proceedings of 16^{th} international student conference Poster*, 2012.

Poster presentations without papers in proceedings

- M. Horký, W. J. Miloch, M. Žáček, Kinetic Studies of Crossfield Plasma Instabilities in Weakly Collisional Plasmas, 17th International Congress on Plasma Physics (ICPP), Lisbon, 2014.
- M. Horký, W. J. Miloch, Wave-particle interaction as a possible source of electron heating in $\mathbf{E} \times \mathbf{B}$ fields driven instabilites, 26th Symposium on Plasma Physics and Technology (SPPT), Prague, 2014.

A.2 Popular-science articles

- M. Horký, Dark Energy Survey, *Aldebaran Bulletin*, **12**, 25, 2014, (in Czech language).
- M. Horký, New Results in the Research of Lightning Discharges, *Aldebaran Bulletin*, **11**, 17, 2013, (in Czech language).
- M. Horký, Fusion-Fission Hybrids, *Aldebaran Bulletin*, **11**, 13, 2013, (in Czech language).
- M. Horký, Transmission Electron Microscopy of Liquids, *Aldebaran Bulletin*, **10**, 32, 2012, (in Czech language).
- M. Horký, Probe MESSENGER and Modelling of the Mercury Magnetosphere, *Aldebaran Bulletin*, **10**, 16, 2012, (in Czech language).
- M. Horký, Czech Satellites MAGION, *Aldebaran Bulletin*, **9**, 47, 2011, (in Czech language).
- M. Horký, Experiment PAMELA: Discovery of Antiprotons in the Van-Allen Belts, *Aldebaran Bulletin*, **9**, 34, 2011, (in Czech language).

A.3 Grants

Responsible researcher - competed projects

- (2012–2014) CTU internal grant SGS12/181/OHK3/3T/13 - Plasma instabilities and plasma-particle interactions. Three year project covering mainly my doctoral research.
- (2014) Norway grant NF-CZ07-INS-3-002-2014 - Analytical and numerical studies of ionospheric plasma instabilities. Project covering research stay at the University of Oslo in the length of one month.

Member of team - ongoing projects

- GAČR grant 14-37086G - Albert Einstein Center for Gravitation and Astrophysics.
- CTU internal grant SGS15/073/OHK3/1T/13 - Waves and instabilities in plasmas - basic research.
- CTU internal grant SGS13/194/OHK3/3T/13 - Electric discharges, basic research, modeling and applications.

Member of team - completed projects

- (2012) GAČR grant GD205/09/H033 - General relativity and its applications in astrophysics and cosmology.
- (2011–2012) CTU internal grant SGS10/266/OHK3/3T/13 - Electric discharges, basic research and application.

Appendix B
Used symbols

$\mathbf{A}$	Vector potential.
$\mathbf{B}$	Magnetic field vector.
B	Magnitude of magnetic field vector.
c_s	Sound speed.
$\mathbf{E}$	Electric field vector.
E	Magnitude of electric field vector.
$F(\omega, \mathbf{k})$	Dispersion relation.
f	Probability density function.
$\mathscr{H}$	Hamiltonian.
$\mathbf{k}$	Wave vector.
$\mathscr{L}$	Lagrangian.
n	Particle density.
$\mathbf{p}$	Momentum vector.
p_0	Magnitude of relativistic momentum.
p	Dynamic pressure.
p_M	Magnetic pressure.
Q	Electric charge.
$\mathbf{R}$	Position vector of gyrocenter.
R_L	Larmor radius.
$\mathbf{r}$	Position vector.
$\overline{\mathbf{T}}$	General tensor quantity.
$\mathbf{u}$	Fluid velocity.
$\mathbf{v}$	Particle velocity.
$\mathbf{v}_\mathrm{d}$	Drift velocity.
v_d	Magnitude of drift velocity.
v_th	Thermal velocity.
$\overline{\mathbf{1}}$	Unit tensor.
α	Index denoting plasma species.
γ	Instability growth rate.
ε_0	Vacuum permitivity.
λ_D	Debye length.
μ	First adiabatic invariant and plasma permeability.
μ_0	Vacuum permeability.
ν	Collision frequency.
ρ	Fluid density.
σ	Conductivity.
ϕ	Scalar potential.
Ω_c	Cyclotron frequency.
ω	Wave frequency.
ω_p	Plasma frequency.